



MEDICAL UNIVERSITY
OF VIENNA

The impact of hemolysis and heme release on the susceptibility to bacterial infections

Doctoral thesis at the Medical University of Vienna
For obtaining the academic degree

Doctor of Philosophy

Submitted by

Rui Martins, MSc.

Supervisor:

Univ. Prof. Dr. Sylvia Knapp, PhD

Department of Internal Medicine I, Laboratory of Infection Biology,
Medical University of Vienna

Research Center for Molecular Medicine (Ce-M-M-) of the Austrian
Academy of Sciences

Vienna, 12/2016

Declaration

The doctoral candidate, Rui Martins, conducted his PhD studies under the supervision of Prof. Dr. Sylvia Knapp, PhD at the Department of Medicine I, Laboratory of Infection Biology, Medical University of Vienna and the Research Center for Molecular Medicine (Ce-M-M-) of the Austrian Academy of Sciences.

For the publication “Heme drives hemolysis-induced susceptibility to infection via disruption of phagocyte functions” included in chapter 2 of this thesis, Rui Martins performed the majority of experiments, analyzed the data and wrote the manuscript. Sylvia Knapp funded the project, supervised the work and wrote the manuscript. Julia Maier, Charles-Hugues Lardeau and Stefan Kubicek provided assistance for the chemical screens. Anna-Dorothea Gorki, Philipp Starkl and Federica Quattrone provided assistance with CRISPR knock-out generation. Omar Sharif performed efferocytosis assays. Simona Saluzzo, Riem Gawish, Karin Lakovits, Anastasiya Hladik and Ana Korosec provided technical assistance with *in vivo* and *in vitro* experiments. Kilian V. M. Huber, Branka Radic-Sarikas, Jacques Colinge and Keiryn Bennett provided assistance with chemical proteomics. Michael C. Aichinger performed, and Thomas Decker supported, experiments with *Listeria monocytogenes*. Kari Vaahtomeri and Michelle Duggan provided technical support with 3D collagen migration assays. Markus Brown and Dontscho Kerjaschki provided assistance with adhesion and rolling experiments. Harald Esterbauer provided *Hmox1^{fl/fl}* mice. Stephanie C. Eisenbarth provided *Dock8^{-/-}* mouse bone marrow. Michael Sixt and Giulio Superti-Furga provided intellectual input and supported this work.

Table of contents

Declaration	ii
Table of contents	iii
List of Figures	v
List of Tables.....	vii
Abstract	viii
Kurzfassung.....	ix
Publications arising from this thesis.....	xi
Abbreviations	xii
Acknowledgements	xv
1. Introduction	1
1.1. The innate immune system	1
1.1.1. Functions, general concepts and context within the immune system	1
1.1.2. Regulation of innate immunity.....	3
1.1.3. Key cells of the innate immune system.....	6
1.1.4. Key mechanisms of resistance to infection	9
1.1.5. Iron homeostasis.....	11
1.2. The actin cytoskeleton	12
1.2.1. Functions and general concepts.....	12
1.2.2. Structure and regulation	13
1.2.3. Actin cytoskeleton control by Rho family GTPases	16
1.2.4. DOCK family GEFs	18
1.2.5. Cell migration and phagocytosis	19
1.3. Bacterial infections	20
1.3.1. Bacteria and the host	20
1.3.2. Immune evasion	21
1.3.3. Nutrient acquisition	22
1.4. Hemolysis and release of free heme	23

1.4.1.	Heme and Hemolysis – Terms and definitions	23
1.4.2.	Heme biosynthesis.....	24
1.4.3.	Hemolytic disorders	25
1.4.4.	Extracellular heme.....	26
1.4.5.	Heme detoxification	27
1.5.	Thesis Aim.....	29
2.	Results	30
2.1.	Abstract.....	31
2.2.	Introduction	31
2.3.	Results	32
2.3.1.	Heme impairs bacterial clearance in vivo	32
2.3.2.	Independence of heme-iron acquisition	34
2.3.3.	Heme potently inhibits phagocytosis	36
2.3.4.	Heme disrupts actin cytoskeleton dynamics	38
2.3.5.	Heme activates Cdc42 via DOCK8.....	40
2.3.6.	Quinine restores phagocytosis in vitro and in vivo	45
2.4.	Discussion.....	47
2.5.	Online methods.....	49
2.6.	Supplementary figures	62
2.7.	Supplementary tables.....	71
2.8.	Publication references.....	72
3.	Discussion	79
4.	References	87
	<i>Curriculum vitae</i>	100

List of Figures

Thesis figures:

Figure 1 – The vertebrate immune system: main branches and components.....	2
Figure 2 – The mammalian toll like receptors.	4
Figure 3 – Mammalian pattern recognition receptors.	5
Figure 4 – Tissue-resident macrophages and associated functions.....	7
Figure 5 – Classical effector mechanisms of neutrophils.....	8
Figure 6 – Phagocytosis of extraneous particles by mammalian professional phagocytes.....	9
Figure 7 – Macrophages and the control of iron homeostasis.....	12
Figure 8 – The cellular cytoskeleton: its components, characteristics and cellular functions.	13
Figure 9 – Actin polymerization dynamics.	14
Figure 10 – Actin cytoskeletal structures.	15
Figure 11 – Mechanisms of Rho GTPase activation, deactivation and sequestering.....	16
Figure 12 – Cdc42 and Rac1 pathways.	17
Figure 13 – Dock atypical GEF family.	18
Figure 14 – Actin cytoskeleton regulation during chemotaxis and phagocytosis.....	20
Figure 15 – Mammalian heme types.	24
Figure 16 – Heme biosynthesis in mammals.....	25
Figure 17 – Heme degradation by heme oxygenase.....	28
Figure 18 – Working model	85

Published figures:

Figure 1 - Heme impairs bacterial clearance <i>in vivo</i>	33
Figure 2 - Increased bacterial burden triggered by heme is independent of heme-iron acquisition	35
Figure 3 - Heme potently inhibits phagocytosis of bacteria.....	37
Figure 4 - Heme induces cell shape changes via actin cytoskeleton remodeling.....	39
Figure 5 - Heme interferes with actin cytoskeleton-dependent functions.....	41
Figure 6 - Identification of the mechanism of heme-induced cytoskeletal interference.....	42
Figure 7 - DOCK8 mediates heme-induced actin cytoskeleton changes and suppression of phagocytosis.....	44
Figure 8 – Quinine restores phagocytosis of bacteria <i>in vitro</i> and <i>in vivo</i>	46

Published supplementary figures:

Supplementary figure 1 - Heme impairs bacterial clearance.....	62
Supplementary figure 2 - Heme inhibits bacterial phagocytosis and the intact heme molecule is required to mediate its effect.	64
Supplementary figure 3 - Heme induces cell shape changes due to effects on the actin cytoskeleton.....	65
Supplementary figure 4 - Heme impairs functions dependent on cytoskeleton rearrangement.	66
Supplementary figure 5 - Heme-induced cell spreading is independent of calcium influx signaling and ROS.....	67
Supplementary figure 6 - Heme further disrupts actin cytoskeleton organization through ARP2/3.....	68
Supplementary figure 7 - Heme interferes with actin cytoskeleton dynamics via DOCK8..	69
Supplementary figure 8 - Quinine restores host bacterial resistance.....	70

List of Tables

Published tables:

Supplementary table 1. Bacteria strains used and generated.....	71
Supplementary table 2. Plasmids used.	71
Supplementary table 3. Oligos used.	72

Abstract

Extensive intravascular hemolysis is a hallmark of sepsis, malaria infection and hemoglobinopathies, such as sickle cell disease or α and β thalassemias, and poses a serious threat to millions of patients worldwide. Erythrocyte destruction during hemolysis leads to the release of their intracellular contents into the circulation, and results in high plasma levels of hemoglobin and the subsequent release of its heme moiety. Excessive plasma heme levels can rapidly overwhelm the protective capacity of heme-scavenging plasma proteins, such as hemopexin, leaving heme free to interact with other plasma components, cell surface proteins and to cross plasma membranes at uncontrolled rates. Once released from hemoproteins, heme can damage cells and organs via the unfettered production of reactive oxygen species, and is one of the major driving factors for organ damage following hemolysis. Importantly, it has long been observed that hemolytic disorders, or hemolysis itself predispose to lethal bacterial infections. This is thought to be due to increased nutritional iron availability for bacteria, as heme is an iron-containing protoporphyrin IX ring, although clear evidence is lacking.

The work presented in this thesis derives from the main hypothesis that heme release is the culprit behind the increased susceptibility to infection following hemolysis, and that heme might negatively influence the immune response to bacteria beyond its potential as an iron source for pathogens.

This work now shows that excess heme levels in the circulation, as found following hemolysis, are sufficient to promote fulminant bacteremia and death in sepsis. Surprisingly, this effect is independent from heme-iron acquisition by bacteria as similar iron overload with free iron failed to replicate the effects of heme, and infection with bacteria unable to utilize heme as an iron source could still be enhanced by excess heme. Instead, heme potently inhibited phagocytosis of bacteria and cell migration, effectively suppressing the immune response to bacteria and creating a favorable environment for bacterial growth. This effect is mediated via the disruption of actin cytoskeletal dynamics through the association of heme with DOCK8 and the hyperactivation of its downstream targets Cdc42 and mDIA2, leading to dramatic changes in cell shape and the inability to adequately respond to bacteria.

Furthermore, as a secondary goal, this work now shows that quinine is able to completely prevent the deleterious effects of heme on phagocytosis, and is able to restore the anti-bacterial response of phagocytic cells both *in vitro* and *in vivo*. This proof-of-concept approach highlights the potential of immunoadjuvant therapies to circumvent failing conventional therapies (e.g. antibiotics).

Kurzfassung

Extensive intravaskuläre Hämolyse kennzeichnet das Krankheitsbild Sepsis, Malariainfektion und Hämoglobin-Erkrankungen wie Sichelzellanämie oder α und β Thalassämie, und wird so zur ernststen Gefahr für Millionen von Patienten weltweit. Zerstörung von Erythrozyten im Zuge der Hämolyse führt zur Freisetzung deren intrazellulärer Inhalte in die Blutbahn und zu einem erhöhten Blutplasma-Hämoglobinspiegel, mit anschließender Freisetzung der Häm-Einheit. Ein Überschuss an Hämoglobin im Blutplasma kann rasch die schützenden Aufnahmekapazitäten von Häm-bindenden Plasmaproteinen wie Hemopexin übersteigen, wodurch freies Häm mit anderen Plasmakomponenten und Zelloberflächenproteinen interagieren oder unkontrolliert Plasmamembranen überqueren kann. Einmal aus Hämoproteinen freigesetzt, kann Häm Zellen und Organe durch unbeschränkte Produktion von reaktiven Sauerstoffradikalen schädigen, und ist dadurch ein Hauptfaktor für Organschäden nach Hämolyse. Schon seit Langem wurde beobachtet, dass hämolytische Erkrankungen oder Hämolyse selbst Patienten für tödliche bakterielle Infektionen anfällig machen. Da Häm ein eisenhaltiger Protoporphyrin IX-Ring ist, wurde dies auf erhöhte Eisenverfügbarkeit für den bakteriellen Stoffwechsel zurückgeführt, obwohl dafür klare Beweise fehlen.

Die vorgestellte Arbeit leitet sich von der Hypothese ab, dass Hämfreisetzung für die erhöhte Infektanfälligkeit nach Hämolyse verantwortlich ist, wobei Häm die Immunantwort gegen Bakterien über seine potentielle Rolle als Eisenquelle hinaus negativ beeinflusst.

Die vorliegende Arbeit zeigt, dass ein überhöhter Häm Spiegel in der Blutbahn, wie er nach Hämolyse vorkommt, hinreichend ist um fulminante Bakteriämie und Tod durch Sepsis zu fördern. Überraschenderweise ist dieser Effekt unabhängig von der Aufnahme von Hämeisen durch Bakterien, da ein ähnlicher Überschuss an freiem Eisen die Effekte von Häm nicht replizierte. Des Weiteren wurde selbst eine Infektion mit Bakterien, die Häm nicht als Eisenquelle nutzen können, durch Überschuss von Häm gesteigert. Stattdessen stellte sich Häm als ein potenter Hemmer der Phagozytose und Zellmigration heraus, wodurch die Immunantwort gegen Bakterien wirksam unterdrückt wird und ein günstiges Umfeld für Bakterienwachstum entstehen kann. Dieser Effekt wird durch Störung der Dynamik des Aktin-Zytoskeletts herbeigeführt, indem Häm mit DOCK8 assoziiert und die Hyperaktivierung von nachgeschalteten Zielproteinen, Cdc42 und mDIA2, hervorruft, was zu dramatischen Veränderungen in Zellform und der Unfähigkeit adäquat auf Bakterien zu reagieren führt.

Als sekundäres Ziel zeigt die vorliegende Arbeit weiterhin, dass Chinin die schädlichen Effekte von Häm auf Phagozytose vollständig unterbinden kann, und die antibakterielle Antwort von

phagozytischen Zellen *in vivo* und *in vitro* wiederherstellen kann. Dieser konzeptionelle Beweis hebt das Potential von immunoadjuvanten Therapieansätzen zur Umgehung von fehlschlagenden konventionellen Therapien (z.B. Antibiotika) hervor.

Publications arising from this thesis

Heme drives hemolysis-induced susceptibility to infection via disruption of phagocyte functions.

Rui Martins, Julia Maier, Kilian V. M. Huber, Anna-Dorothea Gorki, Omar Sharif, Riem Gawish, Karin Lakovits, Michael Aichinger, Charles-Hugues Lardeau, Markus Brown, Kari Vaahntomeri, Michelle Duggan, Donscho Kerjaschki, Harald Esterbauer, Jacques Colinge, Thomas Decker, Keiryn L. Bennett, Stefan Kubicek, Michael Sixt, Giulio Superti-Furga, and Sylvia Knapp

Nature Immunology, published online: 31 October 2016, DOI: [10.1038/ni.3590](https://doi.org/10.1038/ni.3590), print: 17 December 2016 (Vol 12:p1361-1372)

This publication was highlighted in a “news and views” article by Tan & Weninger (2016) in *Nature Immunology*.

Abbreviations

A1M	Alpha-1-microglobulin
ActA	Actin nucleator
ADF	Actin-depolymerizing Factor
ADP	Adenosine diphosphate-
ALAS1	Aminolevulinate Synthase 1
ALAS2	Aminolevulinate Synthase 2
Arp2/3	Actin-related protein 2/3 complex
ATP	Adenosine triphosphate-
BLVR	Biliverdin reductase A
CCL19	C-C motif chemokine ligand 19
CCR2	C-C motif chemokine receptor 2
CCR7	C-C motif chemokine receptor 7
Cdc42	Cell division cycle 42
CO	Carbon monoxide
CPOX	Coproporphyrinogen III oxidase
DFO	Deferoxamine
DHR-1	Dock homology region 1
DHR-2	Dock homology region 2
Diaph3	Diaphanous homolog 3 (generally referred to as mDia2)
DOCK	Dedicator of cytokinesis
DppABCDF	Dipeptide permease
<i>E. coli</i>	<i>Escherichia coli</i>
ECM	Extracellular matrix
eIF2α	Eukaryotic translation initiation factor 2-alpha kinase 1
ENA/VASP	Enabled homolog/vasodilator-stimulated phosphoprotein
F-Actin	Filamentous actin
FECH	Ferrochelatase
FPN	Ferroportin
G6PD	Glucose-6-phosphate dehydrogenase
G-Actin	Monomeric, globular;
GAPs	GTPase activating proteins
GDI s	Guanosine nucleotide dissociation inhibitors
GDP	Guanosine diphosphate

GEFs	Guanine nucleotide exchange factors
GTP	Guanosine triphosphate
HAMP	Hepcidin
Hb	hemoglobin
HMBS	Hydroxymethylbilane synthase
HO-1	Heme oxygenase I
HP	Haptoglobin
HPX	Hemopexin
IFN	Interferon
IgG	Immunoglobulin G
IgM	Immunoglobulin M
IL-10	Interleukin 10
iNOS	Nitric oxide synthase
IRSp53	Insulin receptor substrate p53
<i>L. monocytogenes</i> ..	<i>Listeria monocytogenes</i>
LDL	Low-density lipoprotein
LIMK	LIM domain kinases
LLO	Listeriolysin O
LPS	Lipopolysaccharide
LRP1	Low density lipoprotein receptor-related protein 1 (also known as CD91)
LTA	Lipoteichoic acid
MAPKs	Mitogen-activated protein kinases
MBP	Mannose-binding protein
MCP1	Monocyte chemotactic protein 1 (coded by Ccl2)
mDia2	Diaphanous homolog 3, also known as Diaph3
NADPH	Nicotinamide adenine dinucleotide phosphate-
NETs	Neutrophil extracellular traps
NF-κB	Nuclear factor kappa-light-chain-enhancer of activated B cells
NLR	NOD-like receptor
NR1D1	Nuclear receptor subfamily 1 group D member 1 (known as Rev-ErbA α)
OxLDL	Oxidized low-density lipoprotein
PAK	P21-activated kinases
PAMPs	Pathogen-associated molecular patterns
PBGS	Delta-aminolevulinic acid dehydratase

PH	Pleckstrin homology
PI3K	Phosphoinositide 3-kinase
PMN	Polymorphonuclear leukocytes
PPIX	Protoporphyrin IX
PPOX	Protoporphyrinogen IX oxidase
PRRs	Pattern-recognition receptors
Rac1	Ras-related C3 botulinum toxin substrate 1
Rho	Ras homology
RhoA	Ras homolog family member A
RIG-I	Retinoic acid-inducible gene-1
RLRs	Retinoic acid-inducible gene-1-like family of receptors
RNS	Reactive nitrogen species
ROCK	Rho-associated protein kinase
ROS	Reactive oxygen species
<i>S. pneumoniae</i>	<i>Streptococcus pneumoniae</i>
SCAR/WAVE	SCAR/WASP-family verprolin homologous protein 1
SCD	Sickle cell disease
SH3	SRC homology 3
T3SS	Type III secretion systems
TCR	T cell receptors
TF	Tissue factor
TGF- β	Transforming growth factor β
TLR4	Toll-like receptor 4
TLRs	Toll-like receptors
TNF	Tumor necrosis factor
UROD	Uroporphyrinogen decarboxylase
UROS	Uroporphyrinogen III synthase
WASP	Wiskott–Aldrich syndrome protein

Acknowledgements

I would like to express my gratitude to many people who supported me and generously contributed to the work presented in this thesis.

First and foremost, I would like to thank my supervisor, Sylvia Knapp for the wonderful opportunity to work in her lab, and for the excellent guidance and support, both scientific as well as personal. I am very thankful for the exceptional, and professional mentoring, as well as for having had the freedom to explore new scientific grounds, and the fantastic incentive to be a participative member of the scientific community. It was a tremendously motivating and inspiring, as well as humbling experience which has allowed me to achieve and master many professional and personal milestones.

Profound gratitude goes to all my colleagues in the lab for their readiness to help, even if it meant “waking up with the chickens”, or “burning the midnight oil”. I am also very thankful for the fun, friendly, and fiercely intelligent environment that they created every day in the lab. I want to thank Steffi, Riem and Omar especially for their support and valuable discussions, and Karin, Anastasiya, Bianca and Ana for their kindness and outstanding technical support. I would like to thank Julia Maier in particular for her help and friendship beyond working hours and the joyful whistling and singing that brought color to the orange halls of the AKH. Further, I am very thankful to Thea, Philipp, Simona, Federica and Nina for their all-round support and friendship.

I am also hugely appreciative of all the contributions by everyone involved in publishing the work in this thesis. I am very fortunate to have had your support and it was a pleasure to work with you.

I would like to thank my family and friends for their love, support, fun times and the fact that they bring absolute joy to my life. In particular, I want to thank Ricardo and Dani for their friendship and companionship, the *Ponche* troupe for years of friendship and countless hilarious moments, and my mother and brother for their unconditional love and support.

Last, but certainly not least, I want to thank my partner Katharina for the love, kindness and support you always give me, and our daughter Amelie for being a wonderful beacon of hope, which guides my every thought.

1. Introduction

The work presented in this thesis relates to several topics in the fields of immunology, host-pathogen interaction, microbiology and basic cell biology. These are outlined below and provide an overview of the innate immune system, with special emphasis on the basic mechanisms and functions of phagocytosis and leukocyte migration and how the actin cytoskeleton of phagocytic cells is regulated in these processes. Further, the basic biology behind the interplay between host immunity and invading bacteria is summarized, as well as the causes and implications of hemolysis in the context of hemolytic disorders. Together, the following chapter should provide the background information necessary to understand the scope of this thesis.

1.1. The innate immune system

1.1.1. *Functions, general concepts and context within the immune system*

The immune system of vertebrates has evolved in order to defend and protect against invading microbes (Malagoli, 2016). It is divided in two specialized and distinct branches: the innate (natural) immunity and adaptive (acquired) immunity (Figure 1). Innate immunity represents the first line of defense against pathogens and exerts its defensive functions through the recognition of evolutionarily conserved structures on microbes, mounting of inflammatory responses, followed by pathogen elimination and subsequent resolution of inflammation (Delves & Roitt, 2000a, Delves & Roitt, 2000b). Adaptive immunity is an evolutionarily younger branch of immunity and works synergistically with the innate immune system in order to eliminate pathogens via the generation of highly specific responses tailored against the invading pathogen, and the development of immunological memory, ultimately improving the efficacy of the immune system against repeated exposure to a given pathogen (Delves & Roitt, 2000a, Delves & Roitt, 2000b). In addition, both branches of the immune system rely on cellular and humoral (molecular) components (Figure 1).

The cellular components of the innate immune system comprise primarily phagocytic cells such as monocytes, macrophages and neutrophils, but also mast cells, eosinophils, basophils and natural killer cells and their activity is geared towards the initiation, coordination and resolution of inflammatory processes in response to external challenges (Figure 1) (Medzhitov & Janeway, 2000). Moreover, the innate immune system is involved in crucial processes beyond the popular

notion of immunity, such as surveillance and maintenance of tissue homeostasis, as illustrated by the role of macrophages in iron recycling, storage and homeostasis (Ganz, 2012).

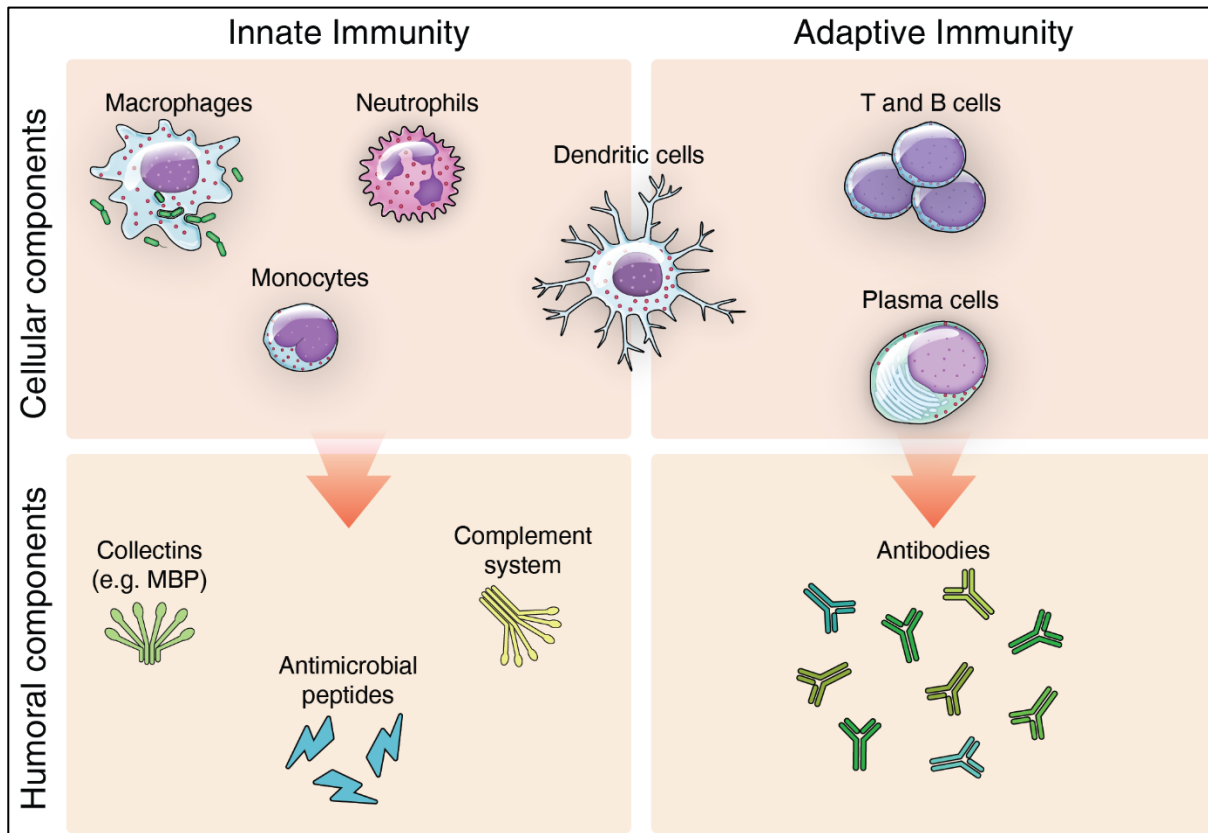


Figure 1 – The vertebrate immune system: main branches and components.

Innate immune cells, as well as other cell types, such as epithelial cells, hepatocytes or endothelial cells are able to produce and respond to a wide array of molecules which further mediate and exert innate immune functions (Medzhitov & Janeway, 2000, O'Neill, Golenbock et al., 2013, Vilcek & Feldmann, 2004). These molecules constitute the humoral (molecular) components of the innate immune system and comprise, antimicrobial peptides, the complement system, collectins such as Mannose-binding protein (MBP), leukotrienes, etc. (Delves & Roitt, 2000a, Delves & Roitt, 2000b, Medzhitov & Janeway, 2000).

The cellular components of the adaptive immune system, on the other hand, comprise mainly lymphocytes, such as T cells, which rely on the interaction with antigen presenting cells, like dendritic cells, in order to expand, mature and become highly specific effector cells, and B cells which are able to take up foreign particles, such as microbes, to mature into plasma cells for the production of highly specific antibodies (Alberts, 2002). The antibodies generated and produced by B cells constitute the molecular component of the adaptive immune system and their action spans from the direct inactivation of pathogens to flagging pathogens for elimination by Fc receptor competent phagocytic cells (Alberts, 2002).

The specificity of the response generated by the adaptive immune system is only possible due to V(D)J recombination and somatic hypermutation (Janeway, 2001). These mechanisms enable the generation of an extremely diverse repertoire of T cell receptors (TCR) and antibodies, on T and B cells, respectively. These cells then undergo clonal selection in order to avoid auto-reactivity and to enhance antigen recognition (Alberts, 2002). Ultimately, the development and selection of clones which react specifically against a given pathogen, constitutes another layer of protection and importantly allow the generation of immunological memory, translating into a greatly improved immunity against re-infection with the same pathogen (Delves & Roitt, 2000a, Delves & Roitt, 2000b).

1.1.2. Regulation of innate immunity

The innate immune system continuously surveys the different tissues, organs and mucosal interfaces and is able to sense and recognize a wide variety of threats, from pathogens to tissue damage or malfunction. In order to do this, innate immune cells need to be able to discriminate between self and a diversity of pathogens or foreign particles, as well as to distinguish normal from damaged or altered cellular states. To this end, innate immune cells rely on a finite number of pattern-recognition receptors (PRRs) (Takeuchi & Akira, 2010). In contrast to TCR and antibodies, which undergo somatic recombination, PRRs are exclusively germline-encoded, and recognize specific microbial components termed pathogen-associated molecular patterns (PAMPs) (Takeuchi & Akira, 2010). These are essential microbial components and as such are highly conserved and less likely to change in order to avoid PRR detection (Kumar, Kawai et al., 2011). As “nonclonal” germline-encoded receptors independent of immunological memory, PRRs confer the immune system an innate mechanism to sense pathogens (Delves & Roitt, 2000a, Delves & Roitt, 2000b). Three major classes of PRRs have evolved to recognize different PAMPs, both by sampling the extracellular milieu, but also by monitoring intracellular microbial presence. Of these classes, Toll-like receptors (TLRs) are the most widely studied PRRs with 10 and 12 different members identified so far in humans and mice, respectively (Figure 2) (Beutler, 2009). TLRs are membrane glycoproteins with extracellular domains responsible for the recognition of PAMPs and cytoplasmic signaling domains to relay the signal upon receptor ligation. TLRs can recognize bacterial, fungal, viral and parasite components, as well as some endogenous markers of damage (Damage-associated molecular patterns; DAMPs) directly on the cell surface or within endosomes (Beutler, 2009, Kumar et al., 2011). For the recognition of intracellular pathogens, immune cells rely on another class of PRRs belonging to the NOD-like receptor (NLR) family (Chen, Shaw et al., 2009). NLRs represent a more diverse family of PRRs and although their expression is not exclusive to innate immune cells,

they represent a crucial component of innate immunity involved in sensing intracellular PAMPs and DAMPs (Chen et al., 2009, Takeuchi & Akira, 2010). Additionally, the retinoic acid-inducible gene-1 (RIG-I)-like family of receptors (RLRs) is involved in intracellular sensing of viral infections (Reikine, Nguyen et al., 2014, Takeuchi & Akira, 2010).

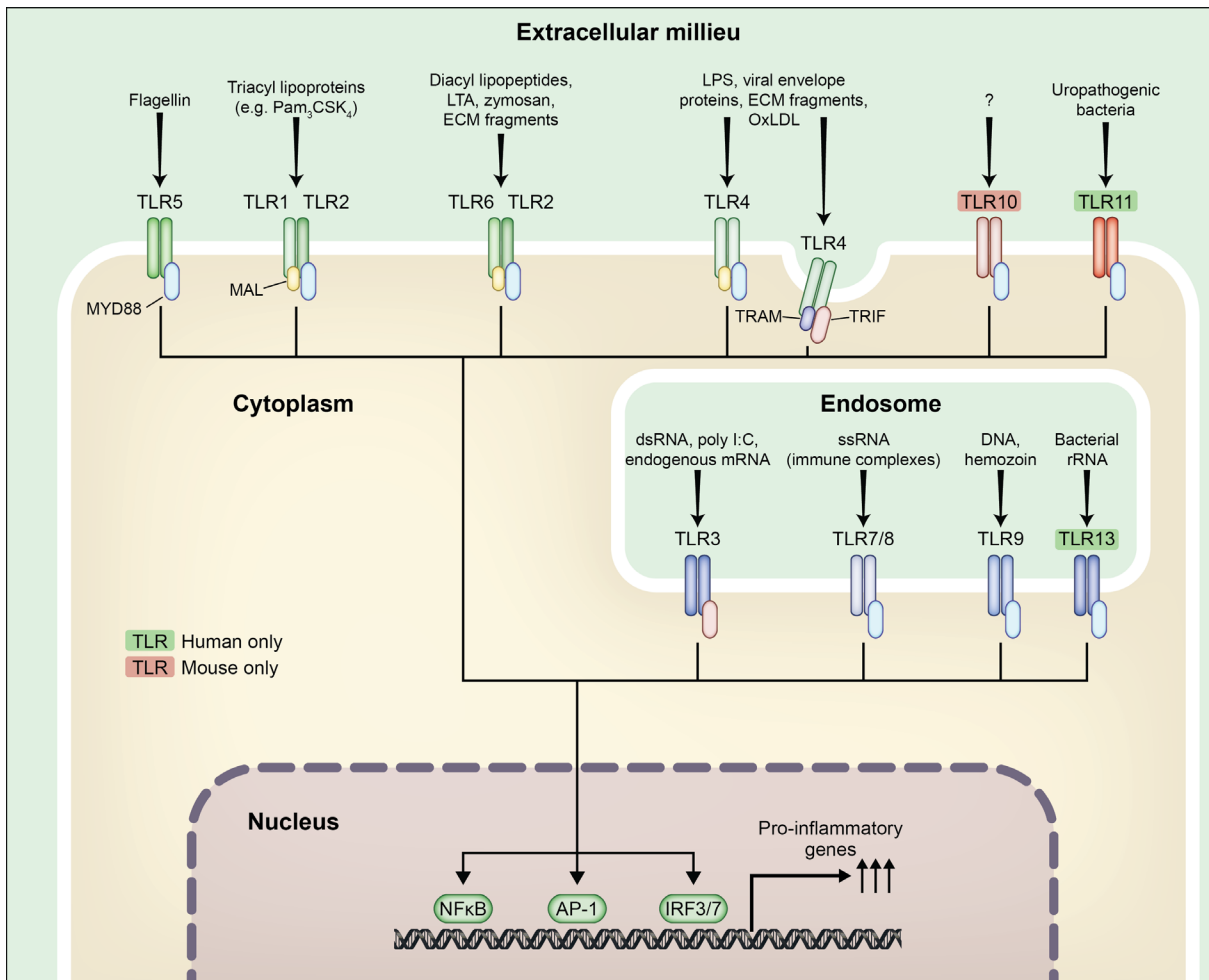


Figure 2 – The mammalian toll like receptors. Legend: LTA = lipoteichoic acid; ECM = extracellular matrix; LPS = lipopolysaccharide; OxLDL= oxidized low-density lipoprotein. Adapted from O'Neill et al. (2013).

The common denominator between the different classes of PRRs is that upon PAMP or DAMP recognition, PRRs activate signaling cascades triggering an inflammatory response in order to deal with the invading pathogen (Takeuchi & Akira, 2010). Nevertheless, not all PRRs activate the same pathways, or have the same end targets since PRR signaling is dependent on both the PRR class and the triggering PAMP or DAMP (Baccala, Gonzalez-Quintal et al., 2009, O'Neill et al., 2013, Takeuchi & Akira, 2010). However, the vast majority of PRR activation targets are part of the nuclear factor kappa-light-chain-enhancer of activated B cells (NF-κB), mitogen-activated protein kinases (MAPKs), interferon (IFN) or caspase-1 pathways (Figure 3) (Baccala et al., 2009). Activation of inflammatory pathways results in the expression of genes involved in host defense against microbial pathogens (Ashley, Weil et al., 2012, Takeuchi & Akira,

2010). This includes the production of anti-microbial peptides, cytokines and chemokines to activate and recruit immune effector cells, as well as cell adhesion molecules to facilitate leucocyte trafficking (Ashley et al., 2012, Chovatiya & Medzhitov, 2014, Kotas & Medzhitov, 2015). Moreover, several PRRs are involved in the recognition of DAMPs, conferring innate immune cells the capacity to detect endogenous damage and states of altered-self (Takeuchi & Akira, 2010) and elicit the appropriate immune response. This represents yet another crucial protective function of the innate immune system in the maintenance of tissue homeostasis. The appropriate inflammatory response against an invading pathogen is of extreme importance since an insufficient response might allow uncontrolled pathogen proliferation, whereas an excessive response can lead to extensive tissue damage, both of which can be life-threatening for the host (Medzhitov, Schneider et al., 2012).

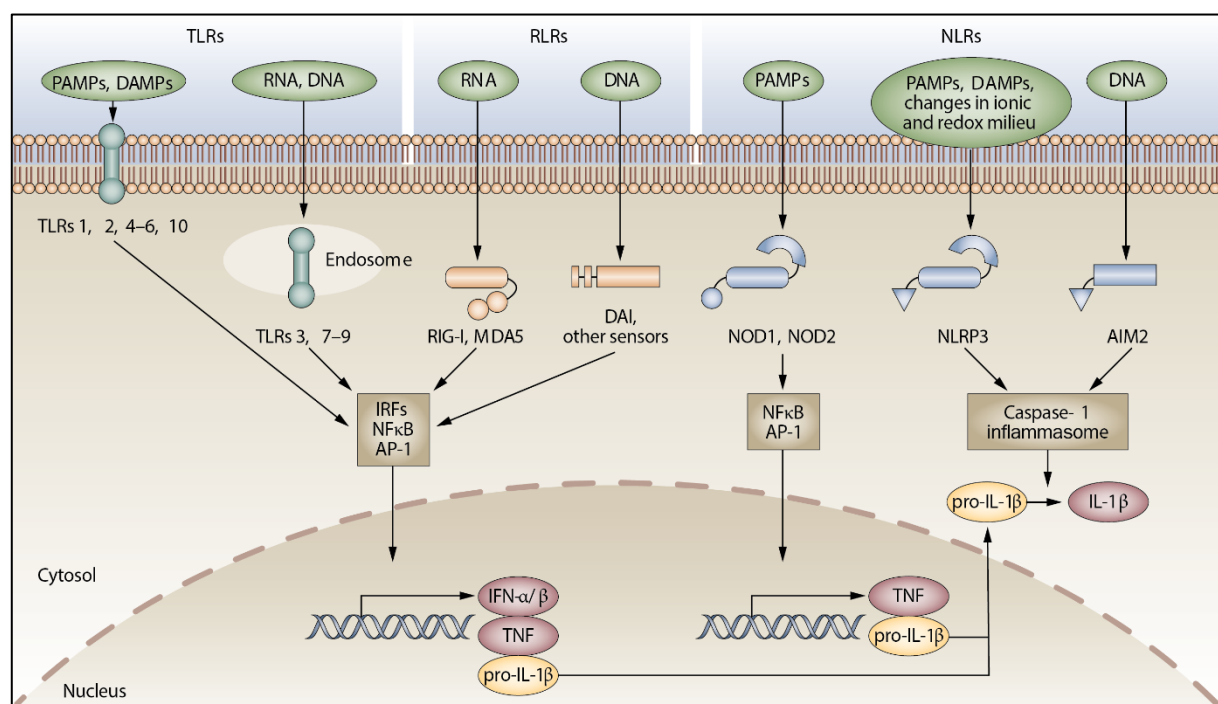


Figure 3 – Mammalian pattern recognition receptors. Taken from Baccala et al. (2009).

In order to restore tissue homeostasis and function following threat neutralization, the accompanying inflammatory reaction needs to be restrained, while at the same time, tissue repair and maintenance mechanisms are activated (Ortega-Gomez, Perretti et al., 2013). Under ideal circumstances, these coordinated and highly regulated processes lead to the resolution of inflammation and return to normal tissue function. The first step towards resolving the inflammatory response is dependent on the abrogation of inflammatory cell migration (e.g. neutrophils). This is achieved through the depletion of chemotactic signals, either by chemokine sequestration or via proteolytic cleavage of circulating chemokines (Soehnlein & Lindbom, 2010). To further attenuate the inflammatory response, activated neutrophils undergo apoptosis

either through intrinsic mechanisms, such as triggered by reactive oxygen species (ROS) generation, or through the action of pro-apoptotic signals, such as tumor necrosis factor (TNF) secreted mainly by macrophages (Akgul & Edwards, 2003, Haslett, Savill et al., 1994, Savill, Wyllie et al., 1989). Apoptotic neutrophils and other cellular debris resulting from tissue damage are then cleared via a phagocytic mechanism termed efferocytosis. This can be promoted via the production or exposure of *find me* and *eat me* signals, ultimately leading to macrophage scavenging of dead cells (Ortega-Gomez et al., 2013). The uptake of dying neutrophils by macrophages further stimulates the production of anti-inflammatory cytokines, such as interleukin 10 (IL-10) or transforming growth factor β (TGF- β) (Voll, Herrmann et al., 1997). Finally, alternatively activated macrophages are pivotal in restoring tissue homeostasis by orchestrating healing through the secretion of growth factors and other anti-inflammatory molecules (Lucas, Waisman et al., 2010, Saclier, Yacoub-Youssef et al., 2013). This process is tissue-dependent and involves extracellular matrix remodeling as well as crosstalk with stem, progenitor and stromal cells (Ortega-Gomez et al., 2013). Ultimately, the concerted effort of innate immunity should ideally result in the recognition and elimination of the threat (e.g. infection, tissue damage), followed by tissue healing and return to homeostasis.

1.1.3. Key cells of the innate immune system

Macrophages

Macrophages are phenotypically diverse tissue-resident innate immune cells, which are involved in a myriad of functions, from homeostatic mechanisms to the initiation of acute inflammatory responses, among others (Figure 4) (Lavin, Mortha et al., 2015). During fetal development, macrophages originate from embryonic hematopoietic progenitors in the yolk sac, prior to the establishment of definitive hematopoiesis, whereas in adult life, macrophages originate from bone marrow-derived precursors, as well as from monocytes under inflammatory conditions (Ginhoux & Jung, 2014, Perdiguero & Geissmann, 2016). Macrophages were initially recognized as central cells of the mononuclear phagocyte system due to their avid phagocytic capacity, granting macrophages the ability to take up a wide variety of particles, such as bacteria, cellular debris, senescent erythrocytes, etc. (Perdiguero & Geissmann, 2016). As such, macrophages play an extremely important role in the initial recognition and elimination of pathogens, but also in clearing up dead or apoptotic cells from damaged tissues. Aside from uptake-dependent functions, all macrophages are able to actively monitor and sense a wide range of exogenous and endogenous molecules due to the expression of many PRRs (Glass & Natoli, 2016). Upon sensing DAMPs and/or PAMPs, macrophages play a pivotal role

in orchestrating the immune response by secreting cytokines and chemokines which recruit other innate effector cells such as neutrophils. Macrophages are present in virtually all tissues, and although they share many functional features among themselves, they specifically adapt to the tissue where they reside by reading tissue factors and environmental cues. These induce tissue-specific transcriptional profiles and functions, making macrophages extremely plastic and versatile cells (Figure 4) (e.g. Kupffer cells in the liver or red pulp macrophages in the spleen) (Ginhoux, Schultze et al., 2016). This is illustrated by their roles in tasks as diverse as muscle regeneration, where macrophage-derived signals control myogenic precursor cell fate (Sacrier et al., 2013), erythropoiesis, where nurse macrophages provide transferrin-bound iron for hemoglobin production (Korolnek & Hamza, 2015), or on blood-borne antigen capture by splenic marginal zone macrophages (A-Gonzalez, Guillen et al., 2013). Furthermore, macrophages are crucial for maintaining iron homeostasis, and are able to take up (mainly through phagocytosis of senescent erythrocytes), recycle, and redistribute iron (through transferrin-bound iron secretion) for further use (Soares & Hamza, 2016).

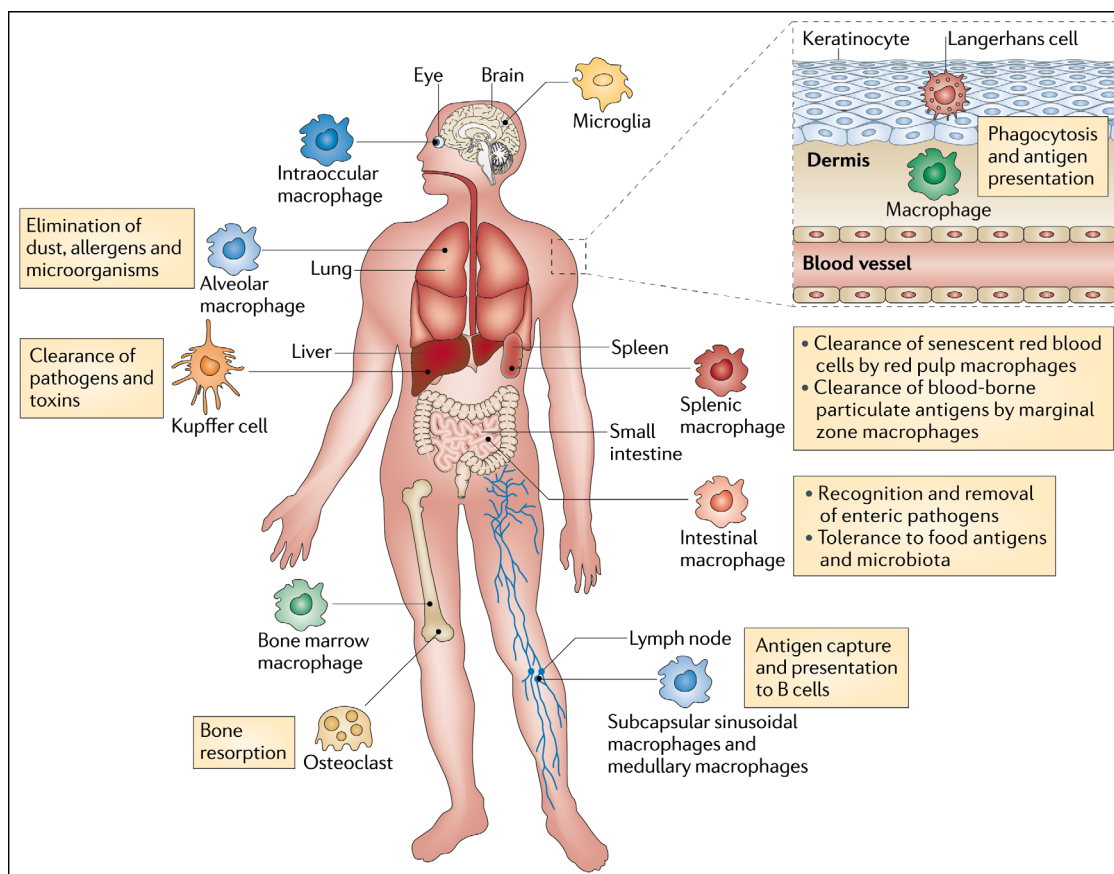


Figure 4 – Tissue-resident macrophages and associated functions. Taken from Murray & Wynn (2011).

Neutrophils

Neutrophils are the most abundant polymorphonuclear leukocytes (PMN) of myeloid origin, best known as short-lived innate effector cells in acute inflammation. Neutrophils are generally

thought of as innate immune “infantry”, which upon activation leave the circulation and swarm the site of infection to eliminate the pathogen (Mocsai, 2013). Their importance for pathogen elimination is pivotal, as reduced number of circulating neutrophils results in severe immunodeficiency (Sokolic, 2013). In order to eliminate pathogens, neutrophils need to sense chemotactic gradients originating from cells in the infected tissue (e.g. tissue-macrophages). This induces the rolling and adhesion of neutrophils to the endothelium, and ultimately, their extravasation into the site of infection (Figure 5). Once there, neutrophils are able to ingest antibody- or opsonin-coated pathogens primarily via Fc or complement receptors for intracellular ROS-mediated killing (Lee, Harrison et al., 2003). Furthermore, neutrophils rely on two other distinct methods to directly kill pathogens: first, through degranulation and release of ROS, lytic enzymes and antimicrobial peptides, and second, via the release neutrophil extracellular traps (NETs) composed of nuclear DNA, to which various proteins adhere (Figure 5) (Brinkmann, Reichard et al., 2004, Kolaczkowska & Kubes, 2013).

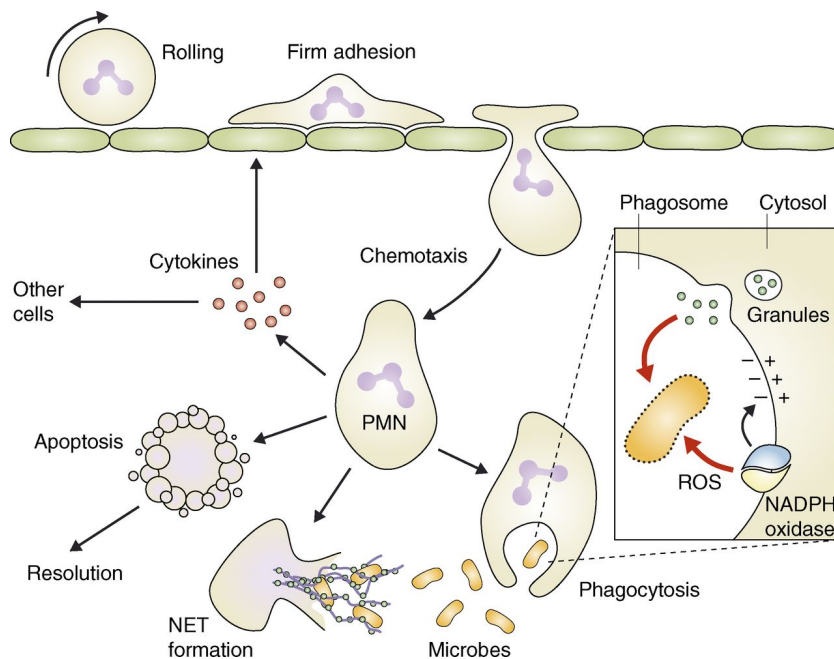


Figure 5 – Classical mechanisms of neutrophil recruitment, pathogen elimination and resolution of inflammation. Taken from Mocsai (2013).

These mechanisms render neutrophils highly inflammatory cells, and dysregulated activation can lead to extensive tissue damage and reduced disease tolerance (Kruger, Saffarzadeh et al., 2015). However, the roles of neutrophils in the course of infection are not limited to pathogen clearance. In fact, neutrophils are also essential to initiate the resolution of inflammation: as neutrophils undergo apoptosis following pathogen elimination, they are cleared by macrophages and provide signals that rewire macrophage activity towards anti-inflammatory and tissue-regenerative phenotypes (Figure 5) (Soehnlein & Lindbom, 2010).

1.1.4. *Key mechanisms of resistance to infection*

Phagocytosis

Phagocytosis of pathogens is a major innate resistance mechanism first identified by Ilya Mechnikov in 1883, via which professional phagocytes (e.g. macrophages, monocytes and neutrophils) are able to ingest microbes. As such, phagocytosis allows the removal of microbes from the circulation and their subsequent killing within the mature phagolysosome (Underhill & Ozinsky, 2002). Microbe uptake relies on microbe-phagocyte contact and recognition, and can be elicited through diverse pathways (Figure 6).

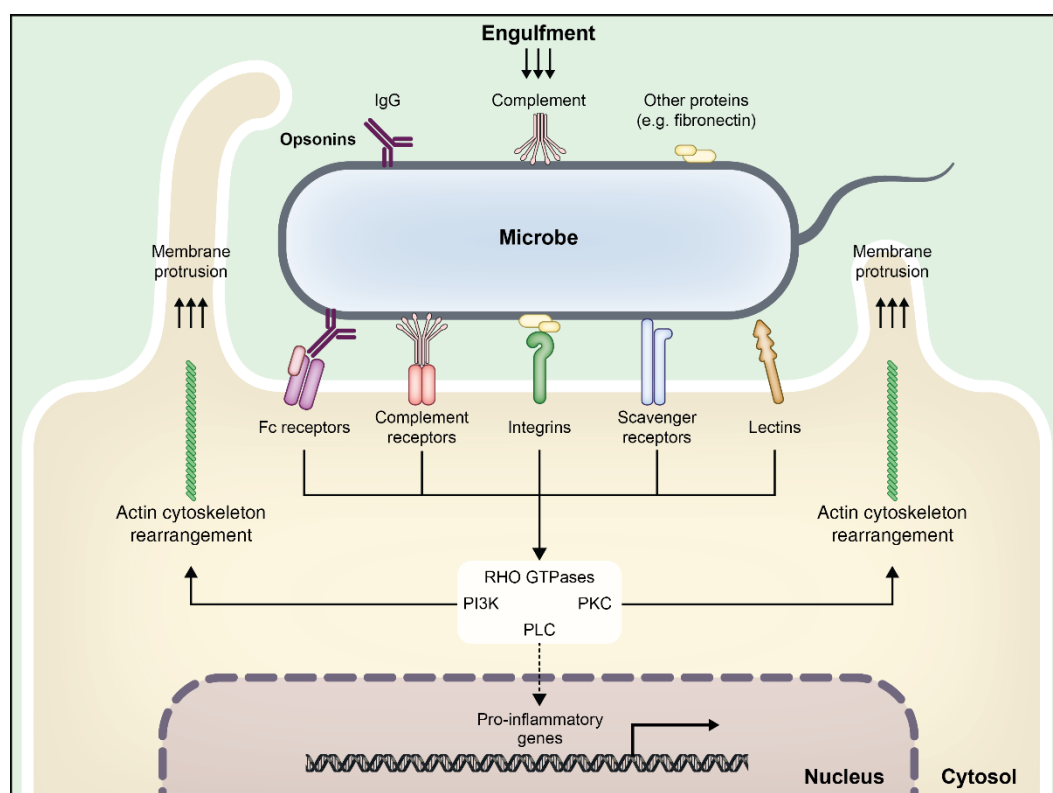


Figure 6 – Phagocytosis of extraneous particles by mammalian professional phagocytes – opsonization and direct recognition by specialized receptors. Adapted from Underhill & Ozinsky (2002).

Specifically, phagocytosis of pathogens can be triggered by the deposition of opsonins on the microbe surface such as immunoglobulin G (IgG) antibodies and complement proteins, or through direct recognition of microbial structures by scavenger receptors. Opsonized microbes are recognized by Fc receptors (for IgG), complement receptors (for complement opsonins) or integrins (for fibronectin/vitronectin), whereas opsonin-independent phagocytosis relies on various receptors, such as scavenger receptors, lectins and TLRs, which directly recognize specific microbial structures as “eat me” signals (Figure 6). Phagocytic receptor ligation triggers the activation of specific pathways inducing the rearrangement of the actin

cytoskeleton, membrane protrusion and the formation of either a phagocytic cup around the particle, or the “sinking” of the particle into the phagocyte.

Furthermore, the internalization of pathogens is a key mechanism in mounting adaptive immune responses, since it allows antigen presenting cells, such as dendritic cells and macrophages, to take up and digest microbes. The digested peptides are then presented as antigens to naïve T-cells, stimulating their activation and triggering a cascade of events ultimately leading up to the production of antigen-specific responses (cytotoxic T-cells, memory T- and B-cells, and antibodies).

Intracellular killing

In order to eliminate pathogens following internalization, professional phagocytes use various mechanisms aimed at destroying pathogen structures, ultimately killing the phagocytosed microbe (Flannagan, Cosio et al., 2009). Because the engulfed particle is trapped within the phagosome in the presence of innocuous extracellular fluid, the phagosome contents need to be rapidly change in order to kill the pathogen. This change occurs via the fusion of the phagosome with either early endosomes, late endosomes, or lysosomes originating from the endocytic pathway leading to its “maturation” (Desjardins, Huber et al., 1994). During this process, the phagosome undergoes several changes, becoming highly acidic, oxidative and proteolytic (Flannagan et al., 2009), leading up to the mature phagolysosome and peak microbicidal activity. Pathogen killing in the phagolysosome is then achieved via several mechanisms, such as lumen acidification via H^+ pumping by the V-ATPase, production of ROS and reactive nitrogen species (RNS) by nicotinamide adenine dinucleotide phosphate- (NADPH) oxidase and nitric oxide synthase (iNOS) respectively, and the production of antimicrobial peptides and proteins, such as cathelicidin, cathepsins, defensins, etc. (Flannagan et al., 2009, Flannagan, Jaumouille et al., 2012). The presence of these diverse microbicidal mechanisms induce direct damage to microbial membranes and structures, or interfere with vital microbial functions, ultimately resulting in death and degradation of the pathogen.

Inflammation

Inflammation is an evolutionarily conserved biological response to damage and danger signals, and as such is elicited upon tissue damage and recognition of invading pathogens by innate immune cells (Medzhitov, 2008). Its primary role is to promote leukocyte influx into the site of injury, induce the rapid production of anti-microbial effector molecules and initiate mechanisms to efficiently eliminate the source of injury (Ashley et al., 2012, Soehnlein & Lindbom, 2010). Following immune recognition of invading pathogens or tissue trauma by PRRs, specific

transcriptional programs are activated (see section 1.1.2 and Figure 2) leading to the secretion of pro-inflammatory mediators such as cytokines, leukotrienes, prostaglandins, histamine, etc. (Ashley et al., 2012). These help recruit, polarize and activate more leukocytes to the site of infection, and signal to the affected tissue to adopt exceptional measures to facilitate or support the inflammatory response. This is well illustrated by the changes the endothelium undergoes during inflammation in order to capture circulating leukocytes and promote their extravasation.

1.1.5. Iron homeostasis

Iron is a vital transition metal for nearly all forms of life, where it is involved in a wide range of biochemical functions and enzymatic reactions, most notably oxygen transport by hemoglobin, or energy generation by mitochondria (Wang & Pantopoulos, 2011). In mammals, iron is predominantly present as heme, coordinated within a protoporphyrin IX (PPIX) ring serving as a prosthetic group for many proteins, with the vast majority stored within hemoglobin in erythrocytes (Ganz, 2013). The intrinsic ability of iron to exchange electrons with various molecules makes it an extremely useful and versatile tool for various redox reactions, metabolic activity and respiration (Andrews & Schmidt, 2007). However, these very same vital properties of iron, and in particular, its ability to react with oxygen-containing molecules to generate ROS, make iron and heme exceptionally reactive and damaging if unrestrained (Wang & Pantopoulos, 2011). As such, iron levels must be tightly regulated in order to prevent tissue damage. In mammals, iron is predominantly stored in hepatocytes, Kupffer cells and red pulp macrophages in the spleen (Ganz, 2013), and its homeostasis is regulated at the organismal level by hepcidin (HAMP), a peptide hormone that inhibits the activity of the iron exporter ferroportin (FPN), in a manner akin to endocrine systems (Andrews & Schmidt, 2007) (Figure 7). The regulation of iron homeostasis is further critically dependent on tissue-resident macrophages, particularly, Kupffer cells, red pulp and bone marrow macrophages, which not only store, but also recycle and redistribute iron to other tissues (Soares & Hamza, 2016). Iron is efficiently recycled primarily in the spleen, and to a lesser extent in the liver, via the phagocytosis of senescent erythrocytes by red pulp macrophages (Soares & Hamza, 2016) (Figure 7). Upon phagocytosis and digestion of senescent erythrocytes, heme is taken up from the phagolysosomes and degraded by heme oxygenase I (HO-1), releasing iron from the protoporphyrin ring which is then either stored intracellularly in ferritin, or released to form iron-transferrin complexes in the plasma (Soares & Hamza, 2016).

The role of macrophages in iron homeostasis is not limited to its regulation under healthy conditions, but is also central for iron withholding upon infection in an effort to limit nutritional

iron availability to invading pathogens (Ganz & Nemeth, 2015). This strategy is aimed at restraining pathogen growth via hepcidin release and inhibition of iron export in a process termed nutritional immunity (Ganz & Nemeth, 2015) (Figure 7).

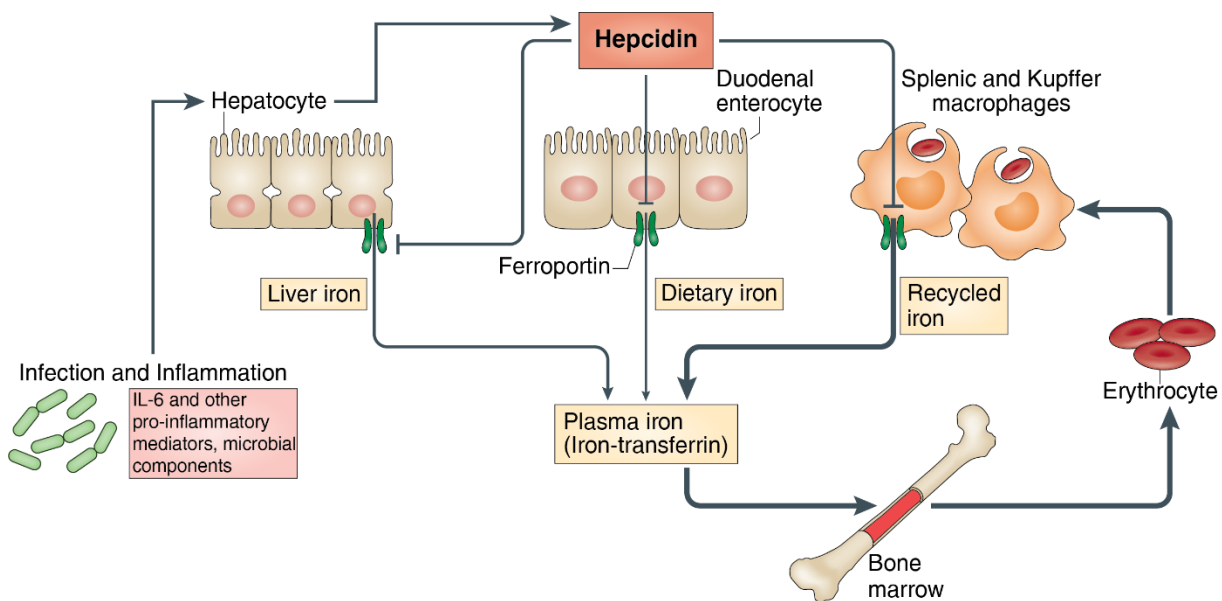


Figure 7 – Macrophages and the control of iron homeostasis. Modified from Ganz & Nemeth (2015).

1.2. The actin cytoskeleton

1.2.1. *Functions and general concepts*

Eukaryotic cells represent the basic biological unit of both unicellular and multicellular eukaryotes. All cellular components are enclosed within a lipid bilayer membrane (plasma membrane) which defines the boundary to the outside environment. However, the plasma membrane affords little to no structural support to cells. Instead, cells depend on a cytoskeletal system, responsible for cellular spatial structure, resistance to deformation, intracellular cargo trafficking and the generation of forces to move and physically interact with the extracellular environment (Wickstead & Gull, 2011). The cellular cytoskeleton is comprised by various intracellular filamentous proteins grouped into three groups: actin, microtubules and intermediate filaments (Fletcher & Mullins, 2010, Huber, Schnauss et al., 2013). The actin cytoskeleton is a highly dynamic network composed of thin (~7nm) actin filaments and is responsible for cell shape, locomotion and generation of forces (Blanchoin, Boujemaa-Paterski et al., 2014) (Figure 8). Microtubules are large filaments (~25nm) composed of alpha- and beta-tubulin heterodimers and are essential for intracellular trafficking, organelle organization, cell polarity and chromosomal movements during cell division (Nogales, 2000) (Figure 8). Intermediate (8~12µm) filaments are flexible yet less dynamic filaments primarily providing

structural support to cells and their nuclei, and are composed of different proteins, such as keratins, neurofilaments, or lamins (Herrmann, Bar et al., 2007) (Figure 8).

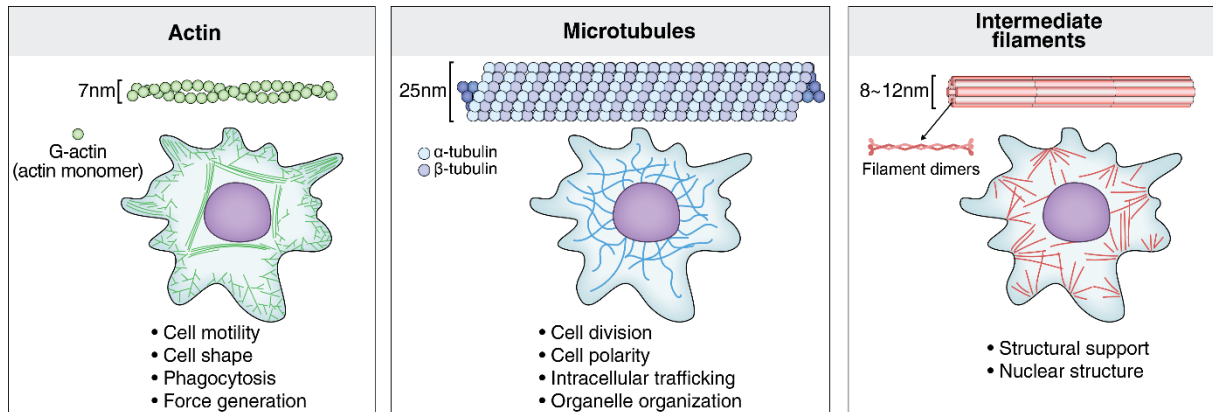


Figure 8 – The cellular cytoskeleton: its components, main characteristics and cellular functions.

Although all three cytoskeletal components (Figure 8) are essential for proper cellular function, immune effector mechanisms rely greatly on the actin cytoskeleton (Mostowy & Shenoy, 2015), which enables immune cells to move, interact and probe their environment, as well as to ingest noxious agents and debris. The actin cytoskeleton is a highly dynamic system which revolves around the fast polymerization and depolymerization of actin filaments in a concerted fashion to reshape the plasma membrane and control cell movement (Dominguez & Holmes, 2011).

1.2.2. *Structure and regulation*

The actin cytoskeleton is composed of actin filaments and a myriad of regulatory and structural proteins. Actin is one of the most abundant proteins in eukaryotic cells and three different isoforms differing in only a few amino acids exist: α - (expressed in muscle tissue), β - and γ -actin (generally expressed in all cells) (Dominguez & Holmes, 2011). Actin belongs to a superfamily of structurally related proteins including sugar kinases, hexokinases and heat shock proteins, but its most important feature is the ability to form filamentous polymers (Dominguez & Holmes, 2011). The switch between monomeric (globular; G-Actin) and filamentous actin (F-Actin), termed actin polymerization, can occur following spontaneous nucleation of adenosine triphosphate- (ATP) bound actin (Dominguez & Holmes, 2011). However, actin nucleation is almost exclusively induced by formins or actin-related protein 2/3 complex (Arp2/3), leading to filament extension from the barbed (+) end (Figure 9A) (Pollard, Blanchoin et al., 2000). Filament maintenance is then controlled by actin's ATPase activity (ATP hydrolysis by actin) and is tightly regulated by a variety of actin-interacting complexes which regulate the rate of dissociation of adenosine diphosphate- (ADP) actin from the pointed (-) end resulting in a "treadmilling" motion (Figure 9A) (Dominguez & Holmes, 2011, Pollard et

al., 2000). Actin filament architecture can be structured in different ways within the cell depending on their purpose and can be roughly divided into contractile and leading edge elements (Blanchoin et al., 2014). Contractile elements are primarily composed of antiparallel actin bundles in stress fibers and crosslinked actin filament networks in cortical actin (Figure 9B) (Blanchoin et al., 2014). Stress fibers provide contractile mechanical forces with the help of myosin, while cortical actin, a thin layer lining the plasma membrane, drives its inward retraction (Figure 9B) (Blanchoin et al., 2014). On the other hand, leading edge elements are composed by parallel actin bundles in filopodia, while lamellipodia and podosomes contain primarily branched and crosslinked actin fibers (Figure 9B) (Ridley, 2011).

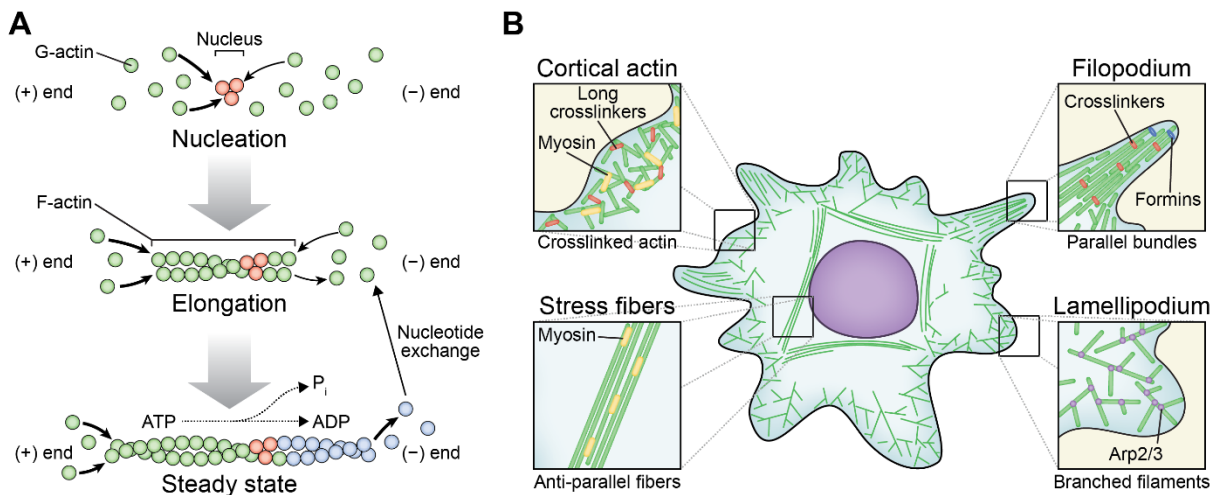


Figure 9 – Actin polymerization dynamics. **A)** The different steps towards actin polymerization, and its equilibrium at steady state via depolymerization, primarily at the pointed (–) end. Polymerization nucleus is displayed in red; Monomeric actin: G-actin; Filamentous actin: F-actin; P_i : phosphate. **B)** The main contractile (cortical actin and stress fibers), and leading edge (filopodia and lamellipodia) actin structures and their general architecture.

In order for the different actin cytoskeletal structures to control cell shape and movement, these need to exert force, either to extend or retract the plasma membrane, and is achieved either via associated nonmuscle myosin use, or directed actin polymerization (Blanchoin et al., 2014). For retraction during cellular locomotion, cortical actin is anchored to the plasma membrane at the trailing end of the cell and uses myosin to contract and “pull” the membrane inward (Figure 10A), whereas stress fibers are anchored to focal adhesion points, thereby control cellular adhesion both at the trailing and leading edges, and promote cell soma migration through their contraction (Figure 10B) (Bezanilla, Gladfelter et al., 2015, Blanchoin et al., 2014). At the leading edge, both lamellipodia and filopodia make use of directed actin polymerization to “push” the cell membrane forward (Figure 10C-D) (Bezanilla et al., 2015). Lamellipodia are thin, quasi-two-dimensional protrusions generated via Arp2/3-mediated actin nucleation following activation of members of the Wiskott–Aldrich syndrome protein (WASP) family,

namely WASPs and SCAR/WASP-family verprolin homologous protein 1 (SCAR/WAVE) proteins (Figure 10C) (Higgs & Pollard, 2001). Arp2/3 activation then leads to filament branching by initiating new F-actin filaments at an angle of 70° of existing ones to generate forward “pushing” branched networks (Figure 10C) (Higgs & Pollard, 2001, Pollard et al., 2000). G-actin availability at the growing edge is maintained via actin-depolymerizing Factor (ADF) /cofilin severing of F-actin at the pointed (–) end, followed by nucleotide conversion and resupply of ATP-actin by profilin (Figure 10C) (Ridley, 2011). Filopodia are thin, finger-like membrane protrusions generated by the extension of parallel F-actin bundles following actin nucleation by formins, particularly by protein diaphanous homolog 3 (Diaph3, generally referred to as mDia2) (Mattila & Lappalainen, 2008, Ridley, 2011). Upon activation of mDia2 by the Ras homology (Rho) GTPase cell division cycle 42 (Cdc42), mDia2 initiates actin nucleation and extension by recruiting profilin-bound ATP-actin to elongate F-actin pushing the plasma membrane outwards (Figure 10D) (Mattila & Lappalainen, 2008).

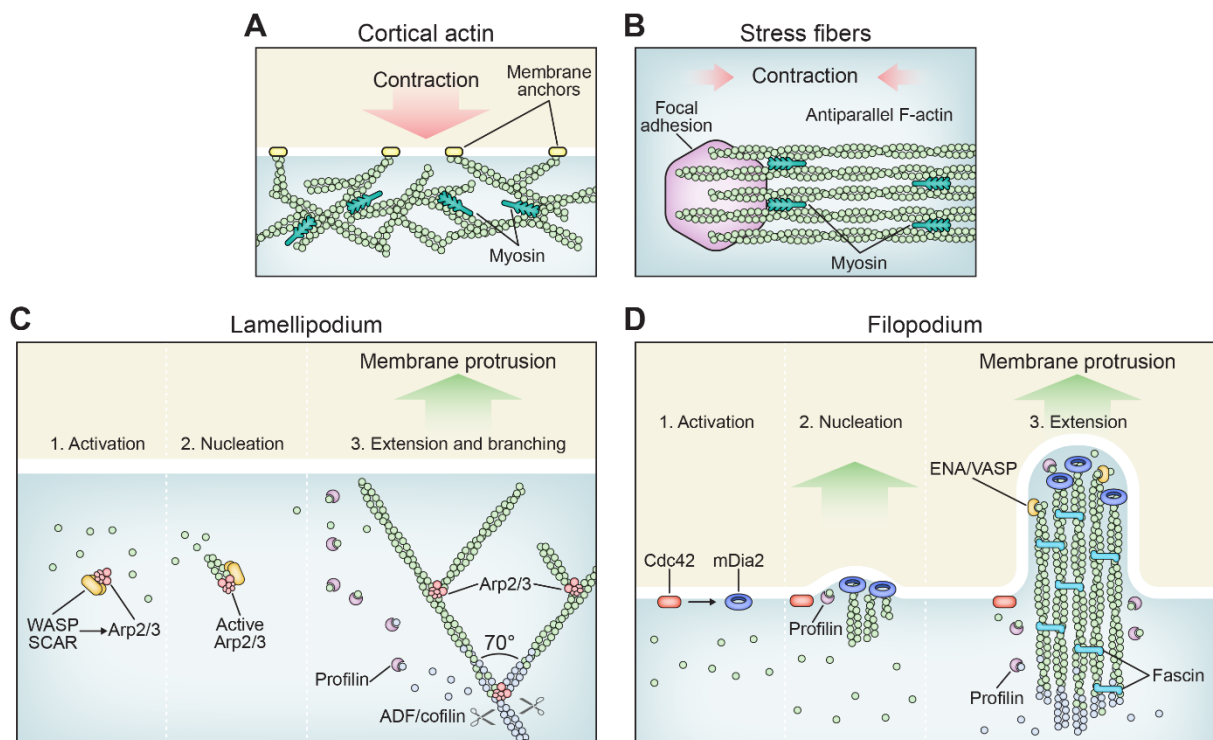


Figure 10 – Actin cytoskeletal structures. **A)** Schematic representation of cortical actin architecture and its contractile activity. The actin cortex is anchored to the plasma membrane and contracts inward owing to myosin activity. **B)** Schematic representation of stress fiber structure. Stress fibers are anchored to focal adhesions and its contraction is mediated by myosin sliding along antiparallel F-actin fibers. **C)** Schematic representation of lamellipodia generation: 1. following its triggering, WASP/SCAR protein family members activate Arp2/3; 2. active Arp2/3 initiates actin nucleation and filament extension; 3. Arp2/3 induces actin branching by binding pre-existing filaments and initiating extension at a 70° angle. **D)** Schematic representation of filopodia extension: 1. active Cdc42 activates the formin mDia2; 2. Active mDia2 recruits profilin-bound actin and initiates actin nucleation; 3. parallel actin filaments are bundled by fascin and extend via mDia2 recruitment of profilin-bound actin and ENA/VASP anti-capping activity.

The long and unbranched actin bundles in filopodia are further supported by the anti-capping activity of the enabled homolog/vasodilator-stimulated phosphoprotein (ENA/VASP) complex at the filopodial tip, keeping the barbed (+) end “open” for continued polymerization, and the tight, parallel bundling of F-actin fibers by fascin (Figure 10D) (Mattila & Lappalainen, 2008).

1.2.3. *Actin cytoskeleton control by Rho family GTPases*

The mammalian Rho GTPase family is composed by 20 conserved members of small (~21 kDa) intracellular signaling proteins, roughly divided into classical and atypical GTPases (Heasman & Ridley, 2008). Rho GTPases function as molecular switches in the control of various cellular processes, such as morphogenesis, neuronal development, cell division or gene expression but are primarily recognized due to their central role in the organization of the actin cytoskeleton (Jaffe & Hall, 2005, Sit & Manser, 2011). Classical Rho GTPase activity is regulated by Rho-interacting proteins which are able to induce the cycling between inactive, guanosine diphosphate (GDP), and active, guanosine triphosphate (GTP) bound states (Jaffe & Hall, 2005). The switch between inactive to active and vice-versa is mediated by guanine nucleotide exchange factors (GEFs), which catalyze the substitution of GDP by GTP to activate the Rho GTPase signaling functions, and GTPase activating proteins (GAPs), which induce the GTPase activity of Rho family members leading to GTP hydrolysis to GDP thus shutting down Rho GTPase signaling (Figure 11) (Heasman & Ridley, 2008, Jaffe & Hall, 2005). Rho GTPase activity can be further modulated by guanosine nucleotide dissociation inhibitors (GDIs), which sequester Rho GTPases, preventing their activation (Figure 11) (Cherfils & Zeghouf, 2013, DerMardirossian & Bokoch, 2005).

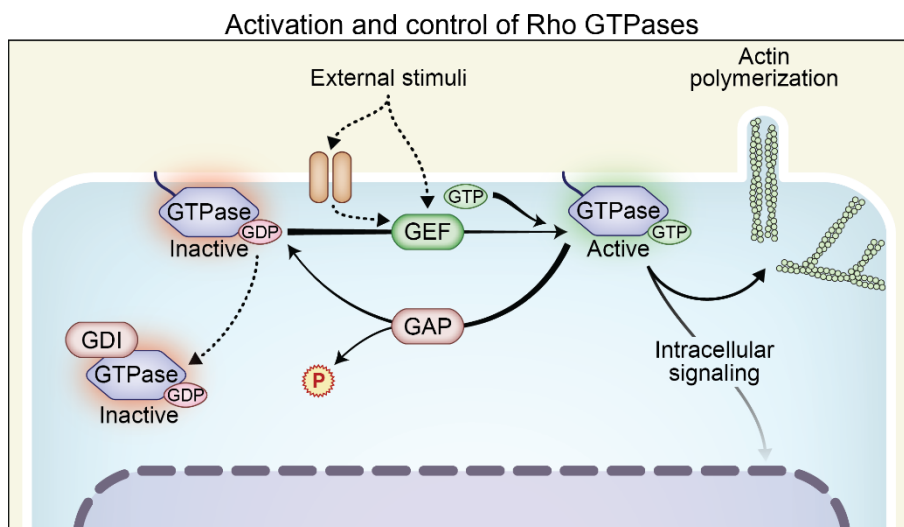


Figure 11 – Mechanisms of Rho GTPase activation, deactivation and sequestering by GEFs, GAPs and GDIs, respectively. GEFs “switch on” Rho GTPase signaling following the exchange of GDP by GTP; GAPs “switch off” Rho GTPase signaling by activating GTPase activity leading to GTP hydrolysis; GDIs sequester Rho GTPases in their inactive GDP-bound state.

Current knowledge of Rho GTPase molecular functions remains very asymmetric, and most data available stems from just three well characterized members: Cdc42, Ras-related C3 botulinum toxin substrate 1 (Rac1), and Ras homolog family member A (RhoA). Cdc42 was initially identified as a protein required for budding and cell division in yeast (Etienne-Manneville, 2004), and has been extensively studied since then. Primarily, Cdc42 has been repeatedly shown as a control switch for the actin cytoskeleton, and is critical in regulating filopodia extension, phagocytosis and cell migration (Sit & Manser, 2011). In addition, Cdc42 is involved in neurite extension, axon growth, cell polarity regulation as well as cell-cell contact and adhesion (Heasman & Ridley, 2008), all processes that actively depend on actin cytoskeletal dynamics. Upon activation, Cdc42 can interact with multiple downstream effectors to control actin cytoskeletal rearrangements (Figure 12A). Active Cdc42 can trigger Arp2/3-mediated actin polymerization by binding and activating WASP proteins or Insulin receptor substrate p53 (IRSp53), and via the binding to the mDia2 formin, which directly nucleates actin and initiates filament elongation and filopodia generation (Heasman & Ridley, 2008, Mattila & Lappalainen, 2008) (Figure 12A). Rac1 primarily induces actin polymerization via WAVE complex-mediated activation of Arp2/3, or mDia2 activation, to induce filament branching and extension in the formation of lamellipodia (Figure 12B). In order to stabilize the actin filaments during membrane protrusion, both Cdc42 and Rac1 are able to activate p21-activated kinases (PAK), which in turn phosphorylate LIM domain kinases (LIMK) leading to cofilin phosphorylation and loss of its activity, thus decreasing filament severing and increasing their stability (Figure 12) (Bamburg & Bernstein, 2010).

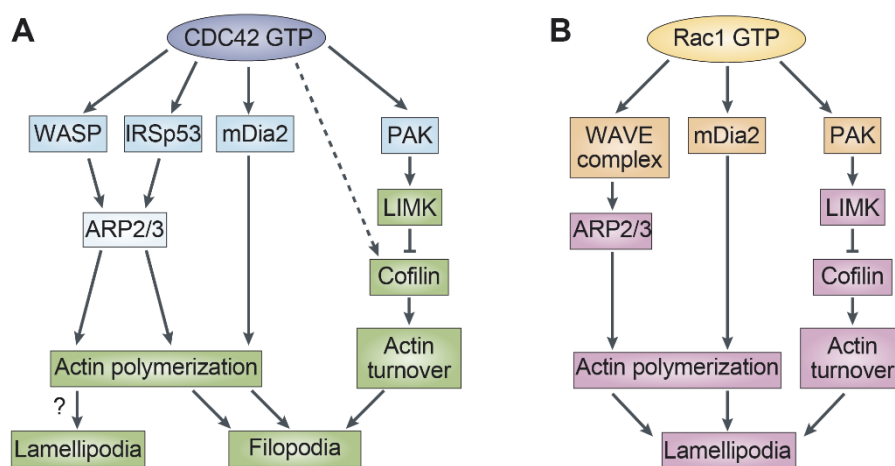


Figure 12 – Cdc42 and Rac1 pathways. Downstream effectors of **A)** active CDC42 and **B)** active Rac1, and the respective pathways leading up to actin rearrangement and membrane protrusion of lamellipodia or filopodia. Modified from Heasman & Ridley (2008).

Although there is considerable functional promiscuity in Rho family GTPase member activity, it is generally accepted that lamellipodia are associated with Rac1 and Cdc42 activity, whereas

filopodia are primarily Cdc42 dependent (Figure 12) (Heasman & Ridley, 2008). However, this does not preclude other Rho GTPases from inducing filopodia or lamellipodia formation, which can be achieved by other Rho family members, such as RhoQ and RhoF (filopodia), or RhoG (lamellipodia) (Heasman & Ridley, 2008).

1.2.4. *DOCK family GEFs*

Classical Rho-activating GEFs are able to mediate the GDP-GTP exchange owing to the presence of a Dbl homology domain, which interacts with Rho GTPases and alters its conformation inducing the release of GDP and the allowing binding of GTP (Rossman, Der et al., 2005, Schmidt & Hall, 2002). However, the dedicator of cytokinesis (DOCK) protein family also displays GEF activity towards Rho GTPases despite the lack of a Dbl homology domain (Laurin & Cote, 2014). Instead, DOCK family members rely on a structurally unrelated dock homology region 2 (DHR-2) that functions as a Rho family-specific GEF (Cote & Vuori, 2002, Laurin & Cote, 2014), thus representing an atypical GEF family. Although all DOCK proteins share the dock homology region 2 (DHR-2) GEF domain and a putative membrane anchoring and lipid binding dock homology region 1 (DHR-1) domain (Premkumar, Bobkov et al., 2010), the DOCK family is further subdivided into 4 subgroups based on sequence homology (Figure 13) (Laurin & Cote, 2014, Nishikimi, Kukimoto-Niino et al., 2013).

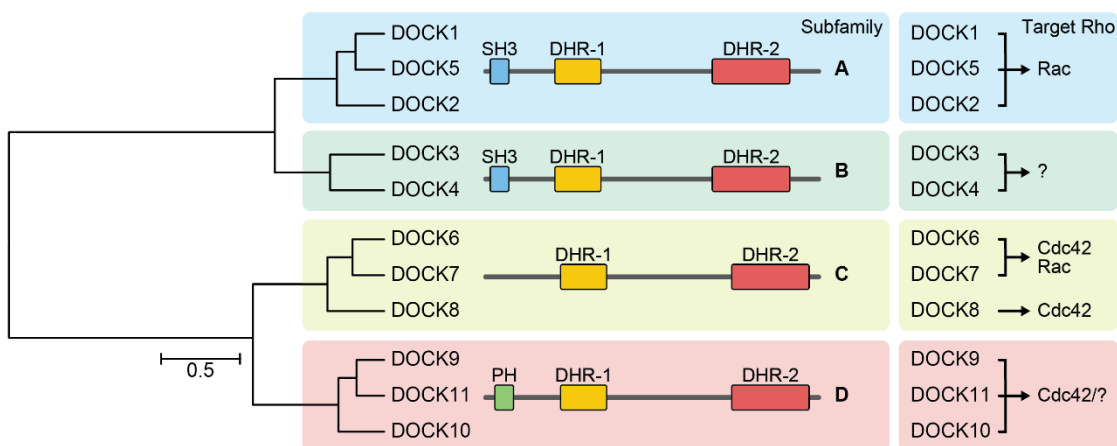


Figure 13 – Dock atypical GEF family. Molecular Phylogenetic analysis by Maximum Likelihood method of the mouse DOCK atypical GEF family using the respective canonical isoform protein sequence. Each subfamily is shown in its own colored box and protein domain arrangement is shown for each subfamily. The known target Rho GTPases for each DOCK protein is shown in the right panel. Structural scheme and target Rho table adapted from Nishikimi et al. (2013).

These differences are reflected also in the presence or absence of SRC homology 3 (SH3) or pleckstrin homology (PH) domains at the N-terminus which mediate protein-protein interactions (Figure 13) (Laurin & Cote, 2014). DOCK proteins are large (170~250 kDa) proteins, and although little is known for some of its members, it is becoming increasingly clear

that they play a major role in the regulation of the actin cytoskeleton (Laurin & Cote, 2014). For instance, DOCK2 has been shown to be an essential Rac1-specific GEF (Figure 13) necessary for hematopoietic cell migration, but is also important for the activation of T cells (Gadea & Blangy, 2014). Similarly, DOCK8 is a Cdc42-specific GEF (Figure 13) which is responsible for regulating cell polarity during chemotaxis and lymphocyte cell shape integrity (Harada, Tanaka et al., 2012, Krishnaswamy, Singh et al., 2015, Zhang, Dove et al., 2014). As such, both *DOCK2* and *DOCK8* deficiency in humans result in severe combined immunodeficiencies (Dobbs, Dominguez Conde et al., 2015, Zhang, Davis et al., 2009).

1.2.5. Cell migration and phagocytosis

Cell migration and chemotaxis are indispensable for proper immune system functioning and is required throughout the development of the immune system as well as during immune responses, as cells need to leave their sites of origin, such as the bone marrow or spleen, enter the blood stream or lymphatic vessels, extravasate to their tissues of residence or sites of infection, and also travel back to lymph nodes to mount adaptive immune responses (Griffith, Sokol et al., 2014). To accomplish that, immune cells rely on the actin cytoskeleton to propel them and are guided by external cues which generally dictate the direction of travel by triggering signaling pathways leading to actin polymerization (Pollard et al., 2000). Chemotactic gradients are sensed by specific receptors on the surface of immune cells and initiate local actin polymerization in a polarized fashion, in the direction of the chemotactic source (Bloes, Kretschmer et al., 2015, Griffith et al., 2014). Chemokines such as monocyte chemoattractant protein 1 (MCP1; coded by *Ccl2*) or C-C motif chemokine ligand 19 (CCL19) are perfect examples which bind to C-C motif chemokine receptor 2 and 7 (CCR2, CCR7), to initiate monocyte, and T, B and dendritic cell recruitment, respectively (Forster, Davalos-Miszlitz et al., 2008, Shi & Pamer, 2011). Upon receptor ligation, G-proteins, phosphoinositide 3-kinase (PI3K) and other kinases signals lead to the activation of Cdc42 and/or Rac GTPases to generate leading edge protrusions such as lamellipodia and filopodia, and RhoA, which controls the retraction of the trailing edge via the activation of Rho-associated protein kinase (ROCK) and its downstream target myosin (Figure 14A) (Curnock, Logan et al., 2002, Raftopoulou & Hall, 2004, Rossman et al., 2005).

Similarly, phagocytosis requires a precise rearrangement of the membrane to engulf microbes or other noxious particles. As such, Rho GTPases play a pivotal role in phagocytosis by coordinating membrane protrusion and contraction forces upon phagocytic receptor ligation, allowing particle engulfment (Flannagan et al., 2012). Phagocytosis can be triggered by a

variety of receptors/signals (see 1.1.4 - Phagocytosis and Figure 6). This is reflected in different modes of phagocytosis whereby the particles are internalized, with some leading to membrane protrusion and microbe envelopment, and others to the “sinking” of the membrane into the cell (Flannagan et al., 2012, Underhill & Ozinsky, 2002). Irrespective of the mechanical mode of engulfment, phagocytes utilize Cdc42 and Rac GTPases to extend the membrane around the particle and RhoA to coordinate membrane contraction and “pull” the particle inward (Figure 14B) (Chimini & Chavrier, 2000, Lee, Cox et al., 2000).

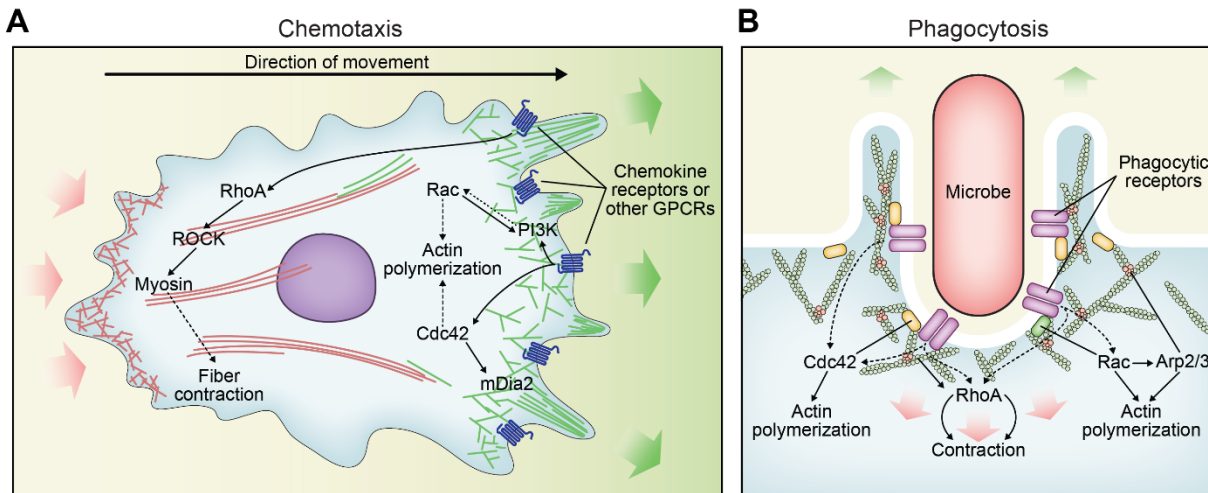


Figure 14 – Actin cytoskeleton regulation during **A)** chemotaxis and **B)** phagocytosis.

1.3. Bacterial infections

1.3.1. *Bacteria and the host*

Bacteria are an extremely diverse kingdom of life with quasi-ubiquitous distribution and phenomenal adaptations to a myriad of environments. As such, higher organisms, like mammals, are in constant contact with a vast array of bacterial species. Many of these are integral to the healthy state in mammals, and comprise a large and diverse “meta-ecosystem” which co-evolved within the host’s body, such as the gut or skin (Grice & Segre, 2011, Sekirov, Russell et al., 2010). There, bacteria can have beneficial roles, such as aiding digestion or synthesizing vitamin B12 in the gut (LeBlanc, Milani et al., 2013, Marchesi, Adams et al., 2016), and preventing inflammation or limiting pathogen invasion on the skin (Lai, Di Nardo et al., 2009, Naik, Bouladoux et al., 2015). Although most bacterial species promote neutral or beneficial interactions with the host, some are opportunistic pathogens, or strictly pathogenic species, and mammalian hosts need to properly distinguish friends from foes at the molecular level in order to recognize and eliminate threats (see sections 1.1.2 to 1.1.4).

Pathogenic bacteria are in a constant “Red Queen’s race” with their hosts and have thus evolved many tools to facilitate invasion and multiplication in the host, thereby seriously compromising host health and fitness. As such, bacterial pathogens account for millions of deaths worldwide every year, arising from foodborne infections, pneumonia or other invasive bacterial diseases (Kaplan, Wirtz et al., 2013, World Health Organization, 2015). To survive in the host and exploit its resources, pathogenic bacteria employ a wide variety of strategies aimed at suppressing, evading or subverting immune responses and scavenging host nutrients (Flannagan et al., 2009, Sarantis & Grinstein, 2012).

1.3.2. Immune evasion

Bacterial pathogens have evolved efficient means to withstand the immune system onslaught by avoiding detection, phagocytosis and intracellular killing by professional phagocytes, or via the manipulation of inflammatory responses (Flannagan et al., 2009). These immune evasion tools comprise the virulence factors which make some bacterial pathogens so dangerous to mammalian hosts. For instance, some bacteria mask surface antigens under a polysaccharide capsule or suppress host pathways triggered by PRRs (Diacovich & Gorvel, 2010, Finlay & McFadden, 2006), effectively avoiding PRR recognition or opsonization. In fact, encapsulated bacteria such as *Streptococcus pneumoniae* (*S. pneumoniae*) are responsible for the majority of community-acquired pneumonia worldwide (Buttery & Moxon, 2002). The main obstacle imposed on pathogens by the immune system is the phagocytosis and intracellular killing, making it the main target for virulent manipulation by bacteria. In the evolution race, bacteria have devised creative solutions such as the hijack of actin cytoskeletal dynamics, escape from the phagosome, inhibition of phagosome acidification or maturation as well as iNOS or NADPH-oxidase inhibition (Diacovich & Gorvel, 2010). For instance, *Listeria monocytogenes* (*L. monocytogenes*) is a true escape artist as it is able to exit the phagosome via the secretion of the pore-forming toxin Listeriolysin O (LLO), which disrupts the vacuolar membrane (Birmingham, Canadien et al., 2008), after which it takes control of actin polymerization via the secretion of the actin nucleator ActA to propel itself inside the cell (Lambrechts, Gevaert et al., 2008). Other species such as *Salmonella* spp., *Shigella* spp. or enteropathogenic *Escherichia coli* (*E. coli*) use so-called type III secretion systems (T3SS) to “inject” effector proteins into host cells and manipulate host cell function (Galan, Lara-Tejero et al., 2014). Due to the critical role of the actin cytoskeleton in immune effector mechanisms, some of these effector proteins, such as the *E. coli* EspH directly target Rho GTPases GEFs leading to decreased Rac1 and Cdc42 activation and disrupted phagocytosis (Dong, Liu et al., 2010). Others, such as *Salmonella* SopE1 and SopE2 mimic host GEFs and activate Cdc42/Rac1 to facilitate entry into

host cells where they survive out of the reach of immune cells (Hardt, Chen et al., 1998, Stender, Friebel et al., 2000).

1.3.3. Nutrient acquisition

Like all living beings, bacteria have nutritional requirements in order to grow and survive regardless of their niche. As such, the capacity of mammalian bodies to host bacterial pathogens depends on the availability of nutrients to bacteria, and their ability to scavenge them (Brown, Palmer et al., 2008). Bacteria require carbon and nitrogen sources to generate cellular components and energy, as well as essential transition metals, such as iron, for enzymatic reactions. Different bacterial species are able to process various carbon sources readily available in host tissues, such as glucose or lactate in the plasma, cholesterol or amino acids, and are able to derive nitrogen from nucleosides, amino acids or proteins in tissues (Abu Kwaik & Bumann, 2015, Brown et al., 2008). Although there is some adaptation depending on which specific carbon and nitrogen sources a given pathogen is able to utilize, it is highly unlikely that carbon or nitrogen availability is a limiting factor in infection. In contrast, transition metals, and in particular iron, are much more tightly controlled by the host (see section 1.1.5). Because iron is an essential nutrient for the vast majority of bacteria, in order for pathogens to successfully infect and survive in the host's body, they have evolved highly efficient iron-scavenging systems (Skaar, 2010). On the other hand, hosts exploit this nutritional bottleneck by withdrawing iron and limiting its bioavailability at the first sign of infection, in a strategy termed nutritional immunity (described in 1.1.5) (Ganz & Nemeth, 2015). Regardless of iron withdrawal strategies, most bacterial pathogens are still able to retrieve iron from the host by using higher-affinity scavengers (siderophores), which are able to seize iron from host iron-binding proteins such as transferrin (Freestone, Haigh et al., 2003, Kvach, Wiles et al., 1977), by secreting proteases which degrade iron containing proteins (Otto, van Dooren et al., 2002), via the expression of receptors for host iron-binding proteins (e.g. ferritin, lactoferrin) (Cassat & Skaar, 2013), or via the localized induction of cell death triggered by the secretion of cell-lysing toxins (Runyen-Janecky, 2013). Notably, as most iron is stored as heme in hemoglobin, it is currently believed that many pathogenic bacteria secrete erythrocyte-lysing pore-forming toxins, termed hemolysins, in a bid to extract heme-iron (Cassat & Skaar, 2013). In order to utilize the iron made available through the use of the virulence factors mentioned before, pathogenic bacteria need to internalize it. To this end, a number of iron and heme transport systems have been identified in various species of bacteria. In particular, TonB-dependent iron acquisition systems has been extensively studied in *E. coli* and other gram-negative bacteria, where they bind metal chelates, such as iron-siderophores and mediate the transport from the

outer membrane into the periplasmic space followed by the import across the inner membrane (Noinaj, Guillier et al., 2010). Similar systems exist for heme transport, although *E. coli* depends entirely on a single inner membrane transport system called dipeptide permease (DppABCDF) for the final step of heme internalization, without which it cannot utilize heme as an iron source (Letoffe, Delepelaire et al., 2006, Wandersman & Stojiljkovic, 2000).

1.4. Hemolysis and release of free heme

1.4.1. Heme and Hemolysis – Terms and definitions

Heme is a vital molecule for nearly all forms of life, composed by a ferrous iron ion (Fe^{2+}) coordinated within a heterocyclic protoporphyrin IX ring made up of four pyrrole groups bridged together (Jordan, 1991, Warren & Smith, 2009). In mammals, there are 6 types of heme molecules, which differ from each other in their protoporphyrin residues (Warren & Smith, 2009). Heme *b* is the most abundant type and serves as the base for the modifications that give rise to all the other heme types found in mammals (Figure 15) (Severance & Hamza, 2009, Warren & Smith, 2009). The different heme types function as prosthetic groups in proteins and enzymes, termed hemoproteins, involved in a variety of cellular functions based on the ability of heme to bind diatomic gases or to facilitate electron transport (Warren & Smith, 2009). Specifically, heme *b* is associated with hemoglobin and myoglobin, heme *a* and *c* are associated with cytochrome *a* and *c*, respectively, heme *l* and *m* are associated with lacto- and myeloperoxidases, respectively, and heme *o* is a stable intermediary of heme *a* (Figure 15). As such, heme is a versatile molecule essential for many biological processes, from ATP production to iron homeostasis (Kadish, Smith et al., 2000). In addition, labile heme (i.e. not bound to a hemoprotein) is able to function as a second messenger itself and can regulate biological processes as diverse as protein translation via the activation of eukaryotic translation initiation factor 2- α kinase 1 (eIF2 α) (Chen, 2007), or the coordination of the circadian clock via the nuclear receptor subfamily 1 group D member 1 (NR1D1; also known as Rev-ErbA α) (Yin, Wu et al., 2010).

However, because of its reactivity, intracellular heme levels must be tightly controlled. In fact, under steady state conditions, virtually all heme is associated with hemoproteins, or chaperoned, and its production is strictly regulated (Gozzelino, Jeney et al., 2010) so as to avoid unspecific damage to intracellular structures (Khan & Quigley, 2011).

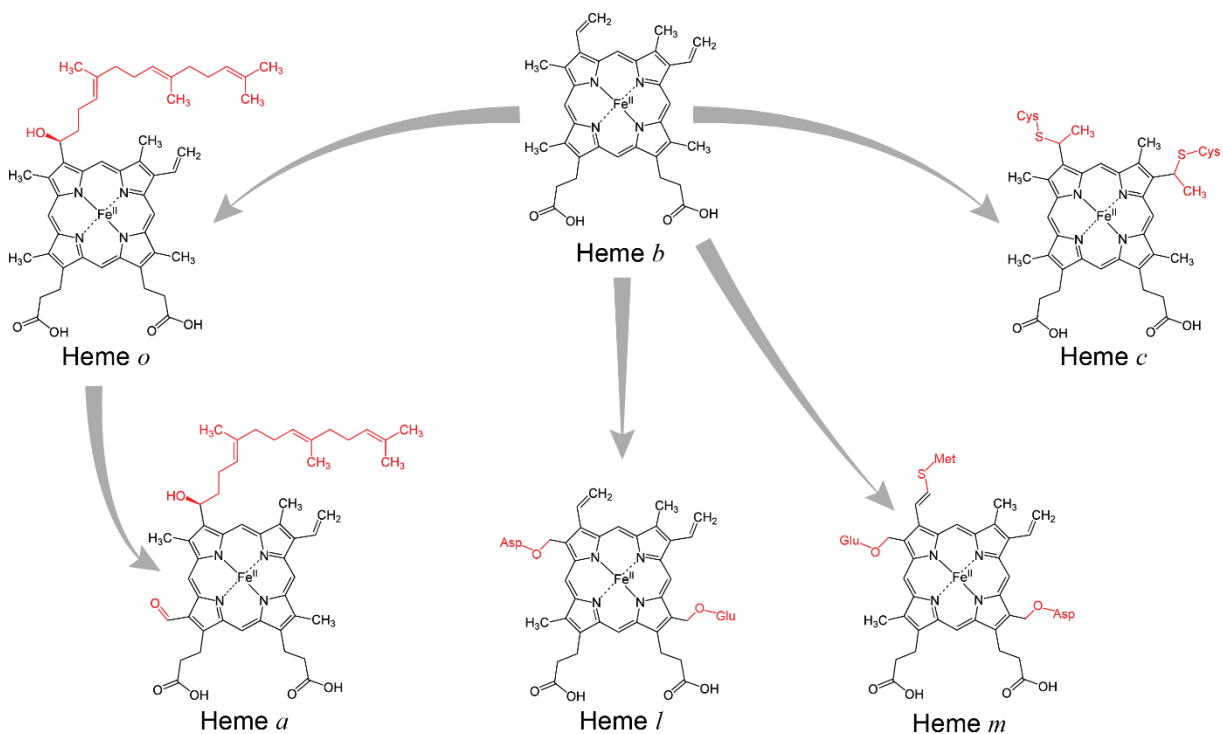


Figure 15 – Mammalian heme types. Heme *b* is the most abundant heme type and the basal form from which the other heme types are produced. Protoporphyrin residue modifications of heme *b* are shown in red. Basic heme *a*, *b*, *o* and *c* molecular structures were extracted from Yikrazuul (2010).

Hemolysis is a term which refers to the lysis of circulating erythrocytes leading to the release of cellular contents into the plasma. As erythrocytes are primarily loaded with vast amounts of hemoglobin ($\sim 250 \times 10^6$ tetramers per erythrocyte), extensive hemolysis can lead to very high concentrations of hemoglobin in the plasma (Schaer, Buehler et al., 2013). Outside of erythrocytes, hemoglobin rapidly oxidizes, and further loses stability and unfolds leading to the release of its heme prosthetic groups (4 heme molecules per hemoglobin tetramer) (Schaer et al., 2013) leading to very high concentrations (up to $50 \mu\text{M}$) of circulating labile heme (Muller-Eberhard, Javid et al., 1968).

1.4.2. Heme biosynthesis

Heme biosynthesis takes place in both mitochondria and the cytosol with some intermediaries being shuttled between the two (Jordan, 1991, Warren & Smith, 2009). It is a process which requires 8 different enzymatic steps and begins with the condensation of succinyl-CoA and glycine into δ -aminolevulinic acid by 5'-Aminolevulinic Synthases 1 or 2 (ALAS1/2) in the mitochondria (Figure 16) (Jordan, 1991). δ -aminolevulinic acid is then exported into the cytosol, where it is progressively modified into coporphyrinogen III (Figure 16), which is imported into the mitochondria (Jordan, 1991). There, coporphyrinogen III is modified successively into protoporphyrin IX, the basic protoporphyrin ring of heme, followed by the insertion of an iron ion into its center by ferrochelatase (FECH; Figure 16) (Jordan, 1991). After

heme synthesis completion, heme can be directly incorporated into hemoproteins in the mitochondria, or exported into the cytosol for hemoprotein incorporation (Jordan, 1991, Warren & Smith, 2009).

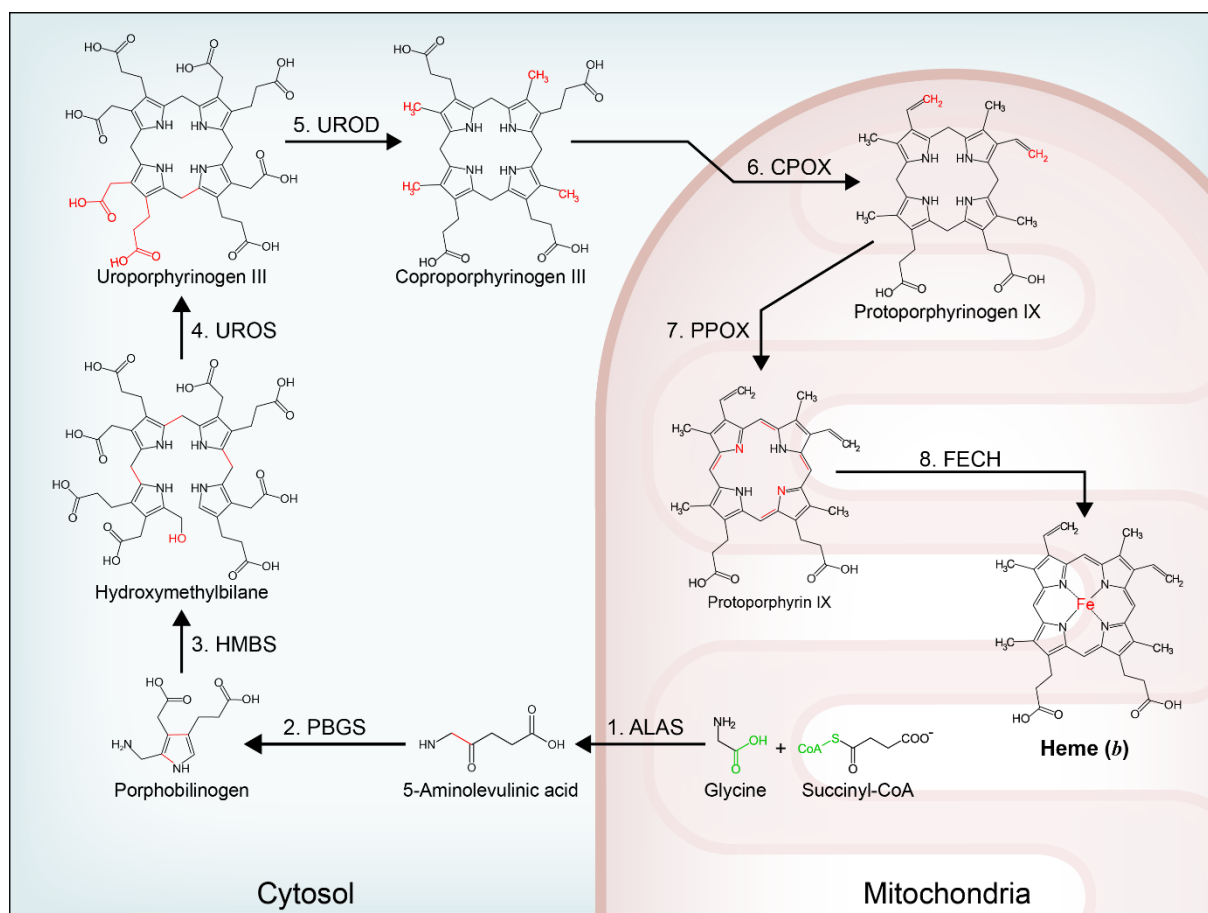


Figure 16 – Heme biosynthesis in mammals. Modified bonds/atoms are shown in red. Glycine and succinyl-CoA merging points are shown in green. ALAS = 5'-aminolevulinatase; PBGS = Delta-aminolevulinic acid dehydratase; HMBS = hydroxymethylbilane synthase; UROS = uroporphyrinogen III synthase; UROD = uroporphyrinogen decarboxylase; CPOX = coproporphyrinogen III oxidase; PPOX = protoporphyrinogen IX oxidase; FECH = ferrochelatase. Molecular structures were adapted from RossBoswell (2012).

1.4.3. *Hemolytic disorders*

Hemolytic disorders is an umbrella term to define disorders where hemolysis is a common denominator and thus encompasses various disease entities. These can arise due to inherited defects in hemoglobin (hemoglobinopathies), as in sickle cell disease (SCD) and α or β thalassemias, or due to cytoskeletal or enzymatic defects, such as in spherocytosis or glucose-6-phosphate dehydrogenase (G6PD) deficiency (Beutler, 2008), respectively. Of these, hemoglobinopathies alone account for 330,000 new cases every year, out of which 83% are due to SCD (Modell & Darlison, 2008). Inherited defects can lead to hemolysis via different pathophysiological mechanisms which culminate in altered erythrocyte membrane stability and rupture (Beutler, 2008, Rees, Williams et al., 2010), and can be due to defective hemoglobin

folding or synthesis (hemoglobinopathies), mutations in cytoskeleton-membrane anchoring proteins, (e.g. ankyrin-1 in spherocytosis) (Eber, Gonzalez et al., 1996), or reduced antioxidant capacity due to defective glutathione production in G6PD deficiency (Beutler, 2008). In addition, hemolytic events can be triggered by extrinsic factors such as severe sepsis, malaria infection or autoimmune hemolysis (Buffet, Safeukui et al., 2011, Freedman, 2015, Larsen, Gozzelino et al., 2010), which combined with inherited disorders affect millions of people worldwide (Modell & Darlison, 2008, Rees et al., 2010, World Health Organization., 2013). Interestingly, it has long been observed that hemolytic disorders predispose to severe and deadly bacterial infections, which is generally believed to be due to increased heme-iron availability for pathogens (Booth, Inusa et al., 2010, Cunnington, de Souza et al., 2012a, Cunnington, Njie et al., 2012b, Ramakrishnan, Moisi et al., 2010, Skaar, 2010, Wiener, 2003), although other disease-specific mechanisms have been better explored, such as functional hyposplenism in SCD (Rees et al., 2010). However, a clear link between hemolysis, heme release and susceptibility to infections is still lacking.

1.4.4. *Extracellular heme*

During intravascular hemolysis, heme is released from the hemoprotein pocket of hemoglobin, and can freely interact with plasma components and exposed cells, such as the endothelium (Schaer et al., 2013), leading to cellular and tissue damage due to the pro-oxidant and cytotoxic properties of labile heme (Gozzelino et al., 2010). This deleterious effect is further aggravated by the underlying anemia and stress erythropoiesis (Fibach & Rachmilewitz, 2008). “Free” heme is able to catalyze Fenton chemistry due to the presence of iron within the heme porphyrin ring, leading to the formation of oxygen radicals (Gozzelino et al., 2010, Vincent, 1989, Vincent, Grady et al., 1988). The generation of ROS by heme is believed to be the main mechanism leading to tissue damage (Gozzelino et al., 2010), as ROS provoke oxidative damage to membrane lipids, proteins and nucleic acids (Dixon & Stockwell, 2014). Because heme is an amphipathic molecule, it is thought that heme intercalates into plasma membranes where it can lead to membrane lipid peroxidation, compromising cellular function (Chiu & Lubin, 1989, Schmitt, Frezzatti et al., 1993). Moreover, high levels of extracellular heme can lead to heme and iron overload in cells involved in the uptake, degradation and excretion of heme or its catabolites (Fortes, Alves et al., 2012, Gozzelino et al., 2010, Larsen et al., 2010, Soares, Gozzelino et al., 2014). In fact, heme overload is associated with the induction of programmed cell death in hepatocytes, where heme sensitizes cells to undergo TNF-mediated apoptosis (Gozzelino et al., 2010), as well as the induction of necroptosis in macrophages (Fortes et al., 2012). Heme has also been shown to be able to bind and inhibit the proteasome,

which in combination with heme-induced oxidative modification of proteins, synergizes and enhances the accumulation of damaged and unfolded proteins, ultimately leading to cell death (Vallelian, Deuel et al., 2015). In addition to the direct damage catalyzed by extracellular “free” heme, it has been described that heme can promote inflammation via the activation of both toll-like receptor 4 (TLR4) (Figueiredo, Fernandez et al., 2007) and the inflammasome (Dutra, Alves et al., 2014), potentially enhancing the inflammatory response, and that heme is able to activate the coagulation cascade in a tissue factor (TF) dependent manner, which can help explain the vaso-occlusion observed in many hemolytic disorders (e.g. SCD) (Dutra et al., 2014). As such, extracellular labile heme satisfies the criteria to be considered a DAMP (Soares & Bozza, 2016), although to date, no dedicated signaling receptors have been identified.

1.4.5. Heme detoxification

Because of the severe danger posed by the presence of elevated circulation heme levels following intravascular hemolysis, higher organisms have evolved efficient protective mechanisms to cope with heme in an effort to quickly return to homeostasis. These involve the concerted effort of serum components and cells involved in iron homeostasis (i.e. macrophages and hepatocytes), which scavenge and degrade heme to prevent its deleterious effects (Gozzelino et al., 2010, Smith & McCulloh, 2015). Upon hemolysis and heme release from hemoglobin, virtually all heme will associate with different serum components at varying affinities (Ascenzi, Bocedi et al., 2005, Chiabrando, Vinchi et al., 2014), with hemopexin (HPX) being the highest affinity and specific serum heme scavenging protein (Muller-Eberhard & Liem, 1974, Paoli, Anderson et al., 1999). Hemopexin binds heme at a 1:1 ratio preventing its reactivity, and is thought to deliver heme to macrophages and hepatocytes via the low density lipoprotein receptor-related protein 1 (LRP1, also known as CD91), after which it is recycled into the bloodstream (Hvidberg, Maniecki et al., 2005), in a manner analogous to hemoglobin scavenging by haptoglobin (HP) and its receptor CD163 (Thomsen, Etzerodt et al., 2013). Although labile heme is bound by hemopexin with the highest affinity, heme is further able to associate with other serum components due to its partially hydrophobic nature, and constantly shuttles between carriers such as albumin, alpha-1-microglobulin (A1M) or low-density lipoprotein (LDL) (Ascenzi et al., 2005). While plasma heme scavenging is able to inhibit direct heme reactivity to some extent, it does not directly contribute towards reducing the amount of circulating plasma heme, and can easily be exhausted following severe intravascular hemolysis (Tolosano, Fagoonee et al., 2010). In order to effectively reduce the amounts of circulating heme, cells resort to enzymatic heme degradation by heme oxygenases, which catalyze the breakdown of heme into equal parts of ferrous iron, carbon monoxide (CO) and biliverdin

(Figure 17) (Gozzelino et al., 2010). Mammals possess two heme oxygenase paralogs: HO-1 (encoded by *Hmox1*), which is a highly inducible enzyme considered the rate-limiting step in heme degradation (Bezanilla et al., 2015), and HO-2, a constitutive lowly expressed enzyme thought to afford baseline protection against redox stress and acting as an oxygen sensor (Maines, Trakshel et al., 1986, Williams, Wootton et al., 2004). In addition, plasma A1M has been described as being able to degrade heme (Allhorn, Berggard et al., 2002), however, its relevance for heme degradation *in vivo* remains questionable, as genetic ablation of *Hmox1* in mice leads to the defective heme degradation despite the fact these animals are A1M-competent (Ferreira, Balla et al., 2008, Gozzelino et al., 2010, Larsen et al., 2010). Both HO-1 and HO-2 cleave the porphyrin ring at the alpha methene bridge releasing the heme iron and a CO molecule (Docherty, Firneisz et al., 1984, Gozzelino et al., 2010, Kikuchi, Yoshida et al., 2005). Similar to heme, iron alone is a potent pro-oxidant capable of inducing cellular toxicity when unrestrained (Puntarulo, 2005), and is quickly contained within ferritin complexes following heme degradation, efficiently protecting against iron-mediated toxicity (Gozzelino et al., 2010).

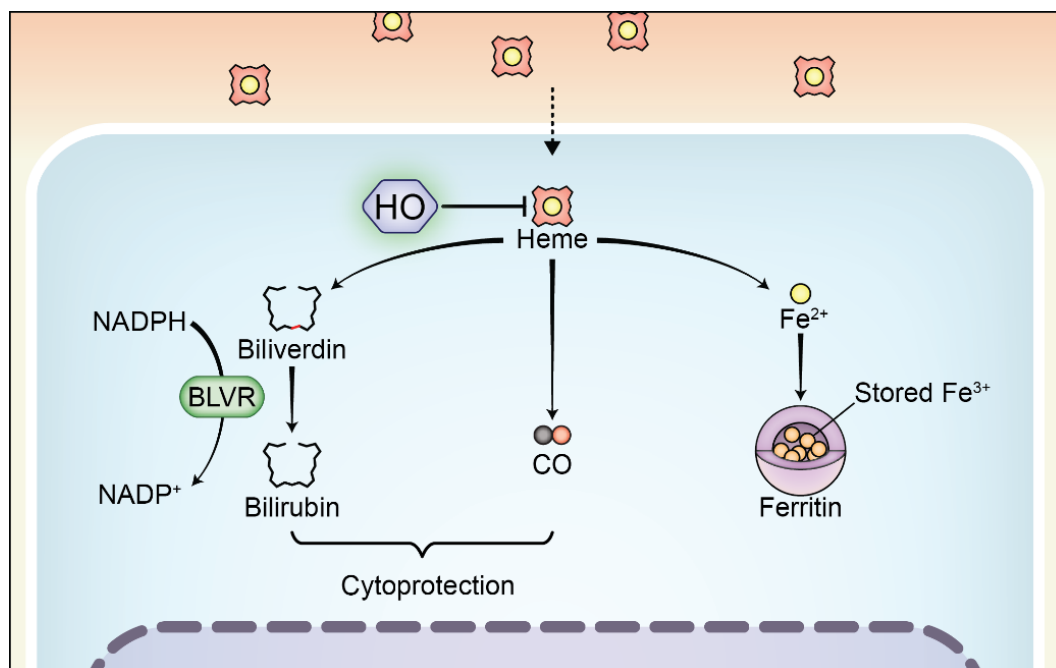


Figure 17 – Heme degradation by heme oxygenase (HO) and the resulting catabolites. HO cleaves heme at the alpha methene bridge producing a molecule of biliverdin, CO and ferrous iron.

The resulting biliverdin molecule is quickly reduced to bilirubin by biliverdin reductase A (BLVR), where bilirubin is thought to function as potent antioxidant, cycling between oxidized and reduced states as an NADPH-dependent redox stress sink (Figure 17) (Wegiel & Otterbein, 2012). Finally, CO resulting from heme degradation has been shown to act as a protective anti-inflammatory gasotransmitter in a variety of conditions by activating cytoprotective pathways (Figure 17) (Motterlini & Otterbein, 2010, Otterbein, Bach et al., 2000). In addition, CO is able

to interact with divalent iron in both labile heme and hemoproteins to exert protective effects further amplifying its therapeutic potential (Ryter, Alam et al., 2006).

1.5. Thesis Aim

Hemolytic disorders such as malaria or sickle-cell disease are well-known to increase susceptibility to bacterial infections. This translates into a serious health threat to millions worldwide, such that prophylactic antibiotics are administered until adulthood with consequences for antibiotic resistance. Although the phenomena of increased susceptibility are known, it is unclear whether and how hemolysis and heme release affect host immunity or invading bacteria. The current notion is that the increased heme-iron availability for bacterial growth arising from the breakdown of red blood cells and the leakage of hemoglobin and heme into the circulation provides a growth advantage for bacteria. However, this notion derives from indirect and incomplete understanding of the role and effects of hemolysis and heme release for infections. Notably, heme is a molecule with pleiotropic once released from the heme pocket of hemoproteins, and is able to catalyze oxidative reactions and induce cellular damage. Thus, we hypothesized that hemolysis and the resulting high levels of heme in the plasma negatively influence the immune response to bacteria by hitherto unknown mechanisms. Therefore, we set out to uncover the effects of increased heme levels for the establishment and outcome of bacterial infections by using a combination of *in vivo* bacterial infection models, as well as using newly generated mutant strains to explore the effects of heme from the pathogen side. In order to characterize the innate immune response in the presence of heme, I used a variety of *in vitro* functional assays and employed a chemical proteomics approach to unravel the molecular mechanism underlying the heme-induced susceptibility to bacterial infection.

Finally, by using a small scale high-throughput chemical screening, we aimed at identifying potential therapeutic agents capable of preventing or reversing the effects of heme on the innate immune response and restore adequate innate effector mechanisms.

2. Results

Heme drives hemolysis-induced susceptibility to infection via disruption of phagocyte functions

Rui Martins^{1,2}, Julia Maier^{1,2}, Anna-Dorothea Gorki^{1,2}, Kilian V M Huber¹, Omar Sharif^{1,2}, Philipp Starkl^{1,2}, Simona Saluzzo^{1,2}, Federica Quattrone^{1,2}, Riem Gawish^{1,2}, Karin Lakovits², Michael C Aichinger³, Branka Radic-Sarikas¹, Charles-Hugues Lardeau¹, Anastasiya Hladik^{1,2}, Ana Korosec^{1,2}, Markus Brown⁴, Kari Vaahtomeri⁵, Michelle Duggan⁵, Donscho Kerjaschki⁴, Harald Esterbauer⁶, Jacques Colinge¹, Stephanie C Eisenbarth⁷, Thomas Decker³, Keiryn L Bennett¹, Stefan Kubicek¹, Michael Sixt⁵, Giulio Superti-Furga^{1,8} & Sylvia Knapp^{1,2}

¹ CeMM Research Center for Molecular Medicine of the Austrian Academy of Sciences, Vienna, Austria; ² Department of Medicine I, Laboratory of Infection Biology, Medical University of Vienna, Vienna, Austria; ³ Max F. Perutz Laboratories, University of Vienna, Vienna, Austria; ⁴ Department of Pathology, Medical University of Vienna, Vienna, Austria; ⁵ IST Austria (Institute of Science and Technology Austria), Klosterneuburg, Austria; ⁶ Clinical Department of Medical and Chemical Laboratory Diagnostics, Medical University of Vienna, Vienna, Austria; ⁷ Department of Laboratory Medicine and Department of Immunobiology, Yale University School of Medicine, New Haven, USA; ⁸ Center for Physiology and Pharmacology, Medical University of Vienna, Vienna, Austria

Received 11 July 2016; accepted 28 September 2016; published online 31 October 2016;
DOI: [10.1038/ni.3590](https://doi.org/10.1038/ni.3590)

Running title

Heme impairs host resistance to bacteria via interference with cytoskeleton dynamics.

Correspondence to:

Sylvia Knapp, MD, PhD

CeMM Research Center for Molecular Medicine of the Austrian Academy of Sciences, and
Department of Medicine I, Laboratory of Infection Biology, Medical University of Vienna
Waehringer Guertel 18-20, 1090 Vienna, Austria

Phone: +43-1-40400-51390; Fax: +43-1-40400-51670;

E-mail: sylvia.knapp@meduniwien.ac.at

2.1. Abstract

Hemolysis drives susceptibility to bacterial infections and predicts poor outcome from sepsis. These detrimental effects are commonly considered to be a consequence of heme-iron serving as a nutrient for bacteria. We employed a Gram-negative sepsis model and found that elevated heme levels impaired the control of bacterial proliferation independently of heme-iron acquisition by pathogens. Heme strongly inhibited phagocytosis and the migration of human and mouse phagocytes by disrupting actin cytoskeletal dynamics via activation of the GTP-binding Rho family protein Cdc42 by the guanine nucleotide exchange factor DOCK8. A chemical screening approach revealed that quinine effectively prevented heme effects on the cytoskeleton, restored phagocytosis and improved survival in sepsis. These mechanistic insights provide potential therapeutic targets for patients with sepsis or hemolytic disorders.

2.2. Introduction

Intravascular hemolysis is a serious complication that accompanies severe inflammatory conditions such as sepsis, is an established complication of hemolytic disorders such as sickle cell disease (SCD), malaria infection or beta-thalassemia, and affects millions of people worldwide¹⁻⁵. In these disorders, extensive hemolysis leads to the release of the heme moiety from hemoglobin, which can rapidly exhaust the body's heme-scavenging capacity and results in high amounts of circulating heme⁵⁻⁸. Excess heme is important for driving disease pathology, primarily as a result of its pro-oxidant properties, which sensitize cells to the cytopathic effects of inflammatory mediators such as tumor necrosis factor (TNF)⁹⁻¹¹. These effects have been demonstrated in models of polymicrobial sepsis and noncerebral malaria, in which mice lacking the heme-degrading enzyme HO-1 (heme oxygenase-1) have increased disease severity and succumb to organ failure^{4,12}.

However, reduced disease tolerance cannot explain the substantially increased susceptibility to bacterial infections in people with hemolytic disorders such as SCD¹³, beta-thalassemia¹⁴ and malaria^{15,16}. Mortality rates of 40% in children with SCD¹ reflect the tremendous threat of bacterial infections in these patients and justify the current recommendation of prophylactic antibiotics until individuals reach adolescence^{17,18}. In spite of the medical importance and apparent link between hemolysis and infection, most studies on heme have either employed sterile stimuli¹⁹ or were performed in the presence of bactericidal antibiotics⁴, effectively precluding the examination of heme effects on antibacterial effector mechanisms. Hemolysis is often considered to be a logical explanation for the increased rate of bacterial infections, as

most pathogens depend on environmental iron sources and heme is an iron-containing protoporphyrin²⁰. Recently, impaired neutrophil effector functions following hemolysis were observed in humans with malaria²¹ or beta-thalassemia¹⁴, and in mouse models of malaria²². These studies have suggested that heme has a role in modulating host resistance mechanisms. However, the mechanism of how excess heme precisely affects host immunity to bacteria remains elusive. We found that, contrary to previous interpretations, heme did not affect bacterial growth through nutrient availability. Instead, heme strongly suppressed phagocyte functions by inducing extensive actin cytoskeleton changes by interfering with DOCK8-mediated Cdc42 activation, ultimately predisposing mice to bacterial dissemination and sepsis. Notably, using a chemical screening approach, we developed a therapeutic proof-of-concept strategy aimed at restoring endogenous host resistance mechanisms.

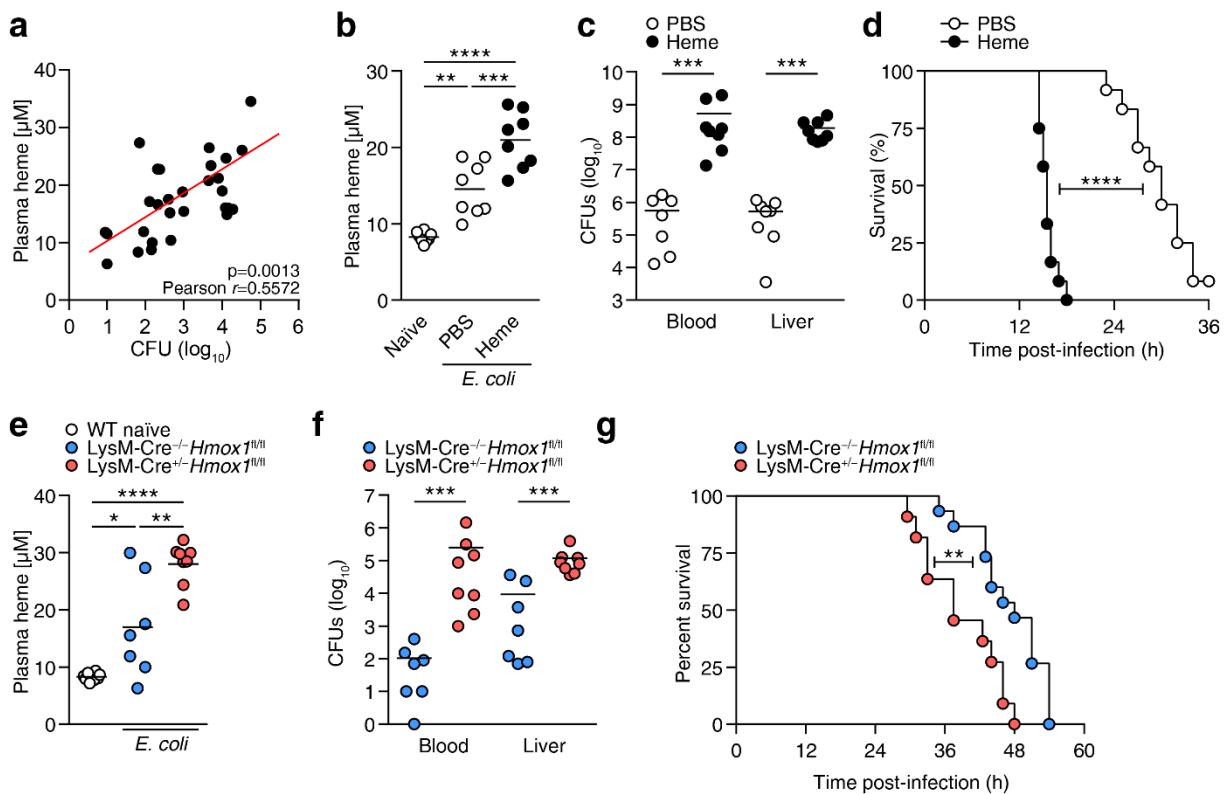
2.3. Results

2.3.1. Heme impairs bacterial clearance in vivo

We sought to determine whether the extent of hemolysis would affect host resistance mechanisms and, consequently, bacterial burden during Gram-negative bacteria-induced sepsis. The number of bacteria present in the blood of septic mice infected with a pathogenic *Escherichia coli* strain (*E. coli*, strain PMV-1 was used throughout this study) directly correlated with heme abundance in the plasma (**Fig. 1a**). To better understand the link between heme abundance and bacteremia severity, we pretreated mice with heme (25 $\mu\text{mol/kg}$ intraperitoneally (i.p.) for all heme treatments *in vivo*) to exogenously increase heme in the plasma before infection with *E. coli* (10^4 colony-forming units i.p.). *E. coli* sepsis itself was accompanied by modest hemolysis, whereas exogenous heme administration led to significantly increased plasma heme levels compared with phosphate-buffered saline (PBS)-treated mice, both 6 and 16 h post-infection (**Fig. 1b** and **Supplementary Fig. 1a**). This was paralleled by a substantial increase in the bacterial burden in heme-treated mice (**Fig. 1c** and **Supplementary Fig. 1b**), and translated into strongly impaired survival compared with PBS-treated mice (**Fig. 1d**).

Macrophages are crucial for the removal of excess heme resulting from hemolysis via the uptake and degradation of heme by HO-1 (ref. 23), encoded by *Hmox1*. To address whether an increase in endogenous heme resulting from defective heme degradation in macrophages would negatively affect bacterial clearance during sepsis *in vivo*, we examined *LysM-Cre^{+/-}Hmox1^{fl/fl}* mice, which lack expression of *Hmox1* in macrophages and neutrophils²⁴, and *LysM-Cre^{-/-}Hmox1^{fl/fl}* control littermates. Following i.p. *E. coli* infection, we observed a significant

increase in plasma heme levels in *LysM-Cre^{+/-}Hmox1^{fl/fl}* mice (**Fig. 1e** and **Supplementary Fig. 1c**), which was accompanied by increased bacterial numbers in blood and liver (**Fig. 1f** and **Supplementary Fig. 1d**) and impaired survival (**Fig. 1g**) when compared with *LysM-Cre^{-/-}Hmox1^{fl/fl}* controls. Similar results were obtained in a separate model of infection with the unrelated Gram-positive pathogen *Listeria monocytogenes* (*L. monocytogenes*) (**Supplementary Fig. 1e,f**).



Publication figure 1 - Heme impairs bacterial clearance *in vivo*. **(a)** Pearson's correlation between heme levels and bacterial burden in wild-type (WT) mice 16 h post-infection with *E. coli* ($n = 30$ mice). **(b,c)** Naive WT mice ($n = 8$) or WT mice pretreated with PBS ($n = 8$) or heme ($n = 8$). Shown are respective heme plasma amounts **(b)** and bacterial counts **(c)** 16 h post-infection with *E. coli*. **(d)** Survival of WT mice pretreated with PBS ($n = 12$) or heme ($n = 12$) and infected with *E. coli*. **(e,f)** Plasma heme levels **(e)** of naive WT ($n = 8$) or infected *LysM-Cre^{-/-}Hmox1^{fl/fl}* ($n = 7$) and *LysM-Cre^{+/-}Hmox1^{fl/fl}* ($n = 8$) mice and respective bacterial counts **(f)** 16 h post-infection with *E. coli*. **(g)** Survival of *LysM-Cre^{-/-}Hmox1^{fl/fl}* ($n = 15$) and *LysM-Cre^{+/-}Hmox1^{fl/fl}* ($n = 11$) mice infected with *E. coli*. Data in **a** are pooled from three independent experiments. Data in **b–f** are representative of two independent experiments. Data in **b, c, e** and **f** are presented as mean, and dots represent individual animals. One-way ANOVA with Tukey's multiple comparison test **(b,e)**, Mann-Whitney test **(c,f)**, Mantel-Cox test **(d,g)**; * $P \leq 0.05$, ** $P \leq 0.01$, *** $P \leq 0.001$, **** $P \leq 0.0001$.

To determine the potential pro-inflammatory effects of heme and to control for increased bacterial numbers in mice with high plasma heme during *E. coli*-induced sepsis, we challenged mice with lipopolysaccharide (40 mg/kg i.p., 16 h). Mice pretreated with heme had similar amounts of plasma interleukin-6 and TNF and similar amounts of the peritoneal chemokines KC and MCP-1, as well as similar cell recruitment as mice pretreated with PBS

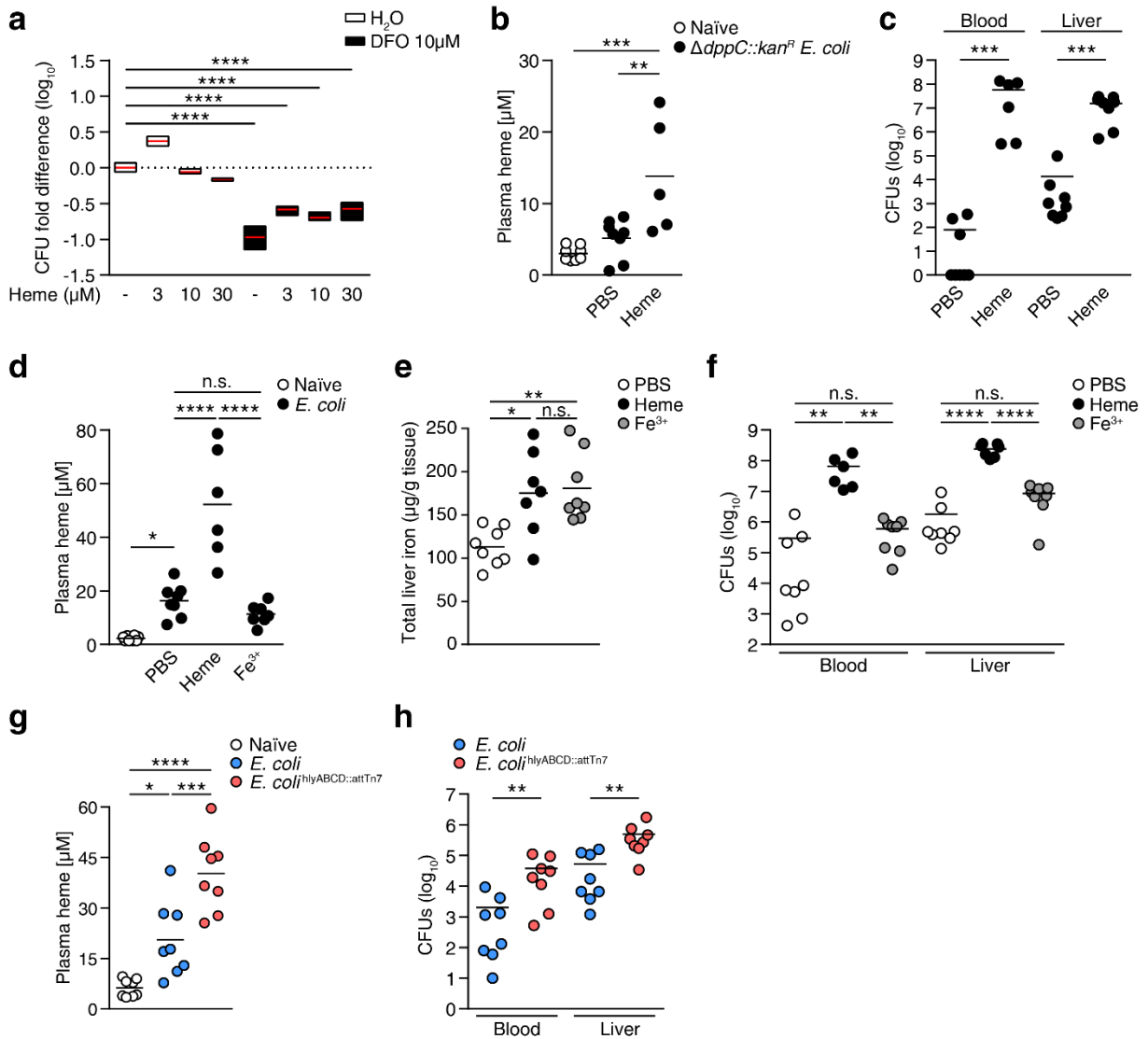
(**Supplementary Fig. 1g–i**), indicating that high plasma heme did not affect the inflammatory response. Thus, enhanced levels of plasma heme, induced by either exogenous heme administration or a lack of HO-1 expression in macrophages, resulted in an increased susceptibility to *E. coli* sepsis.

2.3.2. Independence of heme-iron acquisition

Following infection, hosts reduce the bioavailability of iron through iron withdrawal, which has led pathogenic bacteria to develop compensatory iron acquisition mechanisms²⁵. We tested the importance of heme as an iron source for *E. coli* under limited iron availability *in vitro*. Chelation of growth-medium iron with deferoxamine (DFO, 10 μ M) led to a reduction in bacterial growth, as compared with non-chelated controls (**Fig. 2a**). This defect was not rescued by heme supplementation (**Fig. 2a**), suggesting that heme could not fully compensate for limited iron availability. Pathogenic *E. coli* use several outer membrane heme transporters and periplasmic heme-binding proteins to gather heme²⁶. However, *E. coli* uses a single inner membrane ABC transporter, the dipeptide permease (DppBCDF), to import heme into the cytoplasm, and deletion of any of its components renders *E. coli* unable to grow if heme is the only iron source²⁷. To test whether heme-iron provides a growth advantage to bacteria *in vivo*, we generated an isogenic mutant *E. coli* lacking the DppBCDF-subunit DppC ($\Delta dppC::Kan^R$) that cannot utilize heme-iron (**Supplementary Fig. 1j**). We observed a substantial increase in bacterial load in the blood and livers of heme-treated wild-type mice 16 h post-infection with $\Delta dppC::Kan^R$ *E. coli* compared with PBS-treated mice (**Fig. 2b,c**), suggesting that heme-iron acquisition does not explain enhanced bacterial growth following elevations in heme concentrations. Next, we infected wild-type mice that were pretreated with PBS, heme or an equimolar amount of free iron (ferric ammonium citrate, Fe^{3+}) with wild-type *E. coli*. Plasma heme amounts were comparable in mice pretreated with Fe^{3+} or PBS (**Fig. 2d**), and despite the similarly increased availability of iron in both heme- and Fe^{3+} -treated mice (**Fig. 2e**), only heme-treated mice presented a significantly higher bacterial burden in the blood and liver compared with PBS- or Fe^{3+} -treated mice (**Fig. 2f**). Similar results were obtained in mice infected with *L. monocytogenes* (**Supplementary Fig. 1k**). These results indicate that increased heme concentrations directly lead to increased bacterial counts during sepsis and that bacterial iron requirements are met via heme-independent mechanisms.

The secretion of hemolytic toxins by pathogenic bacteria is an important virulence factor, and is currently considered to be a means of enhancing the availability of iron for bacteria²⁵. To understand the contribution of bacterial hemolysins to hemolysis and bacterial infection, and

because the *E. coli* strain (PMV-1) that we used does not secrete hemolysins, we used the bacterial transposon Tn7 to introduce a single copy of the *E. coli* alpha-hemolysin operon from strain CFT073 into the genome of PMV-1 *E. coli* to generate hemolytic *E. coli*^{hlyABCD::attTn7} (Supplementary Fig. 11).



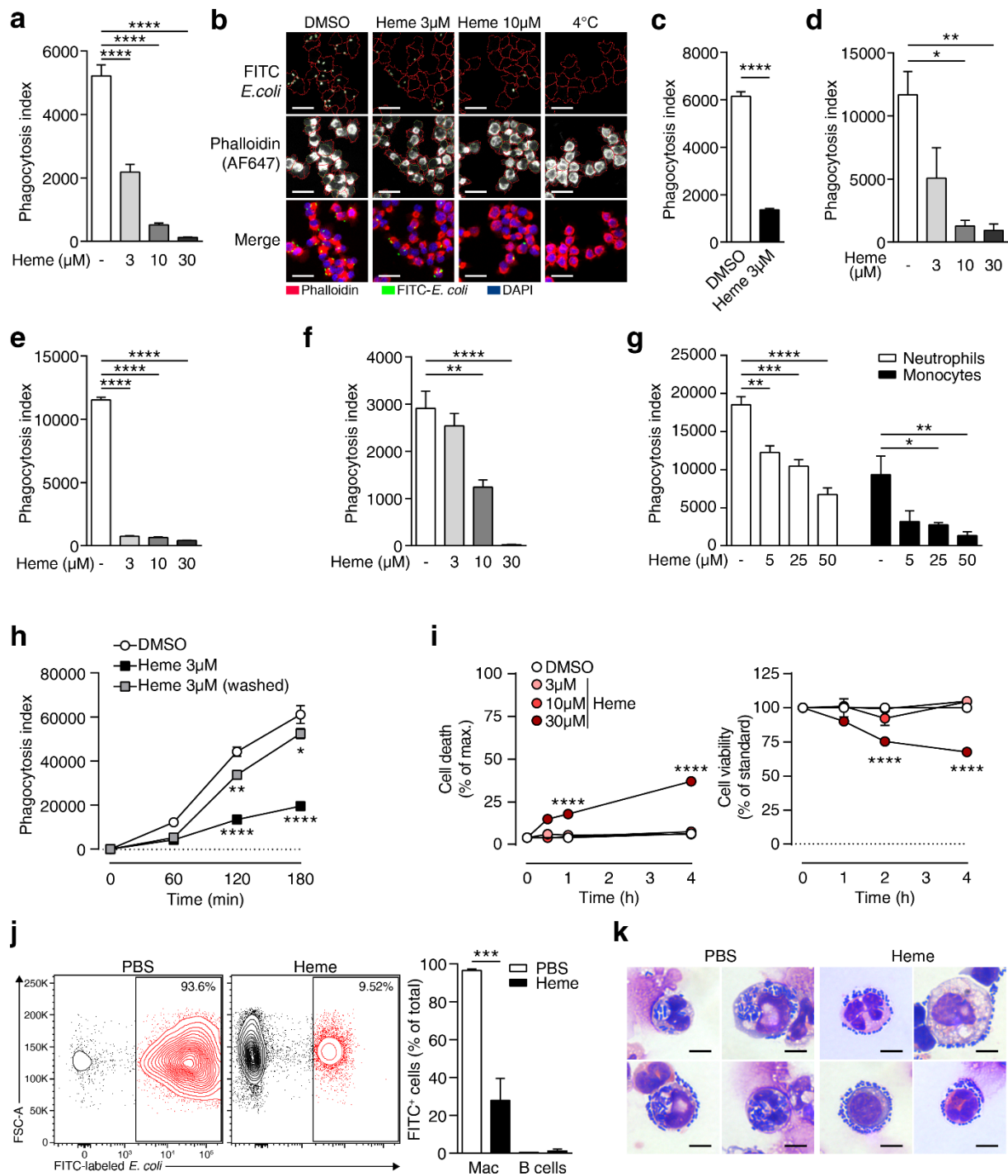
Publication figure 2 - Increased bacterial burden triggered by heme is independent of heme-iron acquisition. **(a)** Mid-log phase difference in the growth of *E. coli* in LB medium or in iron-chelated LB medium (deferoxamine, +DFO), supplemented with DMSO (control) or heme (3, 10 and 30 μM). Data are presented as the log₁₀ difference (normalized to control) in viable colony forming units (CFU) 4.5 h (mid-log phase) post-inoculation of media ($n = 3$ technical replicates per condition). **(b,c)** Plasma heme levels **(b)** of naïve WT mice ($n = 8$) or WT mice pretreated with PBS ($n = 8$) or heme ($n = 6$) and respective bacterial counts **(c)** 16 h after infection with *ΔdppC::kan^R E. coli*. **(d–f)** Plasma heme levels **(d)** of naïve WT mice ($n = 8$) or WT mice pretreated with PBS ($n = 8$), heme ($n = 7$) or an equimolar amount of free ferric iron ($n = 8$; ferric ammonium citrate), and respective total liver iron levels **(e)**, and bacterial counts **(f)** 16 h post-infection with *E. coli*. **(g,h)** Plasma heme levels **(g)** of naïve WT mice ($n = 8$) or WT mice infected with isogenic non-hemolytic ($n = 8$; *E. coli*) and hemolytic ($n = 8$; *E. coli*^{hlyABCD::attTn7}) *E. coli* strains and respective bacterial counts **(h)** 16 h post-infection. Floating bars in **a** are presented as the mean ± minimum and maximum values. Data in **b–h** are presented as mean, and dots represent individual animals. One-way ANOVA with Tukey's multiple comparison test **(a,b,d–g)**, Mann-Whitney test **(c,h)**; n.s. = not significant, * $P \leq 0.05$, ** $P \leq 0.01$, *** $P \leq 0.001$, **** $P \leq 0.0001$.

Infection of wild-type mice with *E. coli*^{hlyABCD::attTn7} further increased heme plasma concentrations (**Fig. 2g**), and resulted in elevated bacterial counts compared with infection with wild-type *E. coli* (**Fig. 2h**), indicating that pathogen-induced hemolysis is an important virulence mechanism for evading host resistance. Together, these data show that bacteria exploit the inflammation- and/or hemolysin-triggered release of heme independently of iron acquisition.

2.3.3. Heme potently inhibits phagocytosis

Next, we investigated how heme influences the host resistance mechanisms that are responsible for restricting bacterial growth. We focused on macrophage effector functions and found that heme pretreatment (15 min, 3–30 μ M unless otherwise indicated) led to a strong, dose-dependent reduction of phagocytosis of *E. coli* by RAW264.7 macrophages compared with DMSO-treated controls (**Fig. 3a,b** and **Supplementary Fig. 2a**). Bacterial phagocytosis by RAW264.7 macrophages was not suppressed by hemoglobin, free iron, or the heme analogs tin-protoporphyrin IX at heme-equivalent concentrations (**Supplementary Fig. 2b–e**). Notably, heme did not alter bacterial binding or bacterial killing by macrophages (**Supplementary Fig. 3f,g**). Incubation of murine primary peritoneal macrophages, bone-marrow-derived macrophages (BMDMs) and neutrophils with heme led to a similar reduction of phagocytosis of *E. coli*, *Pseudomonas aeruginosa*, *Streptococcus pneumoniae* and *L. monocytogenes* (**Fig. 3c,d** and **Supplementary Fig. 2h–k**), and heme strongly suppressed bacterial phagocytosis by human monocyte-derived macrophages (**Fig. 3e** and **Supplementary Fig. 2l**) and neutrophils (**Fig. 3f**), as compared with DMSO controls. In addition, we observed that heme treatment of RAW264.7 macrophages led to a dose-dependent inhibition of apoptotic cell uptake (**Supplementary Fig. 2m**).

To assess the physiological effect of heme-induced inhibition of phagocytosis in the tissue most relevant for hemolysis, we measured bacterial phagocytosis in human whole blood. Induction of hemolysis with phenylhydrazine or addition of heme to whole blood at concentrations mimicking the physiological range of plasma heme in hemolytic patients (5–50 μ M)⁶ led to a dose-dependent impairment of *E. coli* phagocytosis by neutrophils and monocytes, as compared with DMSO controls (**Fig. 3g** and **Supplementary Fig. 2n,o**), indicating that our mouse model was reflective of human hemolytic conditions. To determine whether heme-related cytotoxicity¹¹ causes the inhibition of phagocytosis, we pre-incubated RAW264.7 macrophages with heme (15 min) and washed the cells before addition of bacteria. Removal of heme by washing induced a complete recovery of the phagocytic capacity of macrophages compared



Publication figure 3 - Heme potently inhibits phagocytosis of bacteria. Phagocytosis of FITC-*E. coli* by RAW264.7 macrophages treated with control (DMSO) or heme ($n = 4$ per condition) and assessed by flow cytometry. (b) Confocal microscopy images of RAW264.7 macrophages treated with control (DMSO) or heme and incubated with FITC-*E. coli*. (automatic quantification in **Supplementary Fig. 3a**). Scale bars represent 20 μ m. (c-f) Phagocytosis of FITC-*E. coli* by primary mouse peritoneal macrophages (c), mouse neutrophils (d), human monocyte-derived macrophages (e) and human neutrophils (f), treated with control (DMSO) or heme ($n = 4$ technical replicates per condition) and quantified by flow cytometry. (g) Phagocytosis of bacteria by human blood neutrophils ($CD11b^+$, SSC^{high}) and monocytes ($CD11b^+$, SSC^{low}) from control and heme-treated whole blood ($n = 4$ per condition), as quantified by flow cytometry. (h) Time course of phagocytosis of FITC-*E. coli* by RAW264.7 macrophages treated with control (DMSO), heme, or heme treatment and subsequent washing to remove heme before incubation with bacteria ($n = 4$ technical replicates) per condition and time point; flow cytometry analysis). (i) Percentage of cell death (measured by lactate dehydrogenase (LDH) release; left) and cell

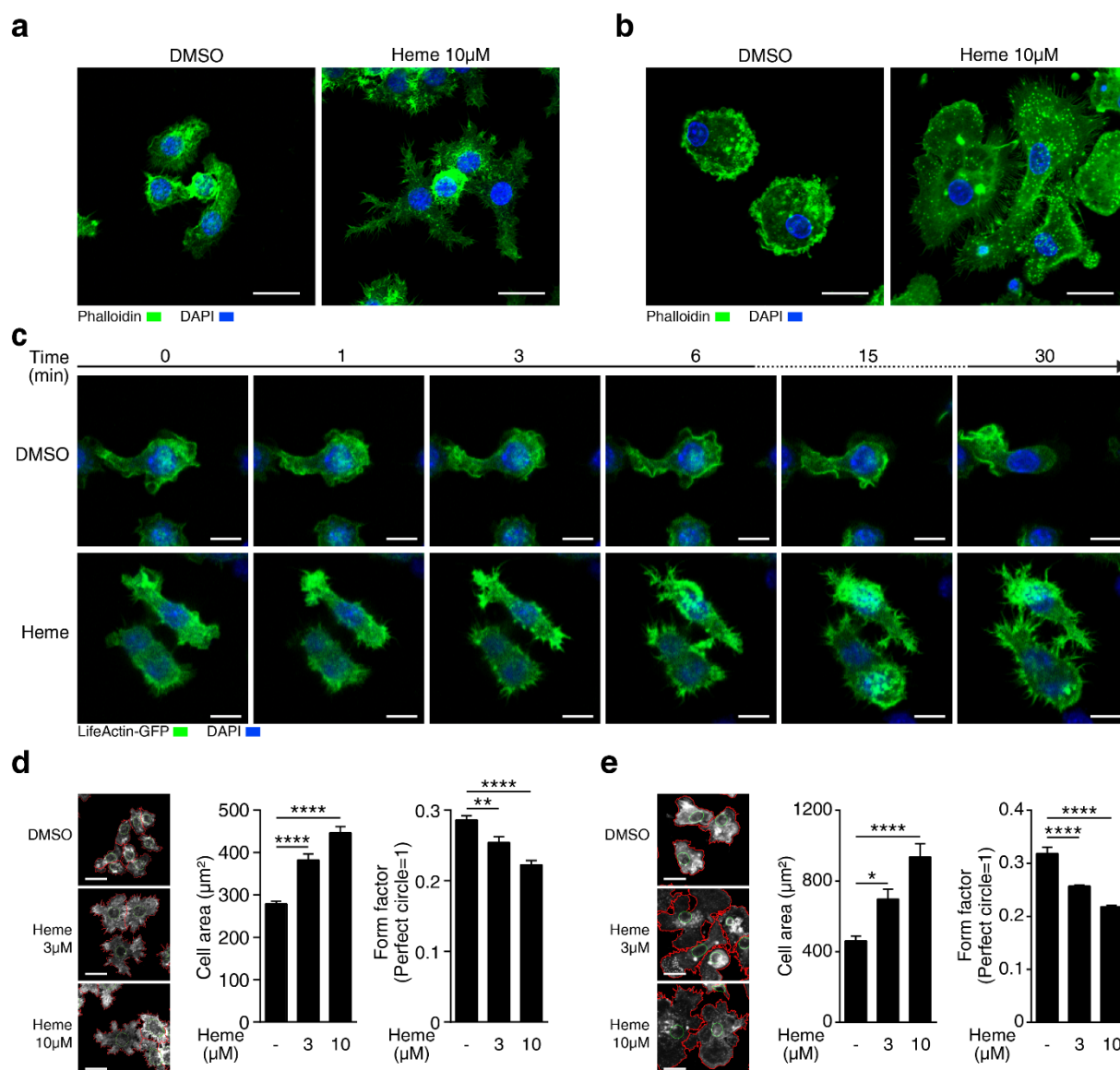
viability (measured by neutral red assay; right) of RAW264.7 macrophages following incubation with control (DMSO) or heme ($n = 4$ technical replicates per condition and time point). Staurosporine treatment (10 μM) was used as a positive control to determine the maximum cell death and loss of viability for LDH release assays and neutral red assays, respectively. **(j)** *In vivo* phagocytosis of FITC-*E. coli* by peritoneal macrophages (percentage FITC⁺F4/80⁺CD11b⁺Ly6G⁻) from PBS- or heme-treated mice ($n = 5$ mice per condition), shown and quantified by flow cytometry. Percentage of FITC⁺ B cells (CD11b⁻CD3⁻B220⁺Ly6G⁻F4/80⁻) shown as control for unspecific binding of bacteria to cells. **(k)** Giemsa stain of cells from peritoneal exudates of mice treated with PBS or heme 16 h post-infection with *E. coli* as in **Figure 1c,d**. Bacteria are stained blue and scale bars represent 5 μm . Data in **a** are representative of four independent experiments. Data in **b, d, e, g** and **i–k** are representative of two independent experiments. Data in **a** and **c–j** are presented as mean \pm s.e.m. One-way ANOVA with Tukey's multiple comparison test (**a,d–g**), two-tailed *t* test (**c,j**), two-way ANOVA with Tukey's multiple comparison test (**h,i**); * $P \leq 0.05$, ** $P \leq 0.01$, *** $P \leq 0.001$, **** $P \leq 0.0001$.

with those in which heme was not removed (**Fig. 3h**), indicating that cell viability was not compromised. In addition, heme only mildly induced cell death at 30 μM (**Fig. 3i** and **Supplementary Fig. 2p**), as has been reported for macrophages¹¹.

To test whether heme affects macrophage phagocytosis *in vivo*, we i.p. injected wild-type mice pretreated with PBS or heme with FITC-labeled heat-killed *E. coli* (FITC-*E. coli*). We found a strong reduction in the percentage of phagocytosing (FITC⁺) F4/80⁺CD11b⁺Ly6G⁻ peritoneal macrophages in heme-treated versus PBS-treated mice (**Fig. 3j**). Reduced *in vivo* phagocytosis was also observed in cytospin preparations of peritoneal exudate cells from mice treated with heme, as compared with PBS, and infected with live *E. coli* to induce sepsis (**Fig. 3k**). These results indicate that heme inhibition of phagocytosis occurs at sub-toxic levels and requires the intact heme molecule.

2.3.4. *Heme disrupts actin cytoskeleton dynamics*

Phagocytosis of pathogens relies on a tightly regulated actin cytoskeleton rearrangement that occurs following recognition of foreign bodies, and any interference with its regulation negatively affects host resistance against bacteria²⁸. Concordantly, we found that exposure of RAW264.7 and human monocyte-derived macrophages to heme led to changes in cell shape, which were accompanied by cell spreading and a strong induction of filopodia formation (**Fig. 4a,b** and **Supplementary Video 1**), which was visible within 3 min of stimulation with heme, but not with DMSO or protoporphyrin (**Fig. 4c**, **Supplementary Fig. 3a** and **Supplementary Videos 2** and **3**). We quantified these changes by automatic image analysis and found that heme-induced cytoskeleton rearrangement led to a significant increase in cell area and perimeter, as well as a decrease in circularity (form factor) (**Fig. 4d,e** and **Supplementary Fig. 3b–d**), indicating that the heme-induced defective phagocytic response was likely tied to cytoskeleton rearrangements.



Publication figure 4 - Heme induces cell shape changes via actin cytoskeleton remodeling. **(a,b)** Cellular morphology of RAW264.7 macrophages **(a)** and human monocyte-derived macrophages **(b)** incubated with control (DMSO) or heme for 15 min. Scale bars represent 20 μ m. **(c)** Live cell imaging of RAW264.7 macrophages expressing LifeAct-GFP treated with control (DMSO) or 3 μ M heme (see **Supplementary Video 2**). Scale bars represent 10 μ m. **(d,e)** Cell shape analysis and automatic quantification of cell area and form factor of RAW264.7 macrophages **(d)** ($n = 177$ – 282 cells analyzed per condition) and human monocyte-derived macrophages **(e)** ($n = 6$ images per condition) incubated with control (DMSO) or heme for 15 min. Scale bars represent 20 μ m. Data in **a** and **d** are representative of six independent experiments. Data in **c** are representative of two independent experiments. Data in **d** and **e** are presented as mean \pm s.e.m.; one-way ANOVA with Tukey's multiple comparison test **(d,e)**; * $P \leq 0.05$, *** $P \leq 0.001$, **** $P \leq 0.0001$.

During immune responses to bacteria, cytoskeletal rearrangement is required beyond phagocytosis and is crucial for cell recruitment and migration²⁹. To investigate whether heme has additional effects, we used a wound-healing assay and found that heme dose-dependently hampered the motility of BMDMs when compared with cells treated with DMSO (**Fig. 5a,b**). Similarly, mouse bone-marrow-derived dendritic cell migration in a three-dimensional collagen gel toward a CCL19 gradient was impaired in the presence of heme, as compared with DMSO

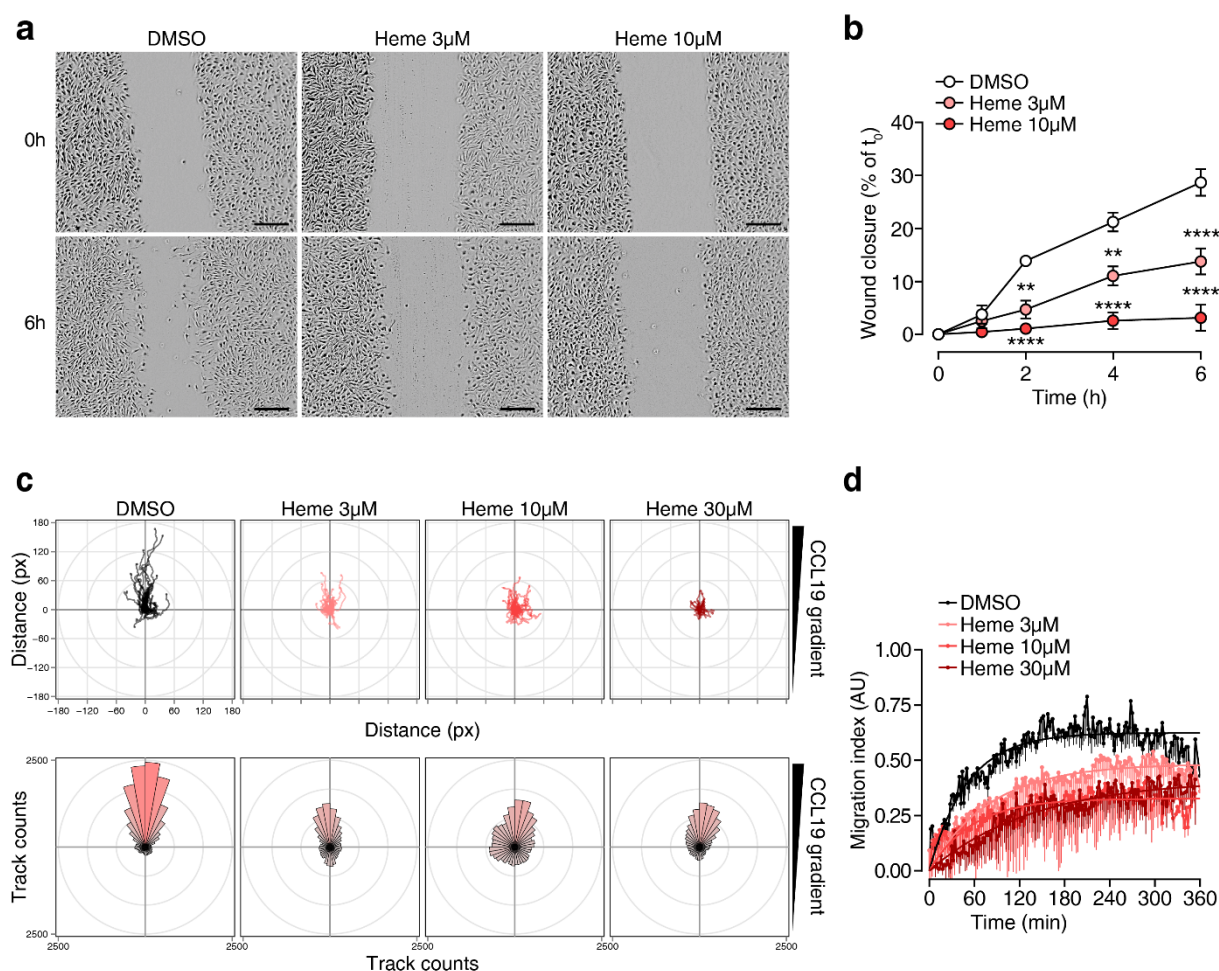
control (**Fig. 5c,d** and **Supplementary Video 4**). In addition, rolling and adhesion of primary human monocytes onto a TNF-activated endothelial layer under flow conditions, which rely on actin polymerization to stabilize integrin anchors onto the endothelium³⁰, were impaired by addition of heme compared with DMSO-treated controls (**Supplementary Fig. 4a,b** and **Supplementary Video 5**).

In vivo, neither heme-treated wild-type or *LysM-Cre^{+/-}Hmox1^{fl/fl}* mice exhibited an increase in peritoneal cell influx 6 h post-infection with *E. coli* when compared with PBS-treated or *LysM-Cre^{-/-}Hmox1^{fl/fl}* controls, respectively (**Supplementary Fig. 4c,d**) despite showing higher concentrations of peritoneal chemokines (KC and MCP-1; **Supplementary Fig. 4e,f**). Furthermore, in a thioglycollate-induced peritonitis model, we found neutrophil migration disrupted in heme-treated as compared with PBS-treated mice *in vivo* (**Supplementary Fig. 4g-i**). Together, these data indicate that heme induces extensive actin cytoskeleton alterations, which results in defective phagocytosis and inflammatory cell migration.

2.3.5. Heme activates Cdc42 via DOCK8

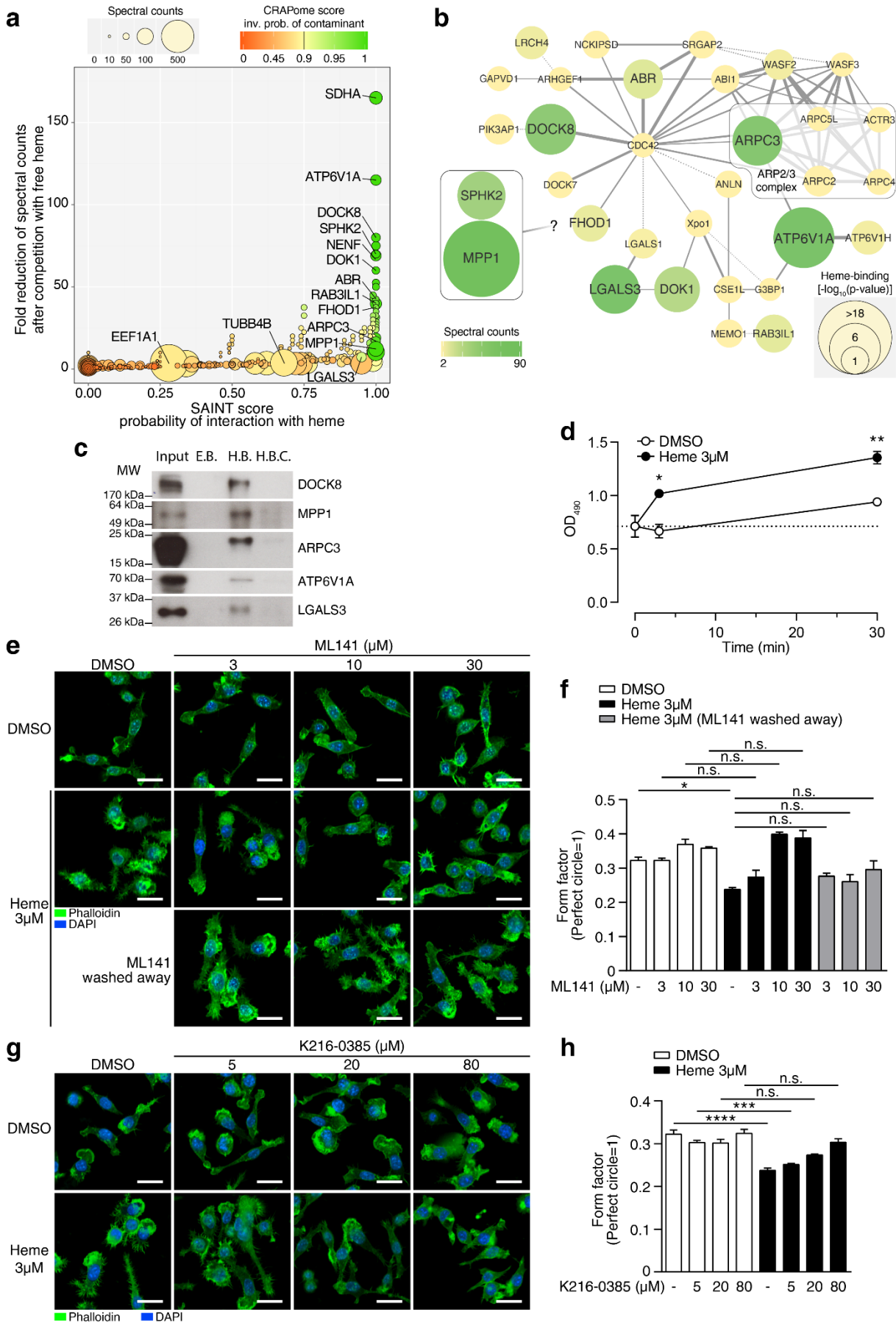
Heme is an amphipathic molecule that can promote the generation of reactive oxygen species (ROS) via Fenton chemistry, thereby leading to membrane damage³¹. As such, the actin cytoskeleton rearrangements induced by heme could be triggered by calcium influx following membrane damage, receptor signaling or ROS sensing. Heme-treated RAW264.7 macrophages cultured in the absence of extracellular calcium or in the presence of a ROS scavenger showed cytoskeleton remodeling that was similar to that of heme-treated positive controls (**Supplementary Fig. 5a-d**), indicating that heme-induced effects on the cytoskeleton are independent of ROS or receptor-triggered calcium signaling.

To decipher the signaling pathways underlying the cytoskeleton changes induced by heme, we incubated lysates of RAW264.7 macrophages with control (empty) or heme-agarose beads and identified binding proteins by liquid chromatography-mass spectrometry (**Supplementary Fig. 6a**). High-affinity interactions were discriminated from abundant or low-affinity interactions by competition with free heme. Binding proteins were scored according to their affinity to heme using the algorithms SAINT³² and CRAPome³³, as well as the fold reduction in spectral counts following competition with excess heme (**Fig. 6a**). Using the STRING database of known and predicted protein-protein interactions³⁴, we generated an interaction network involving various proteins that are known to interact with, or activate, the small GTPase Cdc42, an intracellular signaling regulator, as well as members of the ARP2/3 and WAVE actin cytoskeleton regulator complexes (**Fig. 6a,b**). The heme-association of several candidate proteins in this network was validated by affinity purification with heme-agarose beads, followed by western blotting (**Fig. 6c**).



Publication figure 5 - Heme interferes with actin cytoskeleton-dependent functions. **(a,b)** Migration of BMDM treated with control (DMSO) or heme, as measured by wound closure (scratch) assay ($n = 5$ technical replicates per condition and time point). Scale bars represent $200 \mu\text{m}$. **(c,d)** Dendritic cell migration in a three-dimensional collagen matrix in response to a CCL19 chemokine gradient. Data in **c** represent the tracks and corresponding distances (px) for 100 randomly selected tracks for each condition (upper panels). Lower panels represent track directionality and are presented as a wind rose plot of the number of tracks in a 33° angle from the center of each bin (36 bins, 10° each). Data in **d** are presented as the nonlinear regression for each condition plus the mean \pm s.e.m. for each measurement in each condition. Data in **a** and **b** are representative of two independent experiments. Data in **c** and **d** are pooled from three independent experiments. Data in **b** are presented as mean \pm s.e.m.; two-way ANOVA with Tukey's multiple comparison test (**b**); $****P \leq 0.0001$.

Cdc42 is involved in cell motility and phagocytosis, but is mainly recognized as being a central node in the formation of lamellipodia and filopodia at the leading edge³⁵. Consistent with the observation that heme-treated macrophages rapidly altered their cell shape and concomitantly formed numerous filopodia, we investigated whether heme leads to the activation of Cdc42 and/or ARP2/3 in macrophages. Heme stimulation of RAW264.7 macrophages induced immediate Cdc42 activation for up to 30 min after stimulation (**Fig. 6d**), without inducing changes in total Cdc42 protein amounts (**Supplementary Fig. 6b**). Selective inhibition of Cdc42 with ML141 that allosterically inhibits nucleotide binding effectively blocked all heme-induced changes in cell shape, and this effect could be reversed by removal of ML141 by

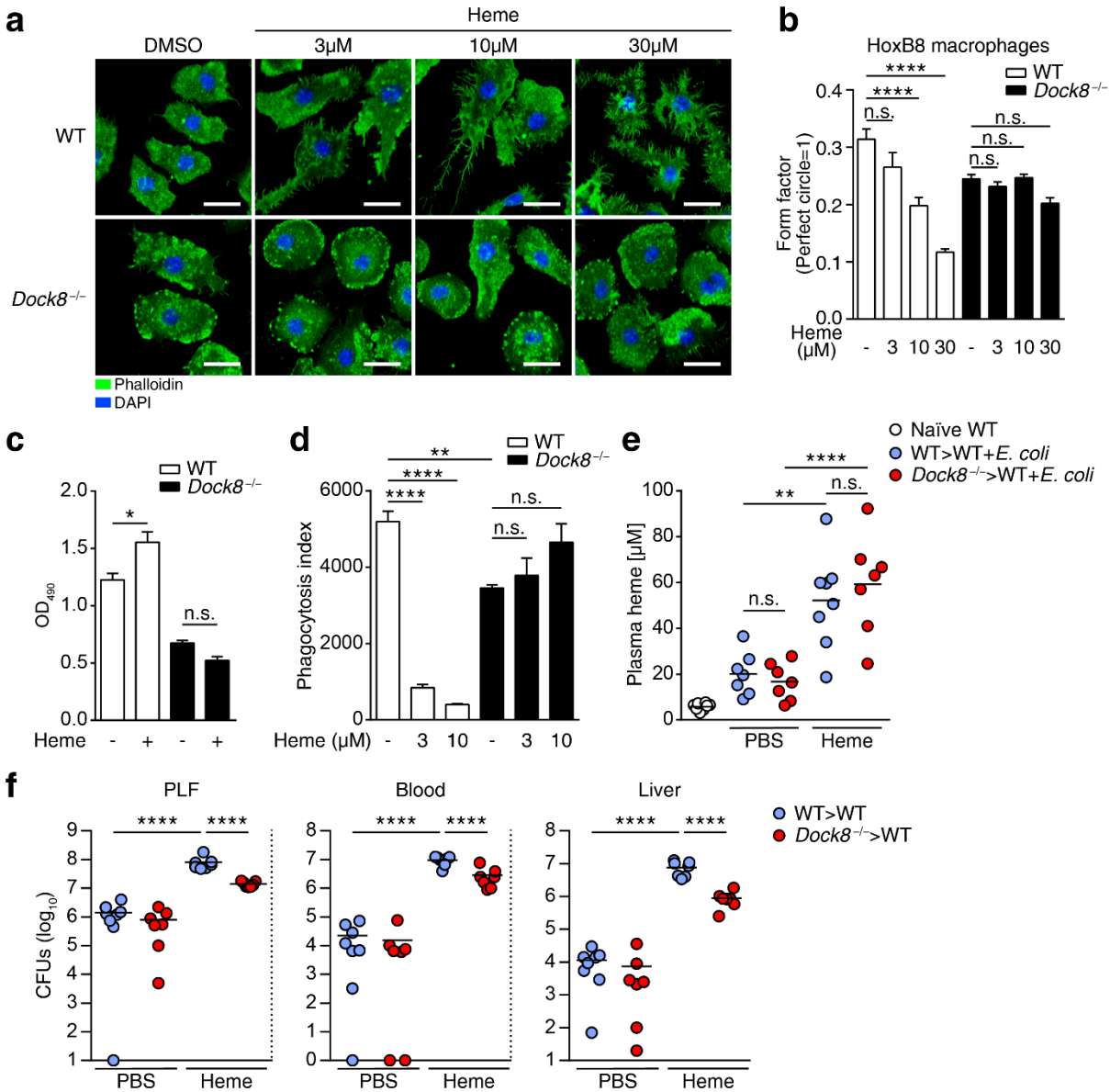


($n = 2$ replicates per experiment). **(b)** STRING database network analysis of heme-associated proteins from **a** that are involved in actin cytoskeleton remodeling. Edge thickness represents interaction confidence as reported by the STRING database v9.1. Solid edges indicate interactions reported for mouse, dashed edges indicate human ortholog projections. **(c)** Western blot validation of heme-associated proteins. E.B., empty beads; H.B., heme beads; H.B.C., heme beads, heme-competed sample. **(d)** Cdc42 G-LISA assay measuring the activation of Cdc42 in RAW264.7 macrophages treated with PBS or heme ($n = 3$ technical replicates per condition and time point). **(e,f)** Representative images of cellular morphology **(e)** of RAW264.7 macrophages pretreated with control (DMSO), ML141 (CDC42 inhibitor), or ML141 treatment and subsequent washing to remove ML141, and treated with control (DMSO) or heme for 15 min, and automatic quantification of form factor **(f)** ($n = 4$ random fields per condition; see automatic quantification of cell area in **Supplementary Fig. 7b**). **(g,h)** Cellular morphology **(g)** of RAW264.7 macrophages pretreated with control (DMSO) or K216-0381 (mDIA2 inhibitor), and treated with control (DMSO) or heme for 15 min, and corresponding automatic quantification of form factor **(h)** ($n = 4$ random fields per condition). Data in **a** and **b** are based on two independent experiments for each condition. Data in **c–f** are representative of two independent experiments. Data in **d**, **f** and **h** are presented as mean \pm s.e.m. Two-way ANOVA with Tukey's multiple comparison test **(d)**, one-way ANOVA with Tukey's multiple comparison test **(f,g)**; n.s. = not significant, $*P \leq 0.05$, $**P \leq 0.01$, $***P \leq 0.001$, $****P \leq 0.0001$. Scale bars represent 20 μm .

washing before heme treatment (**Fig. 6e,f** and **Supplementary Fig. 6c,d**). Consistent with the essential role of ARP2/3 in the formation of lamellipodia³⁵, specific inhibition of the ARP2/3 complex with CK666 that stabilizes ARP2/3 in its inactive conformation blocked heme-induced lamellipodia, but not filopodia, formation (**Supplementary Fig. 6c,e,f**). As a control, CRISPR-targeted deletion of the cytoskeleton signaling protein MPP1 or the cell-adhesion mediator galectin 3 (LGALS3) in RAW264.7 macrophages, which we identified as heme-associated proteins that are not known to interact with Cdc42 (**Fig. 6b**), did not prevent heme-induced actin cytoskeleton reorganization compared with wild-type cells (**Supplementary Fig. 6g,h**). We therefore focused on Cdc42-induced filopodia formation, which can be elicited via the activation of the actin nucleator mDIA2 (ref. 36). Inhibiting mDIA2 using its specific inhibitor, K216-0385, fully abrogated heme-induced filopodia extension (**Fig. 6g,h** and **Supplementary Fig. 6c**).

DOCK8, a member of the atypical guanine nucleotide exchange factor family that has been reported to specifically activate Cdc42 (ref. 37), was among the proteins with highest affinity for heme (**Fig. 6a–c**). To test the role of DOCK8 in mediating heme-induced actin cytoskeleton changes, we used BMDMs generated from wild-type and *Dock8*^{-/-} bone marrow progenitors immortalized via estrogen receptor-driven HoxB8 expression (ER-HoxB8 BMDM). In contrast with wild-type ER-HoxB8 BMDMs, *Dock8*^{-/-} ER-HoxB8 BMDM did not spread or extend filopodia (**Fig. 7a,b**), and failed to activate Cdc42 following treatment with heme (**Fig. 7c**), indicating that DOCK8 was essential for heme-induced activation of Cdc42. Of note, stimulation with the unrelated Cdc42 activator bradykinin led to cell shape changes in both wild-type and *Dock8*^{-/-} ER-HoxB8 macrophages (**Supplementary Fig. 7a**), indicating that the

lack of heme-induced filopodia extensions in the absence of DOCK8 was not a result of intrinsic cytoskeletal defects. Consequently, *Dock8*^{-/-} BMDMs were protected from the inhibitory effects of heme on phagocytosis of *E. coli*, as compared with their wild-type counterparts (**Fig. 7d** and **Supplementary Fig. 7b,c**).



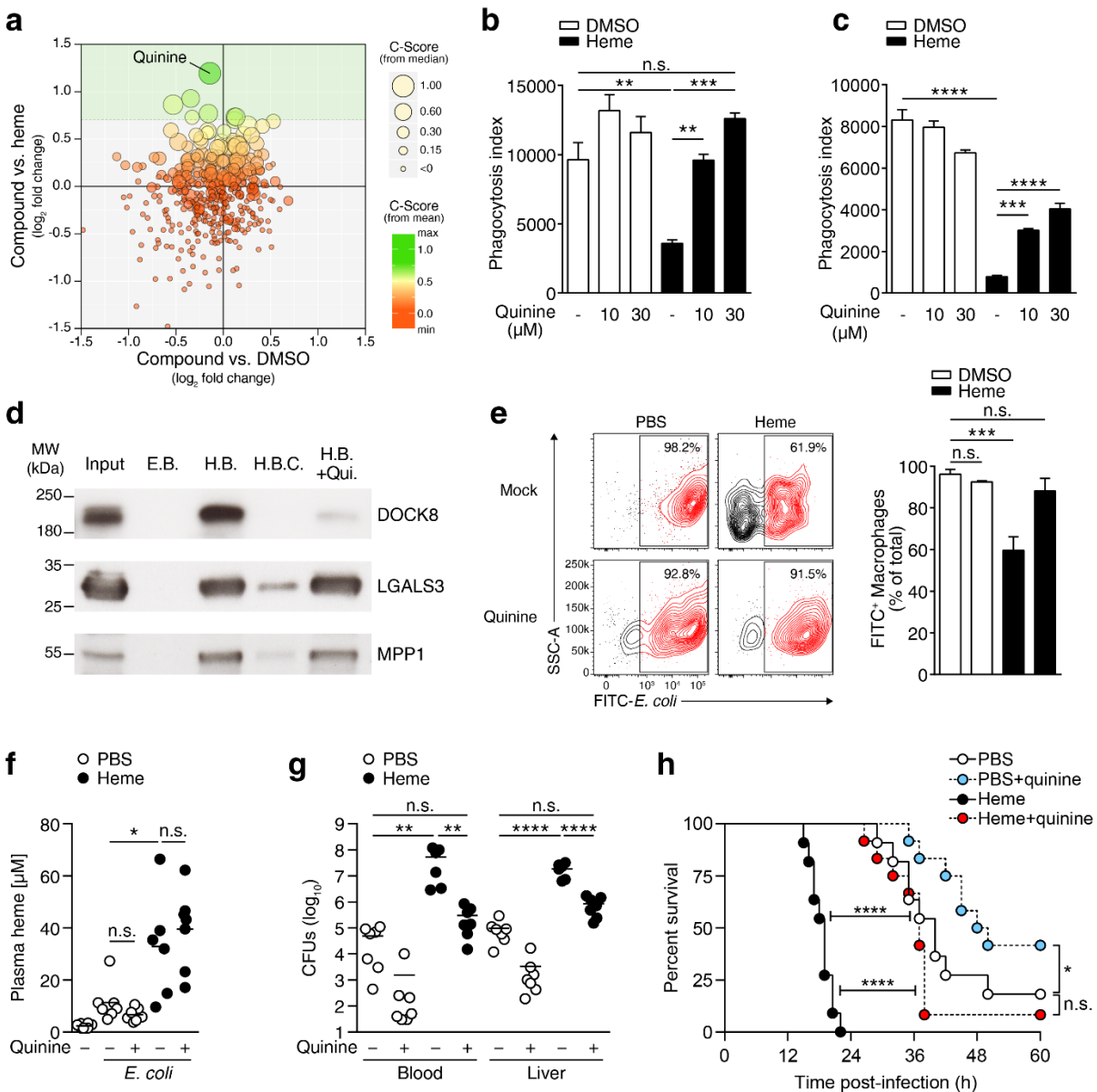
Publication figure 7 - DOCK8 mediates heme-induced actin cytoskeleton changes and suppression of phagocytosis. (**a,b**) Cellular morphology of WT and *Dock8*^{-/-} HoxB8 macrophages (**a**) treated with control (DMSO) or heme for 15 min and corresponding automatic quantification of form factor (**b**) ($n = 4-8$ images per condition). Scale bars represent 20 μm . (**c**) Cdc42 G-LISA assay measuring the activation of Cdc42 in WT and *Dock8*^{-/-} HoxB8 macrophages treated with PBS or heme (10 μM) for 10min ($n = 3$ technical replicates per condition). (**d**) Phagocytosis of FITC-*E. coli* by WT and *Dock8*^{-/-} BMDM pretreated with control (DMSO) or heme ($n = 4$ technical replicates per condition), analyzed by flow cytometry. (**e,f**) Plasma heme levels (**e**) of naive WT mice ($n = 8$) or WT>WT and *Dock8*^{-/-}>WT bone marrow chimeras pretreated with PBS ($n = 7-8$) or heme ($n = 7$) and respective bacterial counts (**f**) 16 h after infection with *E. coli*. Data in **a**, **b** and **d** are representative of two independent experiments. Data in **b-d** are presented as mean \pm s.e.m. and data in **e** and **f** are presented as mean, and dots represent individual animals. One-way ANOVA with Tukey's multiple comparison test (**b-f**), n.s. = not significant, * $P \leq 0.05$, ** $P \leq 0.01$, **** $P \leq 0.0001$.

To assess whether DOCK8 deletion provides protection against the detrimental effects of heme on bacterial clearance during sepsis *in vivo*, we reconstituted lethally irradiated wild-type mice with wild-type (WT) or *Dock8*^{-/-} bone marrow to generate WT>WT and *Dock8*^{-/-}>WT bone marrow chimeras. After successful engraftment, as verified by the percentage of donor (CD45.2⁺) versus recipient (CD45.1⁺) leukocytes 6 weeks after reconstitution (**Supplementary Fig. 7d**), chimeric mice were treated with PBS or heme 30 min before *E. coli* infection. In spite of similarly elevated plasma heme levels in WT>WT and *Dock8*^{-/-}>WT chimeras following heme treatment (**Fig. 7e**), *Dock8*^{-/-}>WT chimeras were significantly protected against excess heme and showed a tenfold reduction in bacterial numbers in liver, blood and peritoneal cavity (**Fig. 7f**). These results indicate that heme acts via DOCK8 to activate Cdc42, leading to dysregulated actin polymerization and impaired bacterial clearance (**Supplementary Fig. 7e**).

2.3.6. Quinine restores phagocytosis in vitro and in vivo

Because inhibition of cytoskeletal effector molecules such as DOCK8 or Cdc42 is not amenable as a therapeutic strategy because of the potential inhibitory effects on cell migration and phagocytosis³⁸, we sought to identify suitable compounds that could prevent the heme-induced inhibition of phagocytosis without affecting baseline phagocytosis of bacteria. To do so, we employed an automated screening platform and tested 389 compounds, including a library representing the variety of approved drugs with regards to their chemical structures and molecular targets. We used high-throughput automated microscopy to measure the phagocytosis efficiency of RAW264.7 macrophages pretreated with the compound library and incubated with heme or DMSO (**Supplementary Fig. 8a**), and scored the compounds on the basis of their efficacy at preventing heme-induced inhibition of phagocytosis (**Fig. 8a** and **Supplementary Fig. 8b**). The top performing drug identified was the antimalarial compound quinine, which fully restored phagocytosis in the presence of heme, without affecting baseline phagocytosis (**Fig. 8a** and **Supplementary Fig. 8b,c**).

Quinine pretreatment protected RAW264.7 macrophages (**Fig. 8b** and **Supplementary Fig. 8c,d**) and human macrophages (**Fig. 8c**) from heme-induced inhibition of phagocytosis and actin cytoskeleton changes (**Supplementary Fig. 8e,f**) compared with DMSO-treated cells. Notably, quinine diminished the association of heme with DOCK8 without affecting the association of heme with MPP1 or LGALS3 in RAW264.7 macrophages (**Fig. 8d**), suggesting that quinine exerted its protective effect by specifically disrupting the heme-DOCK8 association. To test the effects of quinine *in vivo*, we pretreated wild-type mice with PBS or heme, followed by mock or quinine treatment (60 mg/kg) before FITC-*E. coli* i.p. injection.



Publication figure 8 – Quinine restores phagocytosis of bacteria *in vitro* and *in vivo*. **(a)** Effect of compounds on phagocytosis of bacteria by RAW264.7 macrophages. Data are presented as the log₂ fold change in phagocytosis induced by each compound versus DMSO control (x axis) or versus heme (y axis). Bubble size and color represent the compound scores derived from the median and mean phagocytosis values, respectively. **(b,c)** Phagocytosis of FITC-*E. coli* by RAW264.7 macrophages **(b)** and human monocyte-derived macrophages ($n = 3$ technical replicates) **(c)** pretreated with control (saline) or quinine, and treated with control (DMSO) or heme as assessed by flow cytometry. **(d)** Western blot assessment of the influence of quinine on the association of DOCK8, LGALS3 or MPP1 to heme. E.B., empty beads; H.B., heme beads; H.B.C., heme beads, heme-competed sample; H.B.Qui., heme beads, quinine-competed sample. **(e)** *In vivo* phagocytosis of heat-killed FITC-*E. coli* by peritoneal macrophages (F4/80⁺CD11b⁺Ly6G⁻) from mice pretreated with mock (PBS) or quinine, and treated with PBS or heme ($n = 4$ mice per condition), and quantified as the percentage of FITC⁺ macrophages by flow cytometry (representative plots, left). **(f)** Plasma heme levels of naive WT mice ($n = 8$) or WT mice pretreated with mock (PBS) or 60mg/kg quinine, and treated with PBS or heme, and **(g)** respective bacterial counts 16 h post-infection with *E. coli* ($n = 7$ per group of infected mice). **(h)** Survival of WT mice pretreated with mock (PBS) or quinine, and treated with PBS or heme ($n = 11-12$ per group, quinine and heme dose as in **f** and **g**). Data in **b**, **d**, **f** and **g** are representative of two independent experiments. Data in **b**, **c** and **e** are presented as mean \pm s.e.m. Data in **f** and **g** are presented as mean, and dots represent individual animals; C-score analysis **(a)** (Online Methods), one-way ANOVA with Tukey's multiple comparison test **(b,c,e-g)**, Mantel-Cox test **(h)**; n.s. = not significant, * $P \leq 0.05$, ** $P \leq 0.01$, *** $P \leq 0.001$, **** $P \leq 0.0001$.

Quinine treatment abrogated the inhibitory effects of heme on bacterial phagocytosis by peritoneal macrophages (**Fig. 8e**), indicating that quinine could also restore macrophage phagocytosis *in vivo*. Following induction of *E. coli* peritonitis in wild-type mice, quinine treatment did not affect plasma heme levels, but did lead to a reduction in bacterial counts in blood and liver (**Fig. 8f,g** and **Supplementary Fig. 8g,h**), thereby restoring the bacterial clearance capacity of heme-treated mice. Notably, the dose of quinine that we used did not affect bacterial growth *in vitro* (**Supplementary Fig. 8i,j**). Finally, quinine-treatment of heme-treated mice significantly improved survival compared with heme-treated mice that received mock treatment (**Fig. 8h**), indicating that quinine treatment prevented the detrimental effects of exogenous heme administration. Furthermore, quinine treatment also improved the survival of PBS-treated mice compared with mock treatment of PBS-treated mice (**Fig. 8h**). These results indicate that quinine prevents the harmful effects of endogenously elevated heme in the course of Gram-negative bacteria-induced sepsis.

2.4. Discussion

We found that heme released in the course of hemolysis is a critical factor for driving bacterial outgrowth via the disruption of host resistance mechanisms, as it interferes with phagocyte cytoskeletal dynamics. Earlier observations of increased infection rates in the presence of iron, heme, hemoglobin and related compounds have commonly been ascribed to the nutritional benefit of increased iron availability for bacteria^{20,39}. In fact, iron withholding is a widely accepted immune mechanism for restricting bacterial growth by limiting iron bioavailability⁴⁰. Consistent with the notion that all bacterial pathogens are able to circumvent nutritional immunity²⁵, our data indicate that the iron requirement for bacterial growth is met in the course of infection, independent of heme-iron acquisition by the pathogen *in vivo*.

Efficient pathogen removal greatly relies on phagocytosis by macrophages as a first line of defense⁴¹. Following phagocytic receptor engagement, precise signaling triggers local cytoskeletal rearrangements that allow the engulfment of bacteria²⁸. We discovered that this process was disrupted by excess heme, thereby creating a permissive host environment for bacterial infections and sepsis. Given the importance of phagocytosis, it is not surprising that pathogens have evolved means to avoid internalization, often by manipulating the host cell cytoskeleton⁴². In fact, some pathogens directly target Cdc42 activity to prevent phagocytosis in a manner analogous to our findings⁴². It is therefore conceivable that the evolution of erythrocyte-lysing toxins, such as alpha-hemolysin, provide an important means of evading host defense by inducing heme release. As such, our findings provide a new perspective on the role

of these toxins during bacterial infections, independent of their proposed role as a means to increase iron availability. Another aspect to consider relates to the generation of bioactive molecules as a result of heme catabolism by HO-1. Particularly, carbon monoxide (CO) has been implicated as an immunomodulatory second messenger that is able to prime macrophages for increased bacterial killing via indirect NLRP3 inflammasome activation⁴³. This suggests that CO could help to reduce the deleterious effects of excess heme on host resistance.

Our finding that DOCK8 is necessary for the cytoskeleton changes and disruption of bacterial phagocytosis by heme is consistent with recent studies showing that DOCK8 regulates dendritic cell migration via Cdc42 (refs. 37,44). We speculate that heme stimulates DOCK8 guanine nucleotide exchange factor activity, either directly or indirectly via a DOCK8-containing protein complex. Although it is unlikely that this association is relevant under homeostasis, exhaustion of heme-scavenging proteins following severe hemolysis^{7,8} might render it especially important for bacterial infections. As such, *Dock8*^{-/-}>WT chimeric mice were protected from elevated heme during sepsis. However, the improved bacterial clearance in the absence of DOCK8 was incomplete and likely represents a tradeoff between beneficial effects of DOCK8 deletion following hemolysis and inevitable immune defects caused by DOCK8 deficiency^{37,45}. Nevertheless, the net gain in resistance against bacteria further reinforces the relevance of this mechanism during bacterial sepsis. DOCK8 is an intracellular protein that is thought to be anchored to the cell membrane, where it controls cell movement and shape⁴⁶. Thus, understanding precisely how heme gains access to the cytoplasm of innate immune cells could prove to be useful for therapeutic strategy developments, and might be attainable by complexing extracellular heme or by targeting heme transporters to prevent heme internalization.

The effects of excess heme on host resistance that we identified surprised us, considering the weight malaria has had in shaping the human genome. However, it is important to recognize that these events occur mainly following systemic inflammation or in people with homozygous sickle hemoglobin, where even highly conserved mechanisms to scavenge and degrade heme are overwhelmed⁹. It is reasonable to speculate that the need to mitigate the effect of excess heme on vital organs is such that it takes priority over host defense mechanisms, especially given the fact that both functions are essentially coordinated by macrophages.

Rising antibiotic resistance and widespread prophylactic antibiotic use have created an urgent need for new therapeutic strategies. As a proof of concept, we found that quinine treatment was able to prevent cytoskeletal changes and phagocytosis inhibition induced by heme. Quinine is

a long-standing antimalarial drug, whose mechanism of action is not fully understood, although it has been reported that quinine forms complexes with heme⁴⁷, indicating that quinine might interfere with the association of heme with DOCK8 through steric hindrance. This is important, as targeting heme effects upstream of Cdc42 signaling should conserve its normal function. Our results with quinine suggest that adjuvant immunotherapy strategies focused on restoring host resistance are a viable alternative to fighting the increased infection rates resulting from hemolysis.

Taken together, our findings uncover an unexpected effect of heme on the innate immune response and pave the way toward future therapeutic approaches. This could have far-reaching implications, not only for patients with inherited hemolytic disorders, but also for patients with acquired hemolysis, such as malaria, systemic inflammation and sepsis.

2.5. Online methods

Mice

Sex- and age-matched 8–10-week old WT C57BL/6, *LysM-Cre*^{-/-}*Hmox1*^{fl/fl} and littermate *LysM-Cre*^{+/-}*Hmox1*^{fl/fl} mice were used. All mice were kept in SPF conditions, with 12-h light/dark cycle, unrestricted access to food and water, and environmental enrichment. For bone marrow transplant and bone marrow macrophage generation experiments, healthy female WT C57BL/6 and *Dock8*^{-/-} mice were used⁴⁴. All *in vivo* experiments were performed in accordance with Austrian law and after approval by the Institutional Review Board of the Medical University of Vienna and the Austrian Ministry of Sciences (BMWF-66.009/0277-II/3b/2013).

Reagents and ELISA

Heme (hemin), hemoglobin, quinine (quinine hydrochloride dihydrate), 2,2'-bipyridyl, Ammonium iron (III) citrate, Iron (II) sulfate, neutral red, CK666, ML-141, *E. coli* O55:B5 lipopolysaccharide (LPS), phenylhydrazine, *N*-acetyl-*L*-cysteine, trichloroacetic acid, bathophenanthroline disulfonic acid, ascorbic acid, staurosporine, estradiol, bradykinin, DAPI, phalloidin-TRITC, Hoechst 33258 and hemin-agarose were from Sigma. PPIX (protoporphyrin IX, Frontier Scientific), SnPPIX (tin protoporphyrin IX, Santa Cruz Biotechnology), deferoxamine (Desferal, Novartis), DMSO (CryoSure DMSO, WAK – Chemie Medical GmbH), K216-0385 (ref. 48) (ChemDiv), cytochalasin D (Calbiochem), phalloidin-Alexa Fluor 633 and CellMask Orange (Life Technologies), rhM-CSF, and IL-3 (PeproTech), GM-CSF and IL-6 (eBioscience), TMB substrate (Thermo Scientific)

For flow cytometry Ly-6G-PE or PE/Cy7 (clone 1A8), CD11c-APC or PerCP/Cy5.5 (N418), F4/80-PE/Cy7 or FITC (BM8), CD45.1-APC (A20), CD45.2-PerCP/Cy5.5 (104), CD11b Pacific blue (M1/70), CD19-Brilliant Violet 605 or PE (6D5), and Ly-6C-Brilliant Violet 605 (HK 1.4) were from BioLegend. CD3-APC (17A2), B220-PerCP-Cy5.5 (RA3-6B2), CD11b-Alexa Fluor 700 (M1/70), Fixable Viability Dye eFluor 780 were from eBioscience. CD3e-V500 (500A2), CD11c-FITC (HL3), CD45-V500 (30-F11) were from BD biosciences. ELISA kits for mouse KC, MCP-1, TNF and IL-6 were from R&D Systems. For Western blot analysis, rabbit polyclonals against DOCK8 (#11622-1-AP; 1:750), MPP1 (#14715-1-AP; 1:500), ARPC3 (#14652-1-AP, 1:1000), ATP6V1A (#17115-1-AP, 1:750), and Galectin-3 (LGALS3) (#14979-1-AP; 1:750) were from Proteintech. Anti-beta-actin antibody (AC-15, Sigma; 1:3000), anti Cdc42 (4B3, Cytoskeleton; 1:500); goat anti-rabbit IgG, HRP-linked antibody (#7074, Cell Signaling; 1:1000) and goat anti-mouse IgG (H+L), HRP-linked antibody (#170-6516, Bio-Rad; 1:1000) were used. All flow cytometry analysis was done using FlowJo (v10).

Cell isolation, stimulation and culture

Peritoneal macrophages were obtained from the peritoneal lavage fluid of WT mice, resuspended in RPMI-1640 supplemented with 10% FCS and penicillin/streptomycin (pen/strep). Bone marrow cells were collected from tibia and femur of WT and *Dock8*^{-/-} mice and differentiated in RPMI-1640 with 10% FCS, pen/strep and 10% L929 conditioned medium for 7 d to generate BMDMs, or GM-CSF (20ng/ml) for 8 d and 24 h with *E. coli* LPS (200ng/ml) to generate BMDC. DOCK8 deficient precursor cell line and control cell lines were generated by HoxB8 induced conditional immortalization as previously described⁴⁹. Briefly, bone marrow of *Dock8*^{-/-} and WT mice was suspended in RPMI-1640 with 10 ng/ml IL-3, 20 ng/ml IL-6 and 1% supernatant of an SCF producing cell line for 2 d, followed by 5% FLT3 supernatant and 1 μM estradiol and spin infected with retrovirus encoding estrogen inducible ERHBD-HoxB8 (ref. 49). Mouse neutrophils were collected from peritoneal exudates of mice 4 h after thioglycollate treatment, purity >90% was confirmed by Giemsa-stained cytopins. RAW264.7 macrophages (ATCC TIB-71) were maintained in RPMI-1640 with 10% FCS and pen/strep.

Human neutrophils and monocytes were isolated from peripheral blood from healthy donors (after obtaining informed consent from all donors) via OptiPrep density gradient centrifugation (Axis-Shield). Human monocytes were differentiated into human monocyte-derived macrophages (hMDM) in RPMI-1640, 10% FCS, pen/strep and rhM-CSF (10 ng/ml) for 7 d. BMDM, PM, hMDM or RAW264.7 macrophages were allowed to adhere for 3 h before stimulation. Heme (hemin) and PPIX stocks for *in vitro* studies were prepared to 10 mM in

DMSO, stored at -20°C and used within 3 months. SnPPiX and hemoglobin stocks were prepared to 5 mM in PBS. All porphyrin and hemoglobin stimulations were done 15 min before the assay, unless otherwise indicated. Cell lines were routinely checked for *Mycoplasma* contamination.

Bone marrow transplant

Bone marrow chimeras were generated as described before⁵⁰. Briefly, 8-week-old WT recipient mice were lethally irradiated and 5×10^5 bone marrow cells from WT or *Dock8*^{-/-} mice were retro-orbitally injected. 6 weeks later successful engraftment was verified using flow cytometry using the following gating strategy: neutrophils: CD11b⁺, Ly6G⁺; T-cells: CD11b⁻, CD3⁺, CD19⁻; B-cells: CD11b⁻, CD3⁻, CD19⁺; monocytes: CD11b⁺, Ly6G⁻; macrophages: CD3⁻, CD19⁻, F4/80⁺; DCs: CD3⁻, CD19⁻, F4/80⁻, CD11c⁺. Distinction between donor and recipient cells was assessed by CD45.1 or CD45.2 variant expression.

E. coli and sterile peritonitis models

Murine peritonitis was induced as previously described⁵⁰. Briefly, *E. coli* (strain PMV-1, serotype O18:K1)^{51,52} or its isogenic mutants (**Supplementary Table 1**) were cultured in Luria-Bertani medium and mice were infected via i.p. injection with $\sim 10^4$ colony-forming units (CFU) in 200 μl . Where indicated, mice received 100 μl i.p. of PBS, heme (25 $\mu\text{mol/kg}$ body weight) or ammonium iron (III) citrate (25 $\mu\text{mol iron/kg}$ body weight) 30 min before infection with *E. coli*. Heme stock solutions for *in vivo* administration were prepared by dissolving hemin to 5 mM in 0.2M NaOH, pH 7.5 and stored at -80°C . Quinine-treated mice were given one dose (6-h end point) or two doses (16-h end point) 1 h before and 6 h after infection, respectively (60 mg/kg each dose). Serial dilutions of tissue samples were plated to enumerate viable bacteria. In survival studies mortality was monitored every 1 to 2 h. LPS endotoxemia was induced by i.p. injection of *E. coli* LPS (40 mg/kg). For thioglycollate peritonitis, mice were pretreated PBS or heme as described above before injection of 1ml 4% thioglycollate broth⁵³. Blood and peritoneal lavage fluid were collected 6 h post-injection and cell influx into the peritoneal cavity was assessed on cytospin preparations stained with Giemsa, and via flow cytometry (LSRFortessa). Cells were gated on viable CD45⁺ cells and further gated as: neutrophils: Ly6G⁺ CD11b⁺, F4/80⁻, CD3⁻, CD19⁻, and macrophages: F4/80⁺, CD11b⁺, Ly6G⁻, CD3⁻, CD19⁻.

L. monocytogenes infection model

Mice were infected by intraperitoneal injection of 10^6 CFU genetically optimized *L. monocytogenes* strain LO28InIA*⁵⁴. The bacteria were prepared as previously described⁵⁵. For

detection of bacterial loads (CFU assays), mice were sacrificed at the indicated time points, spleens were homogenized and plated on Oxford agar plates for 24 h at 37 °C.

Heme and total liver iron measurements

Plasma levels of heme were measured using its pseudoperoxidase activity as described earlier⁵⁶. Briefly, standard dilutions and samples were diluted in PBS 1% BSA, incubated with TMB substrate and absorbance was measured at 450 nm. Additionally, concentration of standard dilutions was confirmed using the heme-chromogen method⁵⁷, and calculated using Beer's law⁵⁷.

Total liver iron levels were measured as previously described⁵⁸, with the following modifications to detect total iron levels. Briefly, 100 µl (= 20 mg tissue) of liver homogenate were hydrolyzed at 65 °C with 50 µl TCA-HCl solution (16 h), and boiled 1 h at 120 °C to release heme. Clarified samples were incubated with sodium acetate, bathophenanthroline disulfonic acid and ascorbic acid solution for 5 min at RT (21-23°C), absorbance was measured at 540 nm and iron concentration was calculated using $[Fe] = ((A_s - A_b) \times V \times MW) / ((e \times l \times t))$, (A_s : sample absorbance, A_b : blank absorbance, V : volume, MW : molecular weight of iron, e : milimolar absorptivity of bathophenanthroline disulfonic acid, l : path length and t : weight of tissue). Measured concentrations were verified against standard samples with known iron concentrations.

Cloning and bacteria

The *E. coli* dppC gene was deleted using a recombineering approach as described previously⁵⁹. λ-RED plasmid pSIM8 was electroporated into *E. coli* (PMV-1) and the kanamycin resistance gene was PCR-amplified from *E. coli* TKC with the primer set DppC_Kan_For-DppC_Kan_Rev, with 45bp homology arms flanking the dppC gene. Amplicon was electroporated into induced PMV-1-pSIM8 *E. coli*. Correct substitution of dppC by nptII was verified by PCR using the primer set DppC_R1-_For-DppC_R1-_Rev. pSIM8 plasmid was cured and functional dppC deletion was verified by loss of heme-iron utilization (**Supplementary Fig. 1j**) generating $\Delta dppC::Kan^R$ *E. coli*. The hemolysin operon from *E. coli* CFT073⁶⁰, including its upstream regulatory elements⁶¹, was PCR-amplified using primer set Hly_NotI_For-Hly_XhoI_Rev, double-digested with NotI-HF and XhoI and ligated to mini-Tn7 plasmid pGRG36 (ref. 62) to generate pRM24. pRM24 was electroporated into PMV-1 *E. coli*. Insertion of the hemolysin operon onto the *E. coli* attTn7 site was confirmed using the primer sets attTn7_Left_For-attTn7_Left_Rev and attTn7_Right_For-attTn7_Righ_Rev. the plasmid was cured to generate *E. coli* $hly_{ABCD}::attTn7$ (see **Supplementary Tables 1–3**).

CRISPR-Cas9-mediated gene deletion

Mouse *Mpp1* and *Lgals3* genes were deleted in RAW264.7 macrophages using CRISPR-Cas9 system⁶³. Briefly, Cas9 and sgRNA expressing plasmids were generated by digesting the pSpCas9(BB)-2A-Puro (pX459) vector⁶³ with BbsI (New England Labs). Unphosphorylated oligos targeting exon 1 of *Mpp1*, (oligo pair *Mpp1_del_For-Mpp1_del_Rev*) or exon 2 of *Lgals3* (oligo pair *Lgals3_del_For-Lgals3_del_Rev*) were annealed and ligated to linearized vector to generate pX459-*Mpp1_exon1* and pX-459-*Lgals3_exon2*. Resulting plasmids were sequenced using the primer U6_CRISPR_Seq2 to verify the correct ligation of the vector and targeting oligos. RAW264.7 macrophages were plated overnight and transfected with 3.5 µg of each plasmid using Lipofectamine LTX with PLUS reagent (Life Technologies). Puromycin selection (7.5 µg/ml) was started 24 h after transfection, stopped 24 h. After 4–5 d, single-cell cultures were made and individual colonies picked after 10 d for sequencing (*Mpp1_Seq* and *Lgals3_Seq*). Lack of *Mpp1* and *Lgals3* expression was validated by WB.

In vitro bacterial growth assays

Bacteria were cultured in LB medium or minimal salts medium M63 at 37 °C or 32 °C (pSIM8) for the indicated times. LB medium was supplemented with DMSO, or heme plus deferoxamine (DFO) where indicated. M63 medium was supplemented with FeSO₄ (1.8 µM), or 30 µM heme plus 200 µM 2,2'-bipyridyl (bip) to chelate residual iron. Bacteria were enumerated by plating serial dilutions on blood-agar plates.

Bacterial killing assay

Bacterial killing assays were performed as described earlier⁶⁴ using adherent RAW264.7 macrophages (2.5×10^5) that were incubated with mid-log phase *E. coli* PMV1 at MOI 80. Serial dilutions of lysates were plated on blood agar plates to quantify viable CFU, the percentage of killed bacteria was calculated: (CFU ($t = 0$ min) – CFU ($t = x$)).

Phagocytosis, efferocytosis assays

Phagocytosis and efferocytosis assays were done essentially as described earlier⁶⁵. To assess bacterial phagocytosis, $2.5\text{--}5 \times 10^5$ respective macrophage subsets were allowed to adhere for 3 h. 5×10^5 human and mouse neutrophils were placed in round bottom tubes in RPMI-1640. All cells were pretreated with DMSO or heme (15 min) after which FITC-labeled heat-killed *E. coli*, *S. pneumoniae* or *P. aeruginosa* were added (MOI 100) and incubated at 37 °C for 0.5–1 h (except where indicated). For neutrophils, FITC-labeled *E. coli* PMV-1 were pre-opsonized with 15% autologous serum. Negative controls were incubated at 4 °C during the same period.

Adherent macrophages were washed and incubated with proteinase K (50 µg/ml) at 4 °C to remove adherent bacteria, neutrophils were incubated with trypan blue to quench fluorescence of non-internalized bacteria. Uptake of bacteria was assessed via flow cytometry, the phagocytosis index was calculated as (MFI × % positive cells at 37 °C) minus (MFI × % positive cells at 4 °C).

Efferocytosis was assessed essentially as above and described earlier⁶⁵ using RAW264.7 macrophages and CFSE-labeled apoptotic thymocytes (MOI 10) that were incubated at 37 °C for 1 h, and stained with CD11c-APC. Uptake of apoptotic cells was analyzed via flow cytometry (FACScalibur), and calculated as (MFI × %CD11c⁺, CFSE⁺ cells at 37°C) – (MFI × %CD11c⁺, CFSE⁺ cells at 4°C). FITC-labeled bacteria and CFSE-labeled apoptotic cells were prepared as described earlier⁶⁵.

For human whole blood phagocytosis assays, venous blood was collected from healthy donors into EDTA tubes and used as described⁶⁶. Briefly, 100µl undiluted blood was placed in sterile 5-ml tubes and DMSO, heme or phenylhydrazine (125 µg/g) added for 15 min, followed by FITC-labeled *E. coli* (MOI 50) for 20 min. To assess the background FITC-fluorescence from non-internalized bacteria cytochalasin D was added (10 µM) to control tubes. Erythrocytes were lysed using erythrocyte lysis buffer (Qiagen) and cells were stained with Alexa Fluor 700-CD11b and analyzed via flow cytometry. Neutrophils and monocytes were identified as CD11b⁺, SSC^{high} and CD11b⁺, SSC^{low} cells, respectively. The phagocytosis index was calculated as ((MFI × % positive cells) minus (MFI × % positive cells from cytochalasin D treated tubes)).

To test the uptake of live *L. monocytogenes*, adherent BMDM were pre-treated with 10µM heme or DMSO for 15 min before adding live *L. monocytogenes* (MOI 10) for 1h, followed by gentamycin treatment to kill non-internalized bacteria. Cell lysates were plated on Oxford-Agar plates and the colonies counted the next day.

Confocal phagocytosis and binding assay

Phagocytosis was additionally measured using confocal microscopy. 5×10^4 macrophages were seeded on 8-well chambers (µ-slide, Ibidi) and allowed to adhere overnight. The cells were treated with DMSO or heme for 15 min, and in some experiments pretreated for 45 min with mock (PBS) or quinine. FITC-labeled *E. coli* were added (MOI 100) at 37 °C for 1 h, negative controls (and for bacterial binding analysis) were kept at 4 °C. The cells were then washed, fixed with 4% paraformaldehyde, permeabilized with 1% BSA, 0.1% Triton X-100 and stained

with DAPI (1 µg/ml, Sigma) and phalloidin (0.2 µg/ml) conjugated to either TRITC or Alexa Fluor 633. Where indicated, CellMask Orange was used at 0.5 µg/ml instead of phalloidin. Four to eight random fields per condition were imaged using a confocal microscope (LSM700, Zeiss) with a Plan-Apochromat 20×/0.8 M27 objective. Automatic image analysis was performed using the CellProfiler software⁶⁷ (<http://www.cellprofiler.org/>) which was programmed to: a) split images into DAPI, Phalloidin and FITC channels; b) load the channels into the pipeline and identify primary objects (nuclei, DAPI) using Otsu adaptive method with 2-class thresholding, minimized weighted variance and shape method to distinguish clumped objects; c) identify secondary objects (cytoplasm, TRITC or AF633) based on the primary objects (nuclei) identified before using the propagation method with 2-class Otsu global thresholding and minimized weighted variance; d) identify primary objects (bacteria, FITC) using the Otsu global method with 2-class thresholding; e) retrieve only the bacteria present within the cytoplasm of cells. Primary and secondary objects touching the image borders are excluded from analysis. The level of phagocytosis is expressed as the number of internalized bacteria per cell.

In vivo phagocytosis assay

Phagocytosis was assessed *in vivo* as described earlier⁶⁸. WT mice were treated i.p. with PBS or heme (25 µmol/kg body weight) 30 min before i.p. injection of heat-killed FITC-labeled *E. coli* (5×10^7). Peritoneal lavage fluid was harvested 90 min later and exudate cells stained for flow cytometry (LSRFortessa). The percentage of FITC⁺ macrophages (F4/80⁺, CD11b⁺, Ly6G⁻, CD3⁻, B220⁻) was assessed as a measure of bacterial uptake and compared to background FITC⁺ B-cells (CD3⁻, CD11b⁻, Ly6G⁻, F4/80⁻, B220⁺).

Cell death and viability assays

Cell death was assessed via LDH release using the CytoTox 96 Non-Radioactive Cytotoxicity kit (Promega) according to instructions from the manufacturer. Cell viability was assessed via the neutral red assay⁶⁹. Briefly, 7.5×10^4 adherent RAW264.7 macrophages were treated with DMSO, heme or staurosporine (10 µM; positive control) in RPMI for the indicated time points and cell viability was calculated as the percentage of the DMSO control absorbance for each treatment and time point.

Affinity purification

Affinity chromatography using commercially available hemin-agarose was performed as reported previously^{70,71} using 10 mg RAW264.7 macrophage total cell lysate as protein input in duplicates. Control and heme-competed lysates (pre-incubated lysates with heme) were

incubated with beads for 2 h at 4 °C. Beads were washed extensively with lysis buffer and bound proteins eluted with formic acid. After elution, enriched proteins were reduced with dithiothreitol, cysteine residues alkylated by incubation with iodoacetamide and the samples digested with modified porcine trypsin (Promega). 3% (and multiples thereof) of the digested eluates were purified and concentrated by C18 reversed-phase material for subsequent duplicate analysis by gel-free one-dimensional liquid chromatography mass spectrometry (1D-LCMS). Details of the LCMS methodology are as previously described⁷².

Protein identification

Peak extraction and conversion of RAW files into the MGF format for subsequent protein identification was performed with msconvert (ProteoWizard Library v2.1.2708). An initial database search was performed with broader mass tolerance to re-calibrate the mass lists for optimal final protein identification. For the initial protein database search, Mascot (www.matrixscience.com, version 2.3.02) was used. Error tolerances on the precursor and fragment ions were ± 10 ppm and ± 0.6 Da, respectively, and the database search limited to fully-tryptic peptides with maximum 1 missed cleavage, carbamidomethyl cysteine and methionine oxidation set as fixed and variable modifications, respectively. The Mascot peptide ion score threshold was set to 30, and at least 3 peptide identifications per protein were required. Searches were performed against the murine UniProtKB/SwissProt database (www.uniprot.org release 2012-05) including all protein isoforms.

The initial peptide identifications were used to deduce independent linear transformations for precursor and fragment masses that would minimize the mean square deviation of measured masses from theoretical. Re-calibrated mass list files were searched against the same murine protein database by a combination of Mascot and Phenyx (GeneBio, SA, version 2.5.14) search engines using narrower mass tolerances (± 4 ppm and ± 0.3 Da). One missed tryptic cleavage site was allowed. Carbamidomethyl cysteine was set as a fixed modification and oxidized methionine was set as a variable modification. To validate the proteins, Mascot and Phenyx output files were processed by internally-developed parsers. Proteins with ≥ 2 unique peptides above a score T1, or with a single peptide above a score T2 were selected as unambiguous identifications. Additional peptides for these validated proteins with score $> T3$ were also accepted. For Mascot searches, the following thresholds were used: T1 = 14, T2 = 40 and T3 = 10; Phenyx thresholds were set to 4.2, 4.75 and 3.5, respectively ($P < 10^{-3}$). The validated proteins retrieved by the two algorithms were merged, any spectral conflicts discarded and grouped according to shared peptides. A false discovery rate (FDR) of $< 1\%$ for protein

identifications and <0.1% for peptides (including the ones exported with lower scores) was determined by applying the same procedure against a database of reversed protein sequences.

Scoring of identified proteins

Analysis of heme-binding proteins identified by affinity purification and mass spectrometry was performed using the SAINT and CRAPome database bioinformatic tools^{32,33} using empty beads (E.B.) and heme beads, competed with free heme (H.B.C.) as controls. The probability distribution for the calculated CRAPome database scores was inverted to represent the likelihood of each interactor being a contaminant. Gene ontology analysis (DAVID)^{73,74} was used to select a subset of heme-binding proteins involved in the regulation of the actin cytoskeleton, cell and plasma membrane shape, motility, phagocytosis, and related terms. The resulting list was used for network analysis of interactions using the STRING database v9.1³⁴.

Automated chemical screen of phagocytosis

A panel of chemicals and drugs was tested using an automated high-throughput analysis of bacterial phagocytosis. Plate handling was performed using the cell::explorer platform (PerkinElmer). Briefly, 5×10^3 RAW264.7 macrophages were seeded on 384-well clear-bottom plates (4ti-0201 Vision plate, 4titude), allowed to adhere overnight, and a panel of compounds was transferred using an acoustic dispenser (Echo 520, Labcyte) at a final concentration of 10 μ M each and incubated for 3 h at 37 °C. Each condition was run in triplicates and each plate included 32 DMSO (compound) control wells. Each plate layout was prepared twice with one plate treated for 15 min with DMSO (heme control) and the other with 10 μ M heme (see **Supplementary Fig. 8a** for details). FITC-labeled heat-killed *E. coli* were added (MOI 100) for 1 h at 37 °C, and washed twice to remove adherent bacteria. Then cells were fixed (4% PFA), permeabilized and stained with DAPI (1 μ g/ml), phalloidin-TRITC (0.2 μ g/ml) and imaged using automated fluorescence microscopy with a LUCPlanFLN 20 \times NA = 0.45 objective (Operetta, PerkinElmer) and 5 random fields per well were acquired. The Harmony software (PerkinElmer) was then programmed to analyze each image by: a) Find nuclei in the DAPI channel using the M method; b) Find cytoplasm in the TRITC channel from the nuclei identified before using the A method; c) Find spots (bacteria) in the FITC channel within the cytoplasm identified before using the A method; d) calculate the number of spots (bacteria) identified per cell. The phagocytosis (bacteria/cell) from each image were compiled into matching wells and mean and median phagocytosis data from each compound was normalized to its respective plate control (DMSO or heme). The normalized values were log₂ transformed to obtain the log₂ fold change of phagocytosis induced by each compound in the presence of

DMSO or heme. To score the tested compounds (C-Score), the following formula was employed:

$$\frac{\log_2 \text{fold change}(\text{mean or median})_{\text{Heme}}}{1 + |\log_2 \text{fold change}(\text{mean or median})_{\text{DMSO}}|}$$

The resulting C-Scores obtained from mean or median values of phagocytosis for each compound were plotted against each other to estimate the data noise (**Supplementary Fig. 8b**). Compounds with \log_2 mean fold change (over heme) of phagocytosis >0.75 and C-scores >0.5 were considered as significantly restoring phagocytosis. Additionally, compounds for which the C-scores differed by more than 30% from the calculated linear regression were excluded (**Supplementary Fig. 8b**).

Cdc42 activation assay

The activation of Cdc42 was assessed using the Cdc42 G-LISA Activation Assay (Colorimetric format) kit as indicated by the manufacturer (#BK127, Cytoskeleton, Inc.). Briefly, adherent RAW264.7 or HoxB8 macrophages were serum-starved for 2 h before DMSO or heme was added for the indicated time points. Active Cdc42 signal was measured according to the instructions by the manufacturer and corrected for protein content.

Microscopy, image analysis and live cell imaging

For cell shape analysis, RAW264.7 macrophages, BMDM, human monocyte-derived macrophages and HoxB8 macrophages were seeded on 8-chamber slides (μ -slide, Ibidi) at a density of 5×10^4 per well and allowed to adhere overnight. The cells were washed twice with PBS and, where indicated, pretreated in RPMI with ML-141, CK666 or K216-0385 for 1 h, or *N*-acetyl-*L*-cysteine (NAC) for 30min. Where indicated, ML-141 was washed away after pretreatment and the cells were allowed 15 min to recover. The cells were then treated with DMSO, heme or bradykinin for 15 to 30 min. For calcium-influx experiments, the cells were treated with DMSO or heme for 15 min in DMEM or in DMEM lacking calcium (LifeTech). After stimulation, cells were fixed with 4% PFA and stained with DAPI (1 $\mu\text{g/ml}$) and phalloidin-FITC or phalloidin-TRITC (0.2 $\mu\text{g/ml}$). Four to eight random fields per well were acquired using a Zeiss LSM700 confocal microscope equipped with a Plan-Apochromat 20 \times /0.8 M27 objective. The images were loaded into the CellProfiler image analysis software and the pipeline was programmed to retrieve the cell shape parameters for the cell area, perimeter and form factor (circularity) as described earlier⁵⁶. For three-dimensional cell reconstruction Z-stacks were acquired using a Zeiss LSM780 confocal microscope equipped with a Plan-Apochromat 100 \times /1.4 Oil DIC M27 objective. Each slice was then deconvolved

using Huygens Professional (Scientific Volume Imaging) and the corresponding theoretical point spread function. The deconvolved Z-stacks were then used to generate three-dimensional animations of the cells using Huygens Professional SFP renderer module.

Live cell imaging of the actin cytoskeleton was performed using the LifeAct-GFP fusion construct⁷⁵ to generate LifeAct-GFP positive RAW264.7 macrophages (RAW^{LifeAct-GFP}). These were plated at a density of 7.5×10^4 cells/dish, allowed to adhere and stained with Hoechst 33258 (5 μ g/ml). Immediately before time-lapse image acquisition, DMSO, heme or PPIX (10 μ M) were added and cells were imaged every 25 s for 60 to 80 frames using a Zeiss LSM780 confocal microscope equipped with a Plan-Apochromat 40 \times /1.3 DIC M27 objective and an incubator chamber maintaining 37 °C and 5% CO₂.

Migration assays

BMDM motility was assessed using a wound-healing (scratch) assay. WT BMDM were seeded to near confluency onto 12-well plates (5×10^5 cells/well) and allowed to adhere for 3 h. The adherent confluent cell layer was scratched using a 10- μ l pipette tip and the cells washed twice to remove the cell debris. The cells were treated for 15 min with DMSO or heme (3 to 30 μ M) in RPMI-1640 and images of the scratches were collected at the indicated time points using phase-contrast on a DMI6000B inverted microscope (Leica) equipped with an N-Plan 10.0x-0.25 objective and a motorized xyz-stage. The images were loaded into CellProfiler software and image illumination correction functions were applied to each image. The intensity of the corrected images was normalized using ImageJ (v1.47) and the images loaded into the scratch assay analysis software TScratch⁷⁶. The remaining open areas were used to calculate the percentage of the initial open area, which the cells occupy at the different time points.

Cell movement toward a chemokine gradient was performed on collagen gel matrices. Mature BMDC were treated with DMSO or heme at the indicated concentrations in RPMI-1640 and 1.2×10^6 cells/ml were mixed with the collagen gel mix (1.6 mg/ml bovine collagen I, 3.5 mM NaHCO₃ and 1 \times MEM final concentrations) at a ratio of 2:1. The gel mix containing the cells were introduced into custom-made migration chambers (2 mm thick) and incubated for 45 min to allow the gel to polymerize. The polymerized gel chambers were overlaid with CCL19 (250 ng/ml in RPMI-1640, 10% FCS, 1%P/S) and gel images for each condition were simultaneously taken every 2 min for 6 h using a Zeiss Axiovert 40 CFL inverted microscope equipped with custom-built climate chambers (5% CO₂, 37 °C, humidified). The image stacks were loaded into the FiJi image analysis software⁷⁷ and individual cell movement was tracked using a custom plugin to calculate the cell migration index. Track coordinates were introduced onto

Ibidi Chemotaxis and Migration tool (http://ibidi.com/software/chemotaxis_and_migration_tool/) to retrieve centered coordinates and track directionality. Math software R (<https://www.r-project.org/>) with ggplot2 package (<https://cran.r-project.org/web/packages/ggplot2/index.html>) were then used to render both the track distance and wind rose plots.

Cell adhesion and rolling

Sterile Cellix Vena8 Endothelial+ Biochip capillaries were coated overnight with FNC coating mix (Athena enzyme). Immortalized human microvascular endothelial cells (G1S1) were seeded into each capillary and grown to confluence for 24 h at 37 °C under flow (400 µl/min) in EGM-2-MV medium containing 10ng/ml human TNF. Biochips were then attached to the Cellix Nanopump 2.0 and flushed with EGM-2-MV at 8 Dynes/cm². 50 µl of DMSO- or heme-treated (15 min) human monocyte cell suspensions (3.5×10^6 /ml) were loaded into the biochips and images were acquired with an inverted microscope (Zeiss Axiovert 200M) equipped with a CCD camera (Zeiss AxioCam MRc5) every second for 2 min with an exposure time of 344ms. Image sequences were analyzed for cell adhesion and rolling with the cell-tracking tool of Image Pro Plus software.

PCR and western blot

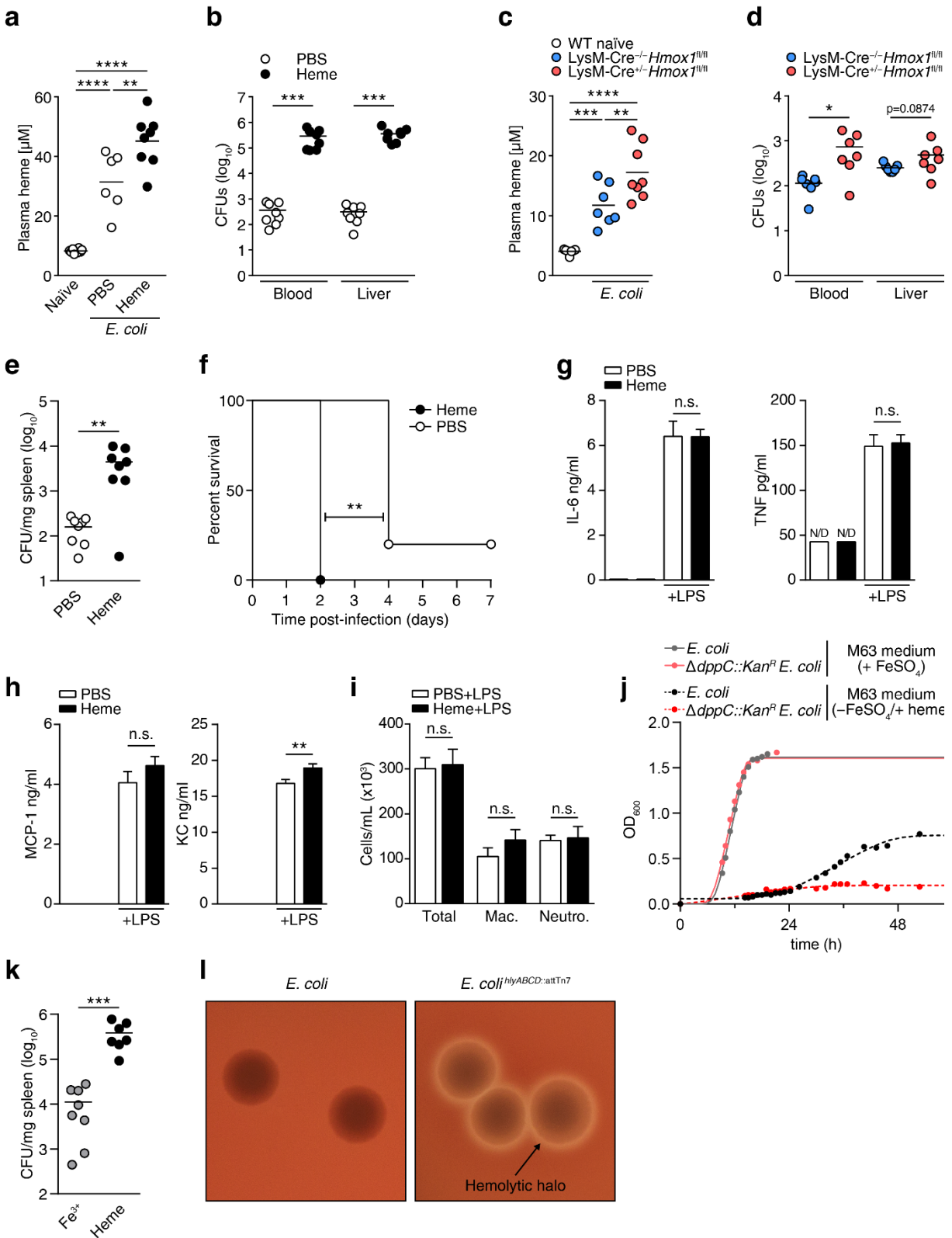
PCR was performed using Taq DNA polymerase, dNTPack (Roche life sciences), High Fidelity PCR Enzyme Mix (Thermo scientific) or Phusion High-Fidelity DNA polymerase (Thermo Scientific) according to instructions from the manufacturers. Primer sequences are indicated in **Supplementary Table 3**. For western blot analysis, cell lysates were prepared in RIPA buffer, mixed 1:1 with 2× SDS sample buffer and boiled for 5 min at 99 °C. Cell lysates or pull-down eluates were resolved in polyacrylamide gels, blotted onto PVDF membranes, and incubated overnight at 4 °C with anti-DOCK8, LGALS3, MPP1, ATP6V1A, ARPC3 antibodies (1:750), anti-CDC42 antibody (1:500) or anti-ACTB antibody (1:1,000), followed anti-rabbit IgG-HRP (1:1,000) or goat anti-mouse IgG (H+L)-HRP (1:3,000) and Amersham ECL Western Blotting Detection Reagent before developing. Some membranes were stripped using stripping buffer, washed and further stained as above.

Statistical analysis

Comparisons between groups were performed using unpaired, two-sided *t*-test for normally distributed data, or Mann-Whitney otherwise. For grouped comparisons, one-way or two-way ANOVA followed by Tukey's multiple comparisons analysis were used where appropriate. Data correlation was assessed using the Pearson product-moment correlation coefficient.

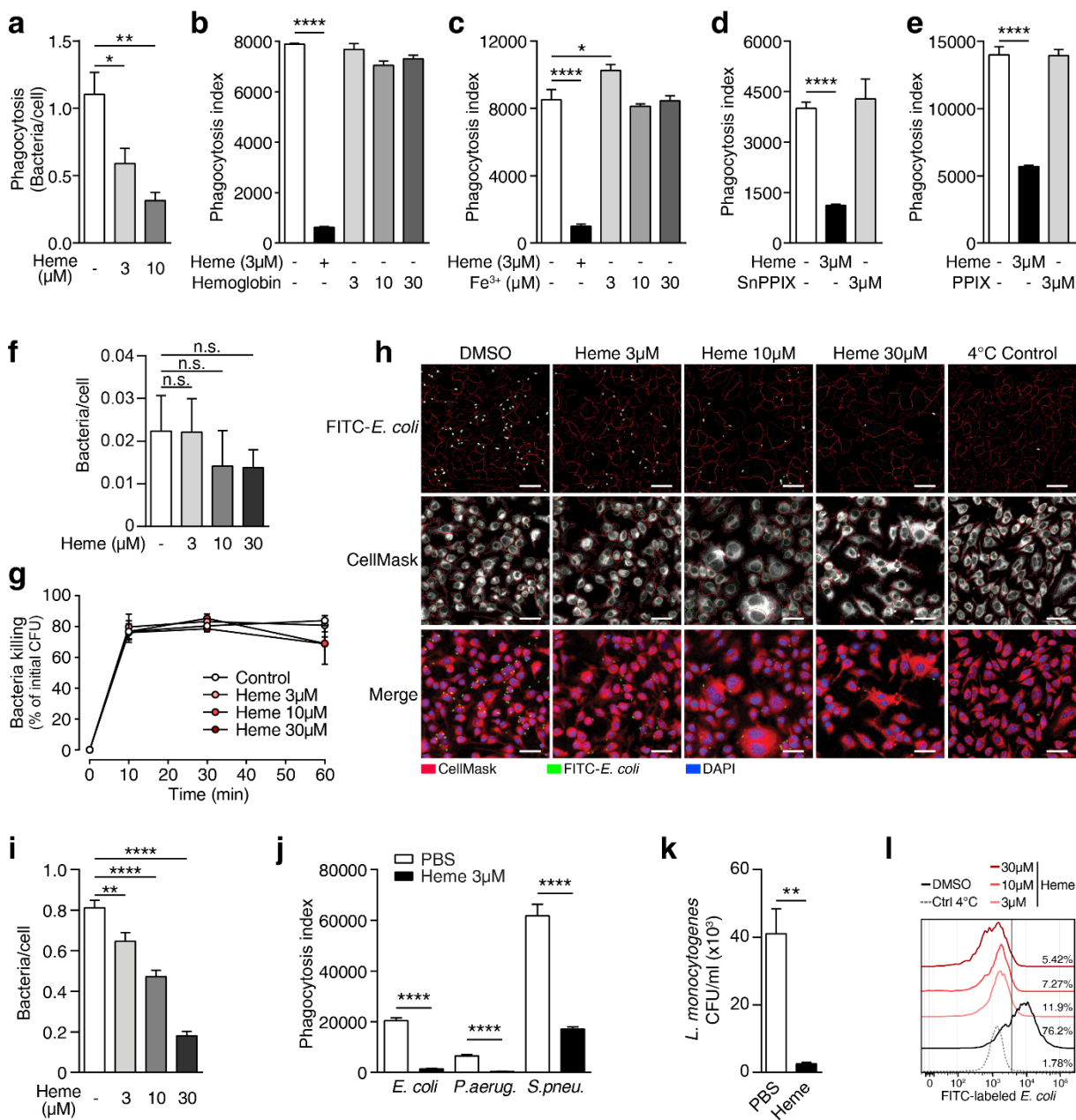
Sample sizes for *in vivo* experiments were calculated based on previous experience using the Power/sample-size calculator (<http://www.stat.ubc.ca/~rollin/stats/ssize/n2.html>). Statistically significant outliers were assessed using Grubb's test ($\alpha = 0.05$) and were excluded from analysis. Animal studies were performed without prior randomization or blinding. Survival data was analyzed by Log rank (Mantel-Cox) test using GraphPad Prism v6.07 Software. Data is presented as mean \pm s.e.m. except where indicated.

2.6. Supplementary figures

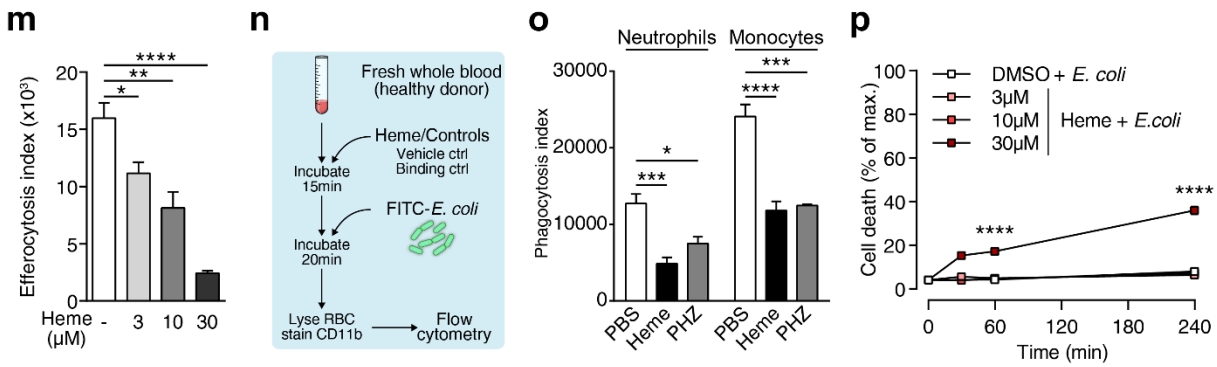


Supplementary figure 1 - Heme impairs bacterial clearance. **(a and b)** Plasma heme levels **(a)** of naïve WT mice (n=8) or WT mice pretreated with PBS (n=8) or heme (n=8) and respective bacterial counts **(b)** 6h post-infection with *E. coli*. **(c and d)** Plasma heme levels **(c)** of naïve WT mice (n=8) or *LysM-Cre^{-/-}Hmox1^{fl/fl}* (n=8) and *LysM-Cre^{+/-}Hmox1^{fl/fl}* (n=8) mice and respective bacterial counts **(d)** 6h post-infection with *E. coli*. **(e)** Bacterial burden of WT mice pretreated with PBS or heme, 24h post-infection with *L. monocytogenes* (n=8 per group). **(f)** Survival

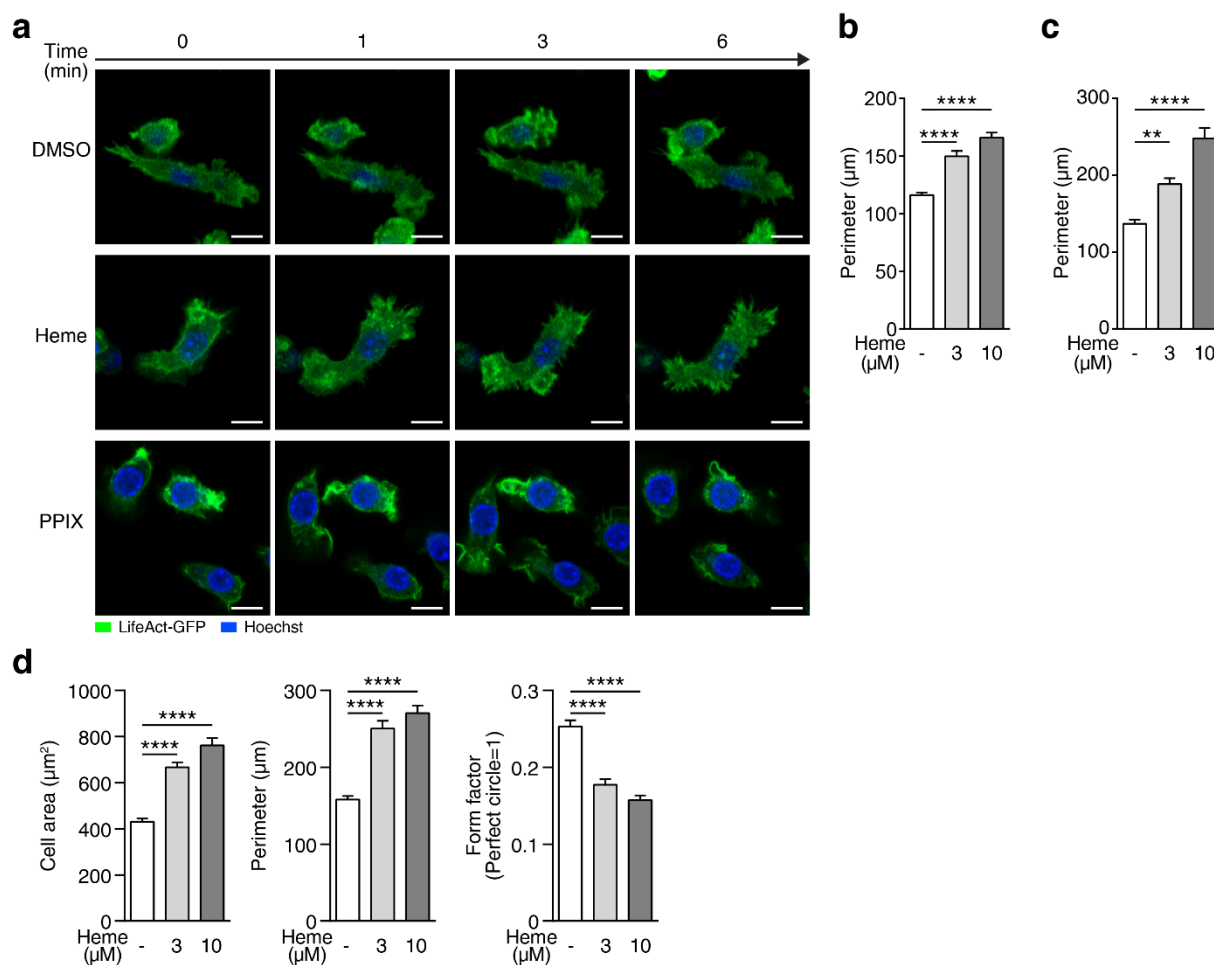
of WT mice pretreated with PBS (n=5) or heme (n=6) and infected with *L. monocytogenes*. (g-i) Plasma cytokine (g) and PLF chemokine levels (h) of WT mice pretreated with PBS or heme 16h after control (PBS) or LPS treatment, and respective PLF absolute cell counts (i) total, macrophage and neutrophil; n=6-8 per group). (j) Growth curves for *E. coli* and $\Delta dppC::Kan^R$ *E. coli* in regular M63 minimal media or elemental iron-free M63 minimal media supplemented with 30 μ M heme. (k) Bacterial burden of WT mice pretreated with heme or equimolar elemental iron (Ferric ammonium citrate), 24h post-infection with *L. monocytogenes* (n=8 per condition). (l) Representative images of isogenic non-hemolytic *E. coli* and hemolytic *E. coli*^{hlyABCD::attTn7} colonies grown on Colombia sheep blood agar plates. Data in (a-d) are representative of 2 independent experiments. Data in (h) are pooled from 2 independent experiments. Data in (a-e, k) are presented as the mean; dots represent individual animals; Data in (g-i) are presented as mean \pm S.E.M.. (a, c, g, h) one-way ANOVA with Tukey's multiple correction test, (b, d, e, k) Mann-Whitney test, (i) two-tailed t-test, (f) Mantel-Cox test; n.s. = not significant, ** p \leq 0.01, *** p \leq 0.001, **** p \leq 0.0001.



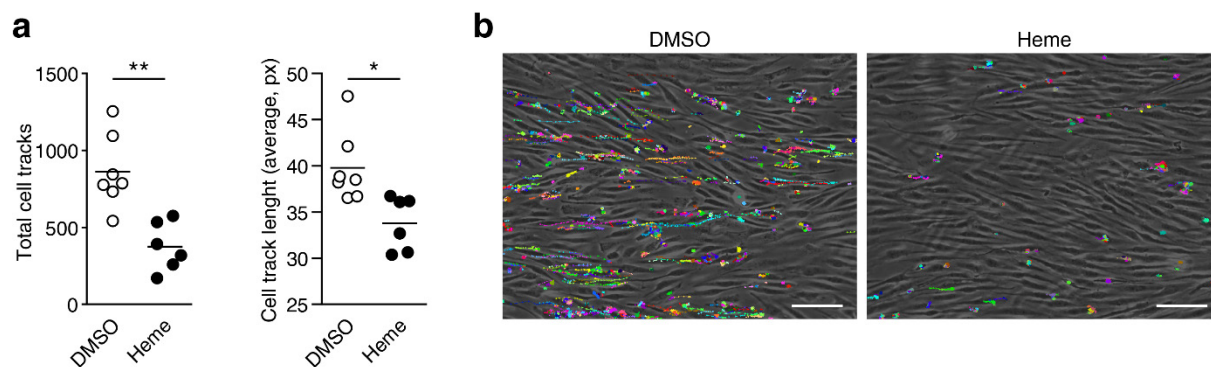
(Supplementary figure 2 – Continued on next page)



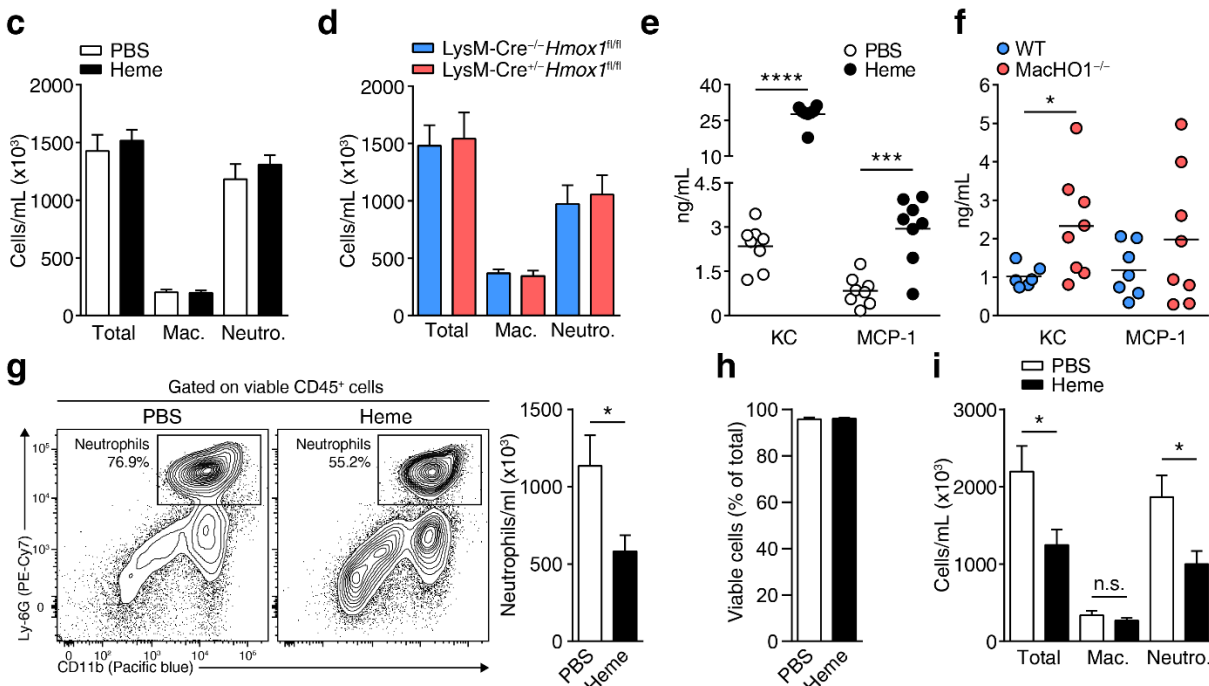
Supplementary figure 2 - Heme inhibits bacterial phagocytosis and the intact heme molecule is required to mediate its effect. **(a)** Automated quantification of phagocytosis of bacteria by control- (DMSO) or heme-treated RAW264.7 macrophages as assessed by confocal microscopy (representative images in Figure 3b) and displayed as bacteria per cell (n=4-5 images per condition). **(b-e)** Phagocytosis of heat-killed *E. coli* by RAW264.7 macrophages pretreated with **(b)** control (DMSO), heme or hemoglobin (n=4 per condition), **(c)** control (DMSO), heme or elemental iron (iron sulfate; n=4 per condition), **(d)** control (DMSO), heme or SnPPIX (n=4 per condition) and **(e)** control (DMSO), heme or PPIX (n=4 per condition). Hemoglobin concentration was calculated as heme content-equivalent concentration. Phagocytosis was quantified by flow cytometry. **(f)** Binding of FITC-labeled *E. coli* to RAW264.7 macrophages pretreated with control (DMSO) or heme (n=5 images per condition) at room temperature and incubated at 4°C for 1h as assessed by confocal microscopy. **(g)** Bacterial killing time course by RAW264.7 macrophages after treatment with control (DMSO) or heme (n=3 per condition). **(h and i)** Representative images **(h)** and quantification of phagocytosis **(i)** of FITC-labelled heat-killed *E. coli* by BMDM pretreated with control (DMSO) or heme (n=510-1009 cells per condition). Scale bar = 25 μm. **(j)** Phagocytosis of heat-killed *E. coli*, *P. aeruginosa* and *S. pneumoniae* by WT BMDM pretreated with control (DMSO) or heme (n=4 per condition) as assessed by flow cytometry. **(k)** Phagocytosis of live *L. monocytogenes* by BMDM pretreated with control (DMSO) or heme (n=4 per condition). **(l)** Phagocytosis of heat-killed FITC-labeled *E. coli* by human monocyte-derived macrophages pretreated with control (DMSO) or heme, shown as the percentage of FITC⁺ macrophages; representative histograms shown (n=3 per condition; related to Figure 3e). **(m)** Efferocytosis of apoptotic thymocytes by RAW264.7 macrophages treated with control (DMSO) or heme (n=4 per condition). **(n)** Scheme showing the workflow for human whole blood phagocytosis assays. **(o)** Phagocytosis of bacteria by human blood neutrophils (CD11b⁺, SSC^{high}) and monocytes (CD11b⁺, SSC^{low}) from control, heme-treated (30μM) and phenylhydrazine (PHZ)-hemolytic whole blood as quantified by flow cytometry. Background signal from bound, non-internalized bacteria was calculated from Cytochalasin D (10μM) treated control samples. **(p)** Percentage of cell death of RAW264.7 macrophages upon incubation with control (DMSO) or heme in the presence of heat-killed *E. coli*, as measured by LDH release (n=4 per condition). Data in **(a, e, f-i, k, l and p)** are representative of 2 independent experiments. Data in **(d)** are pooled from 2 independent experiments. Data in **(a-g, i-k, m, o and p)** are presented as mean ± S.E.M.. **(a-f, i, m, o)** one-way ANOVA with Tukey's multiple correction test, **(g, p)** two-way ANOVA with Tukey's multiple correction test, **(j, k)** two-tailed t-test, * p ≤ 0.05, ** p ≤ 0.01, *** p ≤ 0.001, **** p ≤ 0.0001.



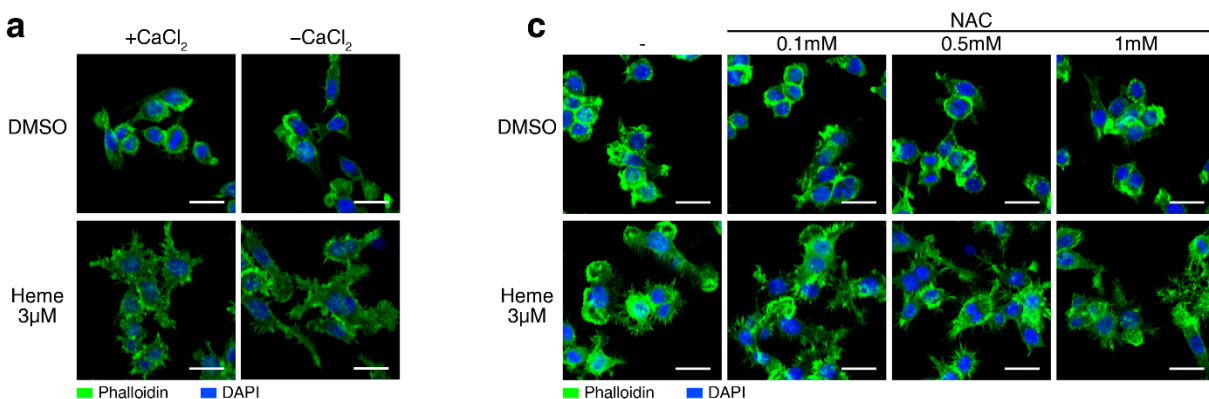
Supplementary figure 3 - Heme induces cell shape changes due to effects on the actin cytoskeleton. **(a)** Live cell imaging of RAW264.7 macrophages expressing LifeAct-GFP treated with control (DMSO), heme or PPIX (see **Supplementary Video 3**). Scale bar = 10 μm. **(b and c)** Cell shape analysis and automatic quantification of cell perimeter of RAW264.7 **(b; n=177-282 cells)** and human monocyte-derived macrophages **(c; n=6 images per condition)** treated with control (DMSO) or heme for 15min (related to **Fig. 4d** and **4e**, respectively). **(d)** Cell shape analysis and automatic quantification of cell area, perimeter and form factor of BMDM incubated with control (DMSO) or heme for 15min (n=169-182 cells). Data in **(b and d)** are representative of 2 independent experiments. Data in **(b, c and d)** are presented as mean ± S.E.M., one-way ANOVA with Tukey's multiple correction test; ** p ≤ 0.01, *** p ≤ 0.001, **** p ≤ 0.0001.



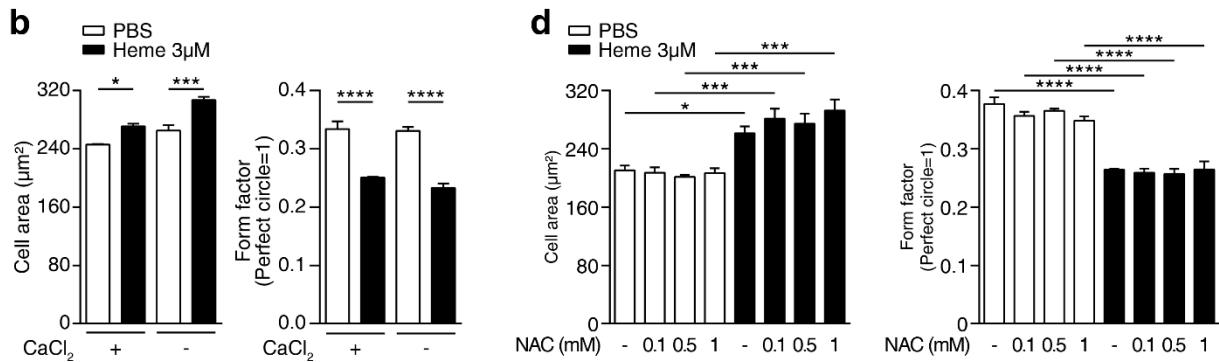
(Supplementary figure 4 – Continued on next page)



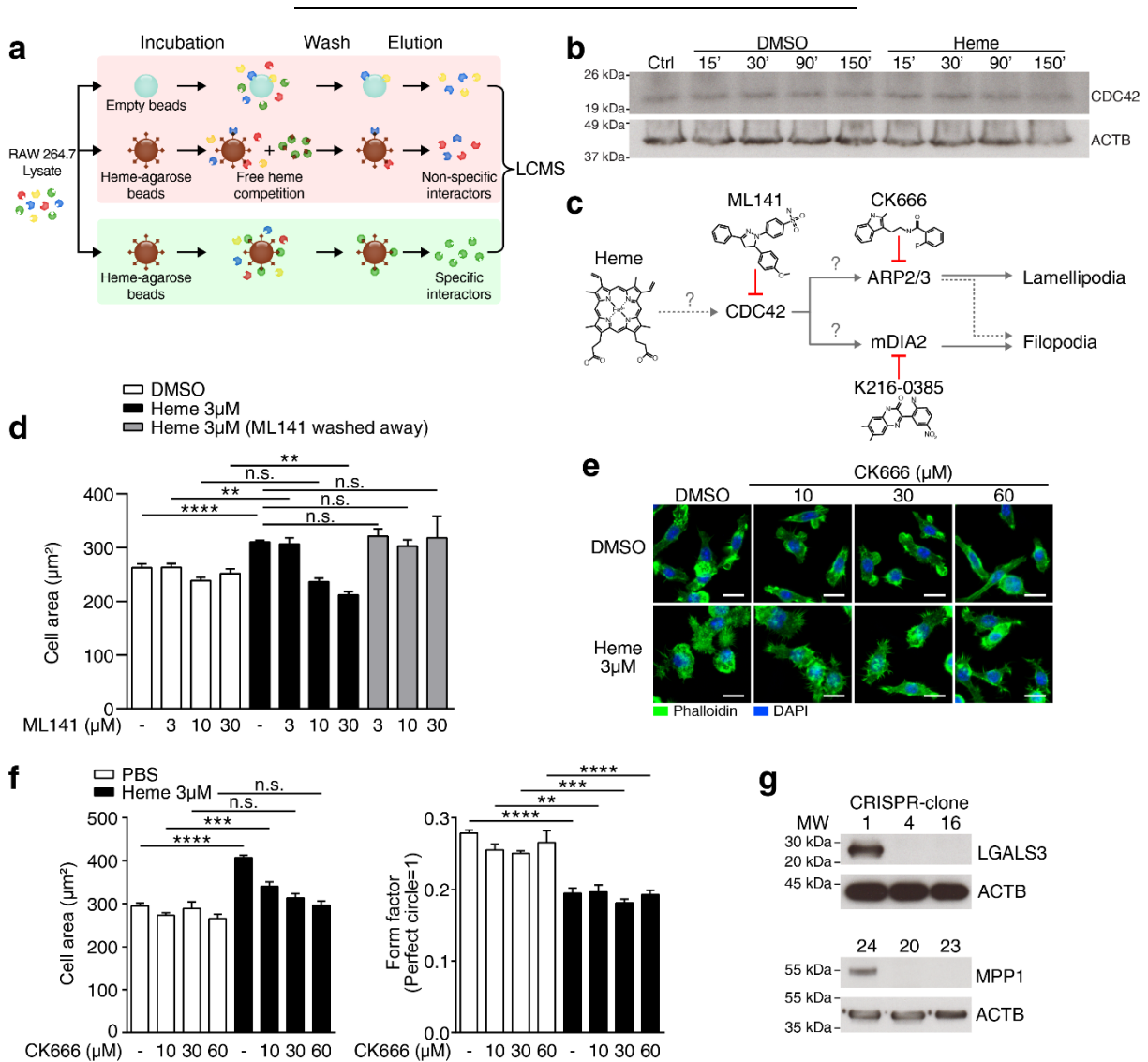
Supplementary figure 4 - Heme impairs functions dependent on cytoskeleton rearrangement. (a) Adhesion (left panel) and rolling (right panel) of human monocytes pretreated with control (DMSO; n=7) or 10μM heme (n=6) on activated human endothelium monolayer, and (b) representative images shown with detected cell tracks overlaid on the endothelium monolayer; scale bar = 100 μm, (see **Supplementary Video 5**). (c) Absolute cell numbers (total, macrophage and neutrophil) in the peritoneal cavity of WT mice pretreated with PBS or heme (n=8) 6h post-infection with *E. coli* (n=8). (d) Absolute cell numbers (total, macrophage and neutrophil) in the peritoneal cavity of *LysM-Cre^{-/-}Hmox1^{fl/fl}* and *LysM-Cre^{+/-}Hmox1^{fl/fl}* mice 6h post-infection with *E. coli* (n=8). (e) Chemokine levels in the peritoneal cavity of mice presented in (c). (f) Chemokine levels in the peritoneal cavity of mice presented in (d). (g) Representative flow cytometry plots displaying the percentage of neutrophils (viable CD45⁺, Ly6G⁺, CD11b⁺, CD3⁻, CD19⁻ cells; left panels), quantification of the absolute number of peritoneal neutrophils (right panel), and (h) the percentage of viable peritoneal cells 6h post-injection of thioglycollate broth to WT mice pretreated with PBS or heme (n=6 per condition). (i) Absolute peritoneal cell numbers (total, macrophage and neutrophil) 6h post-injection of thioglycollate broth to WT mice pretreated with PBS or heme, as assessed by cytospin preparations (n=6 per condition). Data in (a) are pooled from 2 independent experiments. Data in (c-f) are representative of 2 independent experiments. Data in (c-d, g-i) are presented as mean ± S.E.M.; Data in (a, e-f) are presented as mean; dots represent technical replicates (a) or individual animals (e-f). Data in (c, e) are related to Supplementary Fig. 1a and 1b, and (d, f) are related to Supplementary Fig. 1c and 1d. (a, c-i) two-tailed t-test; * p ≤ 0.05, ** p ≤ 0.01, *** p ≤ 0.001, **** p ≤ 0.0001.



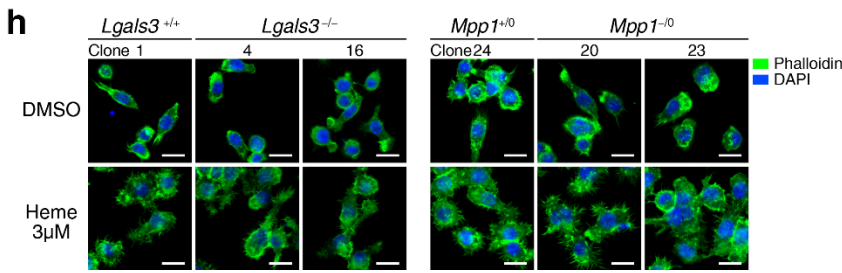
(Supplementary figure 5 – Continued on next page)



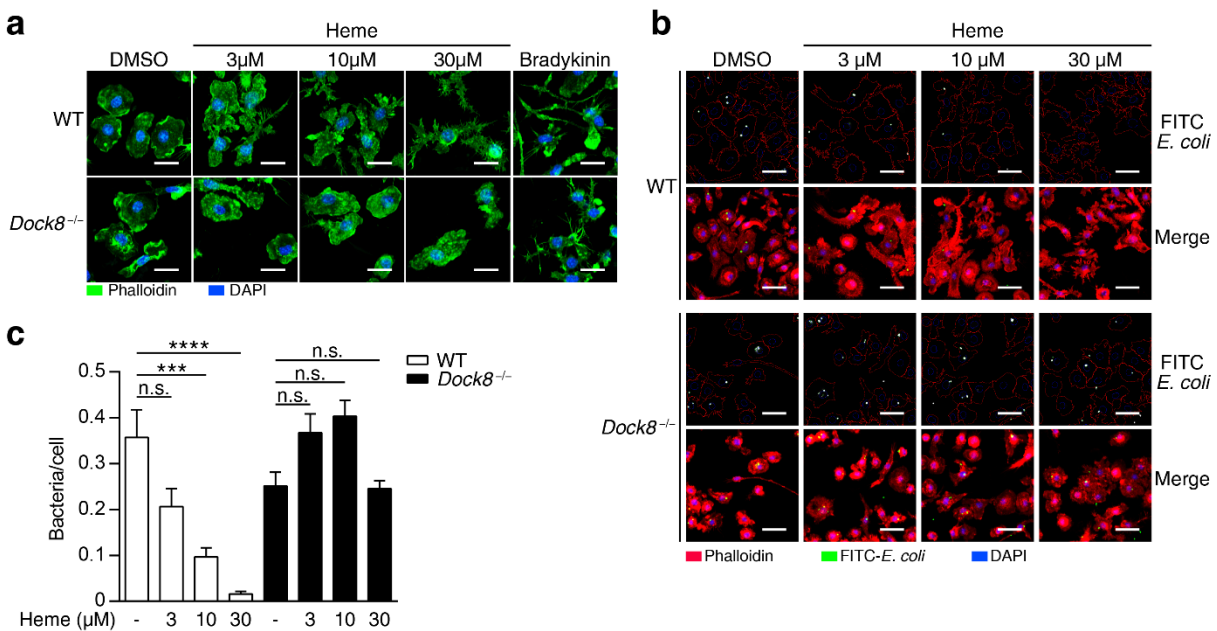
Supplementary figure 5 - Heme-induced cell spreading is independent of calcium influx signaling and ROS. **(a-b)** Representative images and automatic quantification of cell area and form factor of RAW264.7 macrophages treated with control (DMSO) or heme in the presence or absence of calcium in the medium (n=4 images per condition). **(c-d)** Representative images and automatic quantification of cell area and form factor of RAW264.7 macrophages treated with control (DMSO) or heme in the presence or absence of the ROS scavenger *N*-acetyl-L-cysteine (NAC; n=4 images per condition). Data in **(b, d)** are presented as mean ± S.E.M., one-way ANOVA with Tukey's multiple correction test; * p ≤ 0.05, *** p ≤ 0.001, **** p ≤ 0.0001. Scale bars = 20 μm.



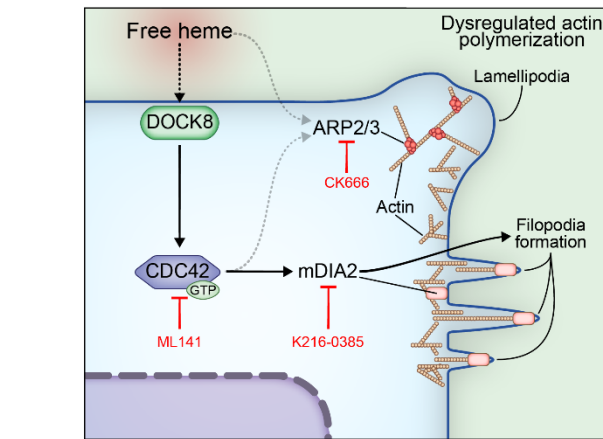
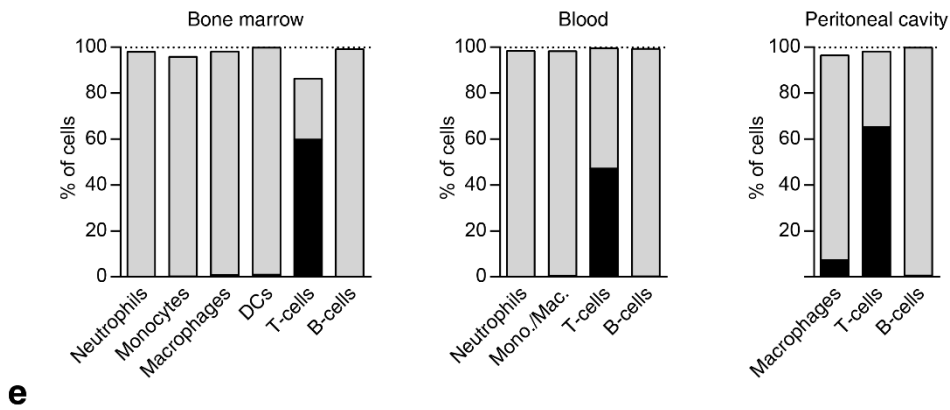
(Supplementary figure 6 – Continued on next page)



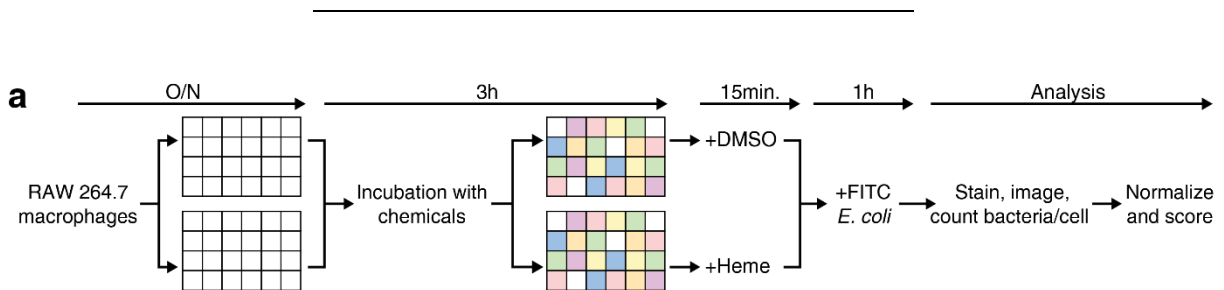
Supplementary figure 6 - Heme further disrupts actin cytoskeleton organization through ARP2/3. **(a)** Chemical proteomic workflow to determine specific heme-binding proteins in RAW264.7 macrophage lysates. **(b)** Western blot showing the protein level of Cdc42 (MW 21kDa) from whole-cell lysates of RAW264.7 macrophage treated with control (DMSO) or heme (10µM) for the indicated time points. Beta actin (ACTB) is shown as loading control. **(c)** Scheme showing the inhibitors used to assess the pathways involved in heme-mediated cell shape changes, and their respective targets. **(d)** Automatic quantification of cell area of RAW264.7 macrophages pretreated with control (DMSO), ML141 (Cdc42 inhibitor) or ML141 treatment and subsequent washing to remove ML141, and treated with control (DMSO) or heme for 15min. (n=4 random fields per condition; see representative images and automatic quantification of form factor in Fig. 7c, d). **(e and f)** Representative images **(e)** and automatic quantification of form factor and cell area **(f)** of RAW264.7 macrophages pretreated with control (DMSO) or CK666 (ARP2/3 complex inhibitor), and treated with control (DMSO) or heme (n=4-8 images per condition). **(e and f)**. **(g)** Western blots showing LGALS3 or MPP1 protein expression in wild-type and CRISPR/Cas9-deleted RAW264.7 macrophage clones, and **(h)** representative images of these cells upon treatment with control (DMSO) or heme. Data in **(d-e)** are representative of 2 independent experiments. Data in **(d and f)** are presented as mean ± S.E.M., one-way ANOVA with Tukey's multiple correction test; n.s. = not significant, * p ≤ 0.05, ** p ≤ 0.01, *** p ≤ 0.001, **** p ≤ 0.0001. Scale bars = 20 µm.



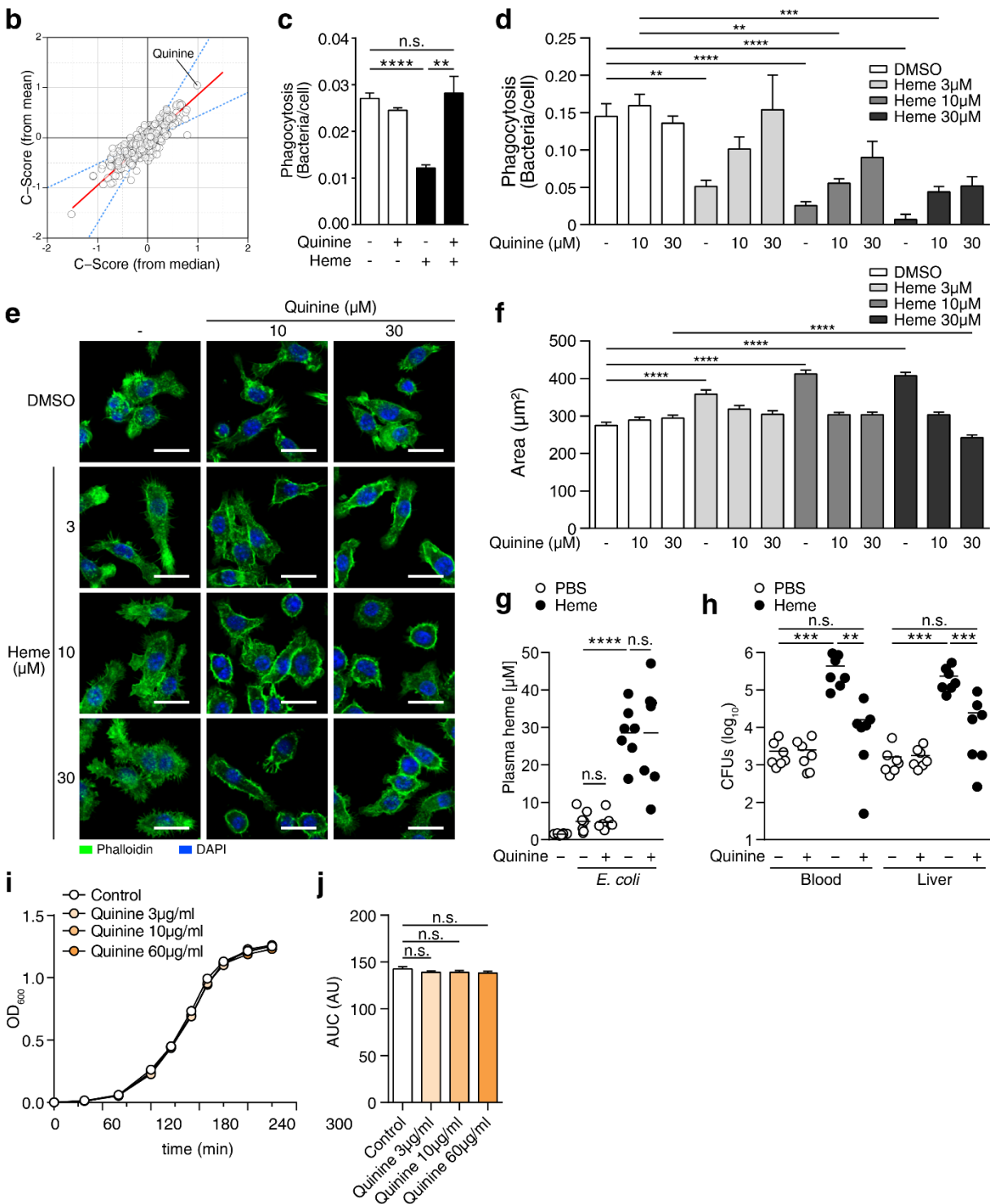
(Supplementary figure 7 – Continued on next page)



Supplementary figure 7 - Heme interferes with actin cytoskeleton dynamics via DOCK8. **(a)** Cellular morphology of WT and *Dock8*^{-/-} HoxB8 macrophages treated with control (DMSO), heme or the CDC42 activator bradykinin (10μM) for 15min. Scale bar = 20 μm. **(b)** and **(c)** Representative images **(b)** and automated quantification of phagocytosis of bacteria **(c)** by WT and *Dock8*^{-/-} BMDM treated with control (DMSO) or heme, as assessed by confocal microscopy and displayed as bacteria per cell (n=6 images per condition). **(d)** Immune cell composition in the bone marrow, blood and peritoneal cavity of chimeric mice, 6 weeks after bone marrow transplant, displayed as percentage of donor (CD45.1⁺) and recipient (CD45.2⁺) cells. **(e)** Scheme depicting the working model proposed. Data in **(b)** and **(c)** are pooled from 2 independent experiments and are representative of 3 independent experiments. Data in **(c)** are presented as mean ± S.E.M., one-way ANOVA with Tukey's multiple correction test; n.s. = not significant, **** p ≤ 0.0001. Scale bars = 20 μm **(a)** and 50 μm **(b)**.



(Supplementary figure 8 – Continued on next page)



Supplementary figure 8 - Quinine restores host bacterial resistance. (a) Chemical screening workflow. (b) Compound screen scoring. (c) Phagocytosis of FITC-labeled heat-killed bacteria by RAW264.7 macrophages pretreated with control (DMSO) or quinine, and treated with control (DMSO) or heme. Data in (c) represent the original phagocytosis values for the top scoring compound from the compound screen (see Fig. 8a Supplementary Fig. 8b). (d) Phagocytosis of FITC-*E. coli* by RAW264.7 macrophages (n=4 images per condition) pretreated with control (saline) or indicated amounts of quinine, and treated with control (DMSO) or heme as assessed by confocal microscopy. (e, f) Cellular morphology and automatic quantification of cell area of RAW264.7 macrophages pretreated with control (saline) or quinine and treated with control (DMSO) or heme (n=172-368 cells per condition). Scale bar = 20 μm. (g) Plasma heme levels of naïve WT mice (n=8) or WT mice pretreated with mock (PBS) or quinine and treated with PBS or heme, and (h) respective bacterial counts 6h post-infection with *E. coli*

(n=7 per group of infected mice). (i) Growth curves and (j) respective area under the curve (AUC) for *E. coli* grown on LB medium supplemented with control (saline) or quinine (n=3 per condition). Data in (d) is representative of 2 independent experiments. Data in (c, d, f, i, j) is presented as mean \pm S.E.M. Data in (g, h) is presented as mean, and dots represent individual animals. Statistical comparisons in (d, f) are calculated versus control conditions (no heme) at the same dose of quinine. (a) C-score analysis – see methods section, (b-d, f-h, j) one-way ANOVA with Tukey's multiple correction test, (i) two-way ANOVA with Tukey's multiple correction test; n.s. = not significant, * $p \leq 0.05$, ** $p \leq 0.01$, *** $p \leq 0.001$, **** $p \leq 0.0001$.

2.7. Supplementary tables

Supplementary table 1. Bacteria strains used and generated.

Strain/serotype	Relevant characteristics	References
<i>E. coli</i> PMV-1 (O18:K1)	clinical isolate (<i>E. coli</i>)	Sewnath, Olszyna ⁵⁰ , Peris-Bondia, Muraille ⁵¹
$\Delta dppC::Kan^R$ <i>E. coli</i> PMV-1 (O18:K1)	dppC replaced with nptII (Kan ^R)	This study
<i>E. coli</i> ^{hlyABCD::attTn7} PMV-1 (O18:K1)	Single copy of α -hemolysin operon inserted onto <i>E. coli</i> PMV-1 attTn7 site	This study
<i>E. coli</i> CFT073 (serotype O6:K2:H1)	<i>E. coli</i> α -hemolysin operon template	Mobley, Green ⁶⁰
<i>E. coli</i> TKC	nptII template (kanamycin resistance)	Sharan, Thomason ⁵⁹
<i>L. monocytogenes</i> LO28InIA*	Mouse-adapted <i>L. monocytogenes</i> LO28InIA ^{S192N/Y369S}	Kernbauer, Maier ⁵⁴
<i>P. aeruginosa</i> PA-103	http://www.lgcstandards-atcc.org/Products/All/29260.aspx	ATCC 29260
<i>S. pneumoniae</i> CIP 104225	http://www.lgcstandards-atcc.org/Products/All/6303.aspx	ATCC 6303

Supplementary table 2. Plasmids used.

Plasmid	Relevant characteristics	Reference
pSIM8	λ -RED recombineering plasmid	Sharan, Thomason ⁵⁹
pGRG36	mini-Tn7 transposon plasmid	McKenzie and Craig ⁶²
pRM24	α -hemolysin operon cloned into pGRG36 (NotI-HF, XhoI)	This study
pX459	CRISPR-Cas9 vector	Ran, Hsu ⁶³
pX459- <i>Mpp1</i> _exon1	CRISPR-Cas9 and sgRNA expressing plasmid targeting <i>Mpp1</i>	This study
pX459- <i>Lgals3</i> _exon2	CRISPR-Cas9 and sgRNA expressing plasmid targeting <i>Lgals3</i>	This study

Supplementary table 3. Oligos used.

Primer	Sequence (5' to 3')
DppC_Kan_For	<u>GGCGTGGTGAACCCGCGTATTCGTCATAAGAAGTAAGG</u> <u>GGACATCTATGGACAGCAAGCGAACCG</u>
DppC_Kan_Rev	<u>TGCACCGATAATTTATCTACATTTAATAACGCCATCTCG</u> <u>AACCTCTCAGAAGAACTCGTCAAAAG</u>
DppC_R1-_For	GAAACGATCCTCATCCTGTCTC
DppC_R1-_Rev	CTGTAGCTGATGCGGTCTACG
Hly_NotI_For	TATCGAAG CGGCC CCATATGCGGGCAAATACGTC
Hly_XhoI_Rev	CTAATTG CTCGAG TTTGCCACAAAACAGTGCAG
attTn7_Left_For	GTCACATGGAGTTGGCAGGA
attTn7_Left_Rev	TCTGCAGCCTGAGCATTGAA
attTn7_Right_For	AGCGTTAAGTCTCAGAGCCG
attTn7_Righ_Rev	CCGAGCCGTATTGAGCAGAT
<i>Mpp1</i> _del_For	CACCGATGACGCTCAAGTCGAGCGA
<i>Mpp1</i> _del_Rev	AAACTCGCTCGACTTGAGCGTCATC
<i>Lgals3</i> _del_For	CACCGTCAAGGATATCCGGGTGCAT
<i>Lgals3</i> _del_Rev	AAACATGCACCCGGATATCCTTGAC
U6_CRISPR_Seq2	GGGCCTATTTCCCATGATTCC
<i>Mpp1</i> _Seq	GGATCCTAGACCCAACCCGA
<i>Lgals3</i> _Seq	TCACAAATGCCTGTAGTCCCC

Underlined: homology arms; bold: restriction/ligation sites

2.8. Publication references

1. Modell, B. & Darlison, M. Global epidemiology of haemoglobin disorders and derived service indicators. *Bull. World Health Organ.* **86**, 480–487 (2008).
2. World Health Organization. *World Malaria Report 2013*. World Health Organization: Geneva, 2013
3. Adamzik, M. *et al.* Free hemoglobin concentration in severe sepsis: methods of measurement and prediction of outcome. *Crit. Care* **16**, R125 (2012).
4. Larsen, R. *et al.* A central role for free heme in the pathogenesis of severe sepsis. *Sci. Transl. Med.* **2**, 51ra71 (2010).
5. Schaer, D.J., Buehler, P.W., Alayash, A.I., Belcher, J.D. & Vercellotti, G.M. Hemolysis and free hemoglobin revisited: exploring hemoglobin and hemin scavengers as a novel class of therapeutic proteins. *Blood* **121**, 1276–1284 (2013).

6. Muller-Eberhard, U., Javid, J., Liem, H.H., Hanstein, A. & Hanna, M. Plasma concentrations of hemopexin, haptoglobin and heme in patients with various hemolytic diseases. *Blood* **32**, 811–815 (1968).
7. Dutra, F.F. & Bozza, M.T. Heme on innate immunity and inflammation. *Front. Pharmacol.* **5**, 115 (2014).
8. Smith, A. & McCulloh, R.J. Hemopexin and haptoglobin: allies against heme toxicity from hemoglobin not contenders. *Front. Physiol.* **6**, 187 (2015).
9. Gozzelino, R., Jeney, V. & Soares, M.P. Mechanisms of cell protection by heme oxygenase-1. *Annu. Rev. Pharmacol. Toxicol.* **50**, 323–354 (2010).
10. Chiabrando, D., Vinchi, F., Fiorito, V., Mercurio, S. & Tolosano, E. Heme in pathophysiology: a matter of scavenging, metabolism and trafficking across cell membranes. *Front. Pharmacol.* **5**, 61 (2014).
11. Fortes, G.B. *et al.* Heme induces programmed necrosis on macrophages through autocrine TNF and ROS production. *Blood* **119**, 2368–2375 (2012).
12. Seixas, E. *et al.* Heme oxygenase-1 affords protection against noncerebral forms of severe malaria. *Proc. Natl. Acad. Sci. USA* **106**, 15837–15842 (2009).
13. Ramakrishnan, M. *et al.* Increased risk of invasive bacterial infections in African people with sickle-cell disease: a systematic review and meta-analysis. *Lancet Infect. Dis.* **10**, 329–337 (2010).
14. Wiener, E. Impaired phagocyte antibacterial effector functions in beta-thalassemia: a likely factor in the increased susceptibility to bacterial infections. *Hematology* **8**, 35–40 (2003).
15. Church, J. & Maitland, K. Invasive bacterial co-infection in African children with *Plasmodium falciparum* malaria: a systematic review. *BMC Med.* **12**, 31 (2014).
16. Scott, J.A. *et al.* Relation between falciparum malaria and bacteraemia in Kenyan children: a population-based, case-control study and a longitudinal study. *Lancet* **378**, 1316–1323 (2011).
17. Cober, M.P. & Phelps, S.J. Penicillin prophylaxis in children with sickle cell disease. *J. Pediatr. Pharmacol. Ther.* **15**, 152–159 (2010).
18. Hirst, C. & Owusu-Ofori, S. Prophylactic antibiotics for preventing pneumococcal infection in children with sickle cell disease. *Cochrane Database Syst. Rev.* **11**, CD003427 (2014).
19. Dutra, F.F. *et al.* Hemolysis-induced lethality involves inflammasome activation by heme. *Proc. Natl. Acad. Sci. USA* **111**, E4110–E4118 (2014).

20. Cassat, J.E. & Skaar, E.P. Iron in infection and immunity. *Cell Host Microbe* **13**, 509–519 (2013).
21. Cunnington, A.J. *et al.* Prolonged neutrophil dysfunction after *Plasmodium falciparum* malaria is related to hemolysis and heme oxygenase-1 induction. *J. Immunol.* **189**, 5336–5346 (2012).
22. Cunnington, A.J., de Souza, J.B., Walther, M. & Riley, E.M. Malaria impairs resistance to *Salmonella* through heme- and heme oxygenase-dependent dysfunctional granulocyte mobilization. *Nat. Med.* **18**, 120–127 (2011).
23. Ganz, T. Macrophages and systemic iron homeostasis. *J. Innate Immun.* **4**, 446–453 (2012).
24. Jais, A. *et al.* Heme oxygenase-1 drives metaflammation and insulin resistance in mouse and man. *Cell* **158**, 25–40 (2014).
25. Skaar, E.P. The battle for iron between bacterial pathogens and their vertebrate hosts. *PLoS Pathog.* **6**, e1000949 (2010).
26. Wandersman, C. & Stojiljkovic, I. Bacterial heme sources: the role of heme, hemoprotein receptors and hemophores. *Curr. Opin. Microbiol.* **3**, 215–220 (2000).
27. Létoffé, S., Delepelaire, P. & Wandersman, C. The housekeeping dipeptide permease is the *Escherichia coli* heme transporter and functions with two optional peptide binding proteins. *Proc. Natl. Acad. Sci. USA* **103**, 12891–12896 (2006).
28. Flannagan, R.S., Jaumouillé, V. & Grinstein, S. The cell biology of phagocytosis. *Annu. Rev. Pathol.* **7**, 61–98 (2012).
29. Moulding, D.A., Record, J., Malinova, D. & Thrasher, A.J. Actin cytoskeletal defects in immunodeficiency. *Immunol. Rev.* **256**, 282–299 (2013).
30. McEver, R.P. & Zhu, C. Rolling cell adhesion. *Annu. Rev. Cell Dev. Biol.* **26**, 363–396 (2010).
31. Wagener, F.A. *et al.* Different faces of the heme-heme oxygenase system in inflammation. *Pharmacol. Rev.* **55**, 551–571 (2003).
32. Choi, H. *et al.* SAINT: probabilistic scoring of affinity purification-mass spectrometry data. *Nat. Methods* **8**, 70–73 (2011).
33. Mellacheruvu, D. *et al.* The CRAPome: a contaminant repository for affinity purification-mass spectrometry data. *Nat. Methods* **10**, 730–736 (2013).
34. Franceschini, A. *et al.* STRING v9.1: protein-protein interaction networks, with increased coverage and integration. *Nucleic Acids Res.* **41**, D808–D815 (2013).
35. Ridley, A.J. Life at the leading edge. *Cell* **145**, 1012–1022 (2011).

36. Heasman, S.J. & Ridley, A.J. Mammalian Rho GTPases: new insights into their functions from in vivo studies. *Nat. Rev. Mol. Cell Biol.* **9**, 690–701 (2008).
37. Harada, Y. *et al.* DOCK8 is a Cdc42 activator critical for interstitial dendritic cell migration during immune responses. *Blood* **119**, 4451–4461 (2012).
38. Lee, D.J., Cox, D., Li, J. & Greenberg, S. Rac1 and Cdc42 are required for phagocytosis, but not NF-kappaB-dependent gene expression, in macrophages challenged with *Pseudomonas aeruginosa*. *J. Biol. Chem.* **275**, 141–146 (2000).
39. Hill, G.B. Enhancement of experimental anaerobic infections by blood, hemoglobin, and hemostatic agents. *Infect. Immun.* **19**, 443–449 (1978).
40. Nairz, M., Haschka, D., Demetz, E. & Weiss, G. Iron at the interface of immunity and infection. *Front. Pharmacol.* **5**, 152 (2014).
41. Flannagan, R.S., Cosío, G. & Grinstein, S. Antimicrobial mechanisms of phagocytes and bacterial evasion strategies. *Nat. Rev. Microbiol.* **7**, 355–366 (2009).
42. Sarantis, H. & Grinstein, S. Subversion of phagocytosis for pathogen survival. *Cell Host Microbe* **12**, 419–431 (2012).
43. Wegiel, B. *et al.* Macrophages sense and kill bacteria through carbon monoxide-dependent inflammasome activation. *J. Clin. Invest.* **124**, 4926–4940 (2014).
44. Krishnaswamy, J.K. *et al.* Coincidental loss of DOCK8 function in NLRP10-deficient and C3HHeJ mice results in defective dendritic cell migration. *Proc. Natl. Acad. Sci. USA* **112**, 3056–3061 (2015).
45. Zhang, Q. *et al.* Combined immunodeficiency associated with DOCK8 mutations. *N. Engl. J. Med.* **361**, 2046–2055 (2009).
46. Nishikimi, A., Kukimoto-Niino, M., Yokoyama, S. & Fukui, Y. Immune regulatory functions of DOCK family proteins in health and disease. *Exp. Cell Res.* **319**, 2343–2349 (2013).
47. Leed, A. *et al.* Solution structures of antimalarial drug-heme complexes. *Biochemistry* **41**, 10245–10255 (2002).
48. Gauvin, T.J., Fukui, J., Peterson, J.R. & Higgs, H.N. Isoform-selective chemical inhibition of mDia-mediated actin assembly. *Biochemistry* **48**, 9327–9329 (2009).
49. Redecke, V. *et al.* Hematopoietic progenitor cell lines with myeloid and lymphoid potential. *Nat. Methods* **10**, 795–803 (2013).
50. Matt, U. *et al.* WAVE1 mediates suppression of phagocytosis by phospholipid-derived DAMPs. *J. Clin. Invest.* **123**, 3014–3024 (2013).

51. Sewnath, M.E. *et al.* IL-10-deficient mice demonstrate multiple organ failure and increased mortality during *Escherichia coli* peritonitis despite an accelerated bacterial clearance. *J. Immunol.* **166**, 6323–6331 (2001).
52. Peris-Bondia, F., Muraille, E. & Van Melderen, L. Complete genome sequence of the *Escherichia coli* PMV-1 strain, a model extraintestinal pathogenic *E. coli* strain used for host-pathogen interaction studies. *Genome Announc.* **1**, e00913-13 (2013).
53. Ploplis, V.A., French, E.L., Carmeliet, P., Collen, D. & Plow, E.F. Plasminogen deficiency differentially affects recruitment of inflammatory cell populations in mice. *Blood* **91**, 2005–2009 (1998).
54. Kernbauer, E., Maier, V., Rauch, I., Müller, M. & Decker, T. Route of infection determines the impact of type I interferons on innate immunity to *Listeria monocytogenes*. *PLoS One* **8**, e65007 (2013).
55. Stockinger, S. *et al.* Characterization of the interferon-producing cell in mice infected with *Listeria monocytogenes*. *PLoS Pathog.* **5**, e1000355 (2009).
56. Huy, N.T. *et al.* An improved colorimetric method for quantitation of heme using tetramethylbenzidine as substrate. *Anal. Biochem.* **344**, 289–291 (2005).
57. Schenkman, J.B. & Jansson, I. Spectral analyses of cytochromes P450. *Methods Mol. Biol.* **320**, 11–18 (2006).
58. Grundy, M.A., Gorman, N., Sinclair, P.R., Chorney, M.J. & Gerhard, G.S. High-throughput non-heme iron assay for animal tissues. *J. Biochem. Biophys. Methods* **59**, 195–200 (2004).
59. Sharan, S.K., Thomason, L.C., Kuznetsov, S.G. & Court, D.L. Recombineering: a homologous recombination-based method of genetic engineering. *Nat. Protoc.* **4**, 206–223 (2009).
60. Mobley, H.L. *et al.* Pyelonephritogenic *Escherichia coli* and killing of cultured human renal proximal tubular epithelial cells: role of hemolysin in some strains. *Infect. Immun.* **58**, 1281–1289 (1990).
61. Cross, M.A., Koronakis, V., Stanley, P.L. & Hughes, C. HlyB-dependent secretion of hemolysin by uropathogenic *Escherichia coli* requires conserved sequences flanking the chromosomal hly determinant. *J. Bacteriol.* **172**, 1217–1224 (1990).
62. McKenzie, G.J. & Craig, N.L. Fast, easy and efficient: site-specific insertion of transgenes into enterobacterial chromosomes using Tn7 without need for selection of the insertion event. *BMC Microbiol.* **6**, 39 (2006).

63. Ran, F.A. *et al.* Genome engineering using the CRISPR-Cas9 system. *Nat. Protoc.* **8**, 2281–2308 (2013).
64. Knapp, S., Matt, U., Leitinger, N. & van der Poll, T. Oxidized phospholipids inhibit phagocytosis and impair outcome in gram-negative sepsis in vivo. *J. Immunol.* **178**, 993–1001 (2007).
65. Sharif, O. *et al.* The triggering receptor expressed on myeloid cells 2 inhibits complement component 1q effector mechanisms and exerts detrimental effects during pneumococcal pneumonia. *PLoS Pathog.* **10**, e1004167 (2014).
66. White-Owen, C., Alexander, J.W., Sramkoski, R.M. & Babcock, G.F. Rapid whole-blood microassay using flow cytometry for measuring neutrophil phagocytosis. *J. Clin. Microbiol.* **30**, 2071–2076 (1992).
67. Carpenter, A.E. *et al.* CellProfiler: image analysis software for identifying and quantifying cell phenotypes. *Genome Biol.* **7**, R100 (2006).
68. Gawish, R. *et al.* Triggering receptor expressed on myeloid cells-2 fine-tunes inflammatory responses in murine Gram-negative sepsis. *FASEB J.* **29**, 1247–1257 (2014).
69. Repetto, G., del Peso, A. & Zurita, J.L. Neutral red uptake assay for the estimation of cell viability/cytotoxicity. *Nat. Protoc.* **3**, 1125–1131 (2008).
70. Fernbach, N.V. *et al.* Acid elution and one-dimensional shotgun analysis on an Orbitrap mass spectrometer: an application to drug affinity chromatography. *J. Proteome Res.* **8**, 4753–4765 (2009).
71. Huber, K.V. *et al.* Stereospecific targeting of MTH1 by (S)-crizotinib as an anticancer strategy. *Nature* **508**, 222–227 (2014).
72. Maurer, M. *et al.* Combining filter-aided sample preparation and pseudoshotgun technology to profile the proteome of a low number of early passage human melanoma cells. *J. Proteome Res.* **12**, 1040–1048 (2013).
73. Huang, W., Sherman, B.T. & Lempicki, R.A. Systematic and integrative analysis of large gene lists using DAVID bioinformatics resources. *Nat. Protoc.* **4**, 44–57 (2009).
74. Huang, W., Sherman, B.T. & Lempicki, R.A. Bioinformatics enrichment tools: paths toward the comprehensive functional analysis of large gene lists. *Nucleic Acids Res.* **37**, 1–13 (2009).
75. Riedl, J. *et al.* Lifeact: a versatile marker to visualize F-actin. *Nat. Methods* **5**, 605–607 (2008).

76. Gebäck, T., Schulz, M.M., Koumoutsakos, P. & Detmar, M. TScratch: a novel and simple software tool for automated analysis of monolayer wound healing assays. *Biotechniques* **46**, 265–274 (2009).
77. Schindelin, J. *et al.* Fiji: an open-source platform for biological-image analysis. *Nat. Methods* **9**, 676–682 (2012).

3. Discussion

Adequate immune responses are crucial to preserve organism homeostasis and integrity, and any dysregulation can lead either to severe infections due to immunosuppression, or immunopathology due to unfettered inflammation (McCusker & Warrington, 2011, Medzhitov & Janeway, 2000). Aside from its role in the recognition and elimination of pathogens, the immune system has vital housekeeping functions and is essential for sensing parenchymal cell health and functional output. As such, the immune system as a whole is a remarkably complex and tightly regulated system across all its branches and various cell types, and is evolutionarily engaged in a race to cope with fast-evolving pathogens. To perform its functions, the immune system relies on various effector mechanisms to recognize and eliminate threats such as bacterial pathogens, and an insufficient immune response can predispose individuals to infection, as clearly illustrated by many primary immunodeficiencies, where the failure of a single immune system component can drastically compromise immunity to pathogens (McCusker & Warrington, 2011). Analogously, exogenous factors negatively influencing the immune response can equally compromise immunity and render the host vulnerable to severe and debilitating infections. Such immunosuppressive effects can be caused by a wide array of factors, ranging from toxic agents, stress, age or malnutrition (Esser, 2016, Scrimshaw, Taylor et al., 1968), to chronic infections or cancer (Ghirelli & Hagemann, 2013, Maartens, Celum et al., 2014). Similarly, disorders characterized by severe hemolysis, such as SCD, α and β thalassemias, severe sepsis, inherited spherocytosis or transfusion of aged red blood cells (Adamzik, Hamburger et al., 2012, Booth et al., 2010, Church & Maitland, 2014, Cunnington et al., 2012a, Larsen et al., 2010, Prestia, Bandyopadhyay et al., 2014, Wiener, 2003) significantly predispose to life-threatening bacterial and viral infections, indicating that hemolytic events are able to either suppress host immunity, or facilitate bacterial and viral replication. Although these disorders have very different etiologies, they share severe hemolysis and susceptibility to infection as common denominators. This supports the basic hypothesis of this thesis, postulating that the hemolytic events and heme release accompanying these disorders predispose to infection via yet unexplored mechanisms.

The aim of this work was to uncover the link between hemolysis and severe bacterial infections, and understand the molecular basis underlying this association, and uses a combination of various *in vivo* infection models to mimic severe hemolysis and bacterial sepsis under different conditions, as well as *in vitro* molecular biology approaches to better understand the effects of hemolysis and heme release on immune effector mechanisms and dissect the pathways mediating susceptibility to infection.

Severe sepsis has been recognized as a potent trigger for hemolysis (Larsen et al., 2010), leading to a stark increase of “cell-free” labile heme levels in the circulation, a finding which is recapitulated in our animal sepsis models elicited by *E. coli* peritonitis. The observation that artificially increasing the levels of heme in the circulation to mimic hemolysis hindered host resistance to infection, thereby increasing the severity of sepsis in infected mice is in agreement with our original hypothesis. Similarly, insufficient heme degradation due to genetic ablation of the main heme-degrading enzyme HO-1 in the myeloid lineage rendered mice more susceptible to *E. coli* sepsis due to the accumulation of higher heme levels in the circulation. Importantly, these data indicated that out of all the components released from erythrocytes upon hemolysis, heme alone is sufficient to replicate the increased susceptibility to infection observed in hemolytic disorders, confirming our hypothesis that high labile heme levels represent the main culprit driving susceptibility to infection.

Heme is composed by an iron ion encased within a protoporphyrin IX ring (Kadish et al., 2000), and represents the most abundant form of iron in mammals, with the majority located within erythrocytes (Severance & Hamza, 2009, Warren & Smith, 2009). This gives rise to the possibility that “cell-free” labile heme in the circulation can facilitate pathogen growth by supplying pathogens with iron for their own nutritional needs. This concept is generally accepted (Cassat & Skaar, 2013, Hill, 1978) and is further supported by the idea of nutritional immunity (Hood & Skaar, 2012), whereby hosts limit iron bioavailability after an infectious threat is detected, with the goal of deterring pathogen growth. However, virtually all bacterial pathogens have evolved efficient ways of scavenging host iron, suggesting that nutritional immunity can be easily circumvented by “professional” pathogens (Skaar, 2010), thus acting primarily as a homeostatic mechanism geared towards preventing and limiting opportunistic infections. Although heme-acquisition is certainly necessary for a minute number of pathogens which are unable to synthesize heme, such as *Haemophilus influenza* (Stull, 1987), the question still remained of whether elevated heme levels in the circulation enhance infection by serving as an iron source for the remaining bacteria which are able to synthesize heme. This seemed not to be the case, as heme supplementation was unable to efficiently compensate for the partial chelation of growth medium “free” iron *in vitro*. Conclusive evidence supporting this notion came from *in vivo* sepsis experiments, where infection with *E. coli* unable to utilize heme as an iron source due to the deletion of the DppC subunit of its inner membrane transporter (DppABCDF) (Letoffe et al., 2006), was still enhanced by the presence of elevated plasma heme levels. Because DppC deletion does not affect outer membrane heme transport, the possibility that spontaneous degradation of heme trapped in the periplasm could provide

residual iron, albeit unlikely, remained. However, the likelihood that heme-iron acquisition by bacteria was causing the enhanced bacterial growth in the presence of high heme levels was ultimately dispelled by further *in vivo* experiments, as the administration of an equimolar amount of “free” iron failed to replicate the enhanced bacteremia found in heme-treated animals, both upon *E. coli* and *L. monocytogenes* infections. This is in line with the observation that pathogens are able to circumvent host iron withdrawal and nutritional immunity and indicates that the iron requirements of some pathogens are met via heme-independent mechanisms, such as siderophore-mediated iron acquisition or the scavenging of host iron-binding proteins (e.g. transferrin, ferritin, lactoferrin) (Freestone et al., 2003, Kvach et al., 1977, Skaar, 2010). Nevertheless, it should be noted that even though heme-iron acquisition played no role in the increased infection severity and bacteremia triggered by heme, it is possible that heme sensing by pathogens is recognized as a sign they are within a mammalian host, thus eliciting the expression of virulence genes (Miller, Hoffman et al., 2007). This could further contribute to the effects of hemolysis and elevated plasma heme levels, and although unlikely to play a major role, further studies would be needed to elucidate the extent of such an effect.

Instead of potentiating bacterial growth during infection through heme-iron delivery to bacteria, elevated plasma heme levels had a stark inhibitory effect on phagocytosis of bacteria by professional phagocytes, such as macrophages and neutrophils. The implications of such a defect on a crucial innate effector mechanism were reflected by the increased bacteremia and severity of infection, as it allowed invading bacteria to spread and multiply with little resistance (Berkowitz, 1991). It is not surprising that a strong inhibition of phagocytosis would render the animals susceptible to bacteria and sepsis. However, because labile heme itself has been described as having a pro-inflammatory effect and the ability to function as an alarmin (Soares & Bozza, 2016), we were surprised to find that excess heme levels could in parallel have such an immunosuppressive effect.

Labile heme can have well-known cytotoxic effects to many cell types (Ferreira et al., 2008, Gozzelino et al., 2010), including macrophages (Fortes et al., 2012), which are thought to be mediated via the generation of damaging ROS through Fenton chemistry (Gozzelino et al., 2010, Vincent, 1989, Vincent et al., 1988). Importantly, we could rule out cytotoxicity as the cause for the decreased phagocytic ability of macrophages *in vitro*. However, as the extent of hemolysis and labile heme in the circulation during infection *in vivo* can occasionally rise beyond our measured cytotoxicity threshold in macrophages, it is possible that immune cell death further compounds the deleterious effects of heme in cases of extreme hemolysis in the course of bacterial sepsis. For efficient pathogen removal and killing to occur, pathogens need

to be recognized prior to phagocytosis, and subsequently destroyed in the mature phagolysosome (Flannagan et al., 2009, Flannagan et al., 2012). Heme stimulations did not influence bacterial binding to macrophages, or intracellular killing upon bacteria internalization, which indicated that the effect of heme was specific to the phagocytic step.

Phagocytosis is a multistep process requiring the precise coordination of different pathways (Flannagan et al., 2012, Underhill & Ozinsky, 2002), and is crucially dependent on a fast and accurate rearrangement of the actin cytoskeleton, to generate the forces necessary to reshape the plasma membrane around the particle to be ingested, and to reel it into the cytoplasm (Chimini & Chavrier, 2000, Flannagan et al., 2012, Underhill & Ozinsky, 2002). In line with this, we found that heme had a profound effect on the cytoskeletal dynamics of macrophages, leading to an apparent dysregulated extension of leading edge structures (lamellipodia and filopodia) thereby disrupting phagocytosis. The dynamics of this effect were very fast, and visible after only 3 minutes of exposure to heme. Because the effect of heme on the cytoskeleton of macrophages was so swift and pervasive, we could safely rule out the effect of gene expression profile alterations potentially mediated by heme, as even highly responsive gene elements would likely require longer until enough protein had been translated (Milo & Phillips, 2016). Instead, the celerity by which heme stimulation led to cytoskeletal alterations suggested that this effect is rather mediated by immediate signaling cascades, and could be the result of cell surface receptor engagement, and/or the activation of intracellular signaling molecules. This was indeed the case, as an unbiased chemical proteomics approach demonstrated that heme was able to specifically associate with several actin cytoskeleton-regulating proteins. This sparked the discovery that the way heme induces cytoskeletal changes and impairs phagocytosis is dependent on the activity of the atypical GEF DOCK8 and its downstream Rho GTPase Cdc42, as well as the formin mDIA2. The dissection of this pathway was crucial towards understanding the molecular basis of heme-mediated immunosuppression. DOCK8 is a large intracellular plasma membrane-anchored protein which is thought to act as a signal relay from cell surface cues to downstream cytoskeleton regulators through its GEF activity towards Cdc42 (Harada et al., 2012). Whether DOCK8 is part of a heme-interacting protein complex or directly interacts with heme remains unanswered and future studies are needed to identify potential upstream events leading to DOCK8 activation, or to structurally characterize exactly how heme might bind DOCK8 and induce the activation of its DHR2 domain.

Our chemical proteomics experiments showed that other cytoskeletal regulators are able to associate with heme, among which we found several members of the ARP2/3 complex. The ARP2/3 complex is pivotal in many actin cytoskeleton-related processes, particularly in the

extension of branched-actin filaments such as those in lamellipodia (Higgs & Pollard, 2001, Ridley, 2011), which was in line with the observation that specific ARP2/3 inhibition abrogated heme-induced lamellipodia formation. Although ARP2/3 activity can be controlled by a wide array of mechanisms (Higgs & Pollard, 2001), we can safely speculate that its activity upon heme stimulation is downstream of Cdc42, as Cdc42 inhibition equally abrogated heme-induced and ARP2/3-dependent lamellipodia formation. Whether the association of the identified proteins with heme represent direct interactions, or co-precipitation with actin regulating complexes remains unanswered and further studies could prove exceptionally useful for the development of future therapeutics and our overall understanding of the structural aspects underlying the deleterious effects of heme on cytoskeletal function.

Adequate actin cytoskeleton rearrangement during innate immune responses is not only vital for phagocytosis, but also for leukocyte migration and chemotaxis (Bezanilla et al., 2015, Fletcher & Mullins, 2010, Vicente-Manzanares & Sanchez-Madrid, 2004). As expected, the disruption of cytoskeletal dynamics by heme impaired chemotaxis and motility of immune cells, both *in vitro* and *in vivo*, and likely contributes to the increased bacteremia and sepsis severity in the presence of elevated labile heme levels in the circulation. However, other immune effector mechanisms crucially depend on adequate actin cytoskeleton rearrangement, such as antigen uptake, processing and presentation, and any defect in these processes will invariably lead to inefficient antibody production and immunological memory formation (Moulding, Record et al., 2013). More experiments are required to test the hypothesis that cytoskeletal dynamics disruption by heme also impair adaptive immunity, and could be instrumental in redefining the impact of hemolysis and heme release on susceptibility to infection. In fact, it has long been noted that vaccine failure in SCD patients is a common event, despite extended vaccination programs (Ahonkhai, Landesman et al., 1979, Overturf, Field et al., 1979). In line with this, SCD patients show poor IgG and IgM antibody responses upon vaccination (Bjornson & Lobel, 1987, Overturf, Selzer et al., 1982), which is recapitulated in mouse models of SCD (Szczepanek, McNamara et al., 2012, Szczepanek, Secor et al., 2013). Furthermore, T cell memory formation is affected in SCD patients (Bertucci, El-Dahr et al., 2013). These defects are often solely attributed to hyposplenism due to constant splenic exposure to high levels of heme from senescent and defective erythrocytes (Brousse, Buffet et al., 2014). Nevertheless, reduced dendritic cell migration into lymph nodes, coupled to reduced phagocytosis and antigen presentation due to cytoskeletal impairment by heme, could play an unexpected role in the suppression of adaptive immune responses in people with SCD. In agreement with this hypothesis, people suffering from SCD are more prone to influenza

infection, and often suffer from prolonged and increased disease severity (Bundy, Strouse et al., 2010, Inusa, Zuckerman et al., 2010, Strouse, Reller et al., 2010), indicating that adaptive immunity is likely compromised. The hypothesis that heme-mediated cytoskeletal disruption contributes towards defective adaptive immune responses remains an extremely interesting open question, but requires further experimentation to assess its relevance to hemolytic disorders and explore its specific underlying mechanisms.

The immunosuppressive effects of excess heme uncovered in the course of this work were surprising in light of the tremendous evolutionary pressure exerted by malaria on human evolution (Kwiatkowski, 2005). As such, it is essential to reconcile these findings with the presence of such a vulnerability in the gene pool, in order to understand why no efficient negative selection occurred. While seemingly counterintuitive, it is important to note that highly efficient heme-scavenging and degradation mechanisms exist in mammals, and have likely evolved precisely to protect against such deleterious effects of free heme (Gozzelino et al., 2010, Smith & McCulloh, 2015, Tolosano et al., 2010). However, even such highly conserved protective mechanisms can be overwhelmed as a result of severe intravascular hemolysis (Muller-Eberhard et al., 1968, Schaer et al., 2013, Smith & McCulloh, 2015). This suggests that the energetic cost of running such protective mechanisms against cell-free heme constitutively is only evolutionarily affordable up to a certain accumulation of plasma heme, after which heme is able to more efficiently exert its immunosuppressive and organ-damaging effects (Ascenzi et al., 2005, Dutra & Bozza, 2014, Ferreira et al., 2008, Fortes et al., 2012, Larsen et al., 2010). It is also reasonable to speculate that some immunosuppressive action of excess cell-free heme are aimed at mitigating the extensive organ damage triggered by heme, by preventing its exacerbation due to unfettered inflammation and immunopathology. Recent studies have shed light on this possibility (Cunnington et al., 2012a, Cunnington et al., 2012b, Gozzelino, Andrade et al., 2012, Soares et al., 2014), but whether this is valid for the findings herein would require further experimentation to fully grasp the biological meaning underlying the effects of heme on cytoskeletal rearrangement. Although highly speculative, an interesting alternative hypothesis is that populations highly exposed to malaria, or where SCD alleles are present at high frequency, could have concomitantly fostered the appearance of heme-insensitive allele variants in members of the affected pathways, such as in *DOCK8*. Tackling this question would require a combination of population genetics, structural biology, and functional experiments, but bears the potential to thoroughly improve our understanding of heme-mediated pathology.

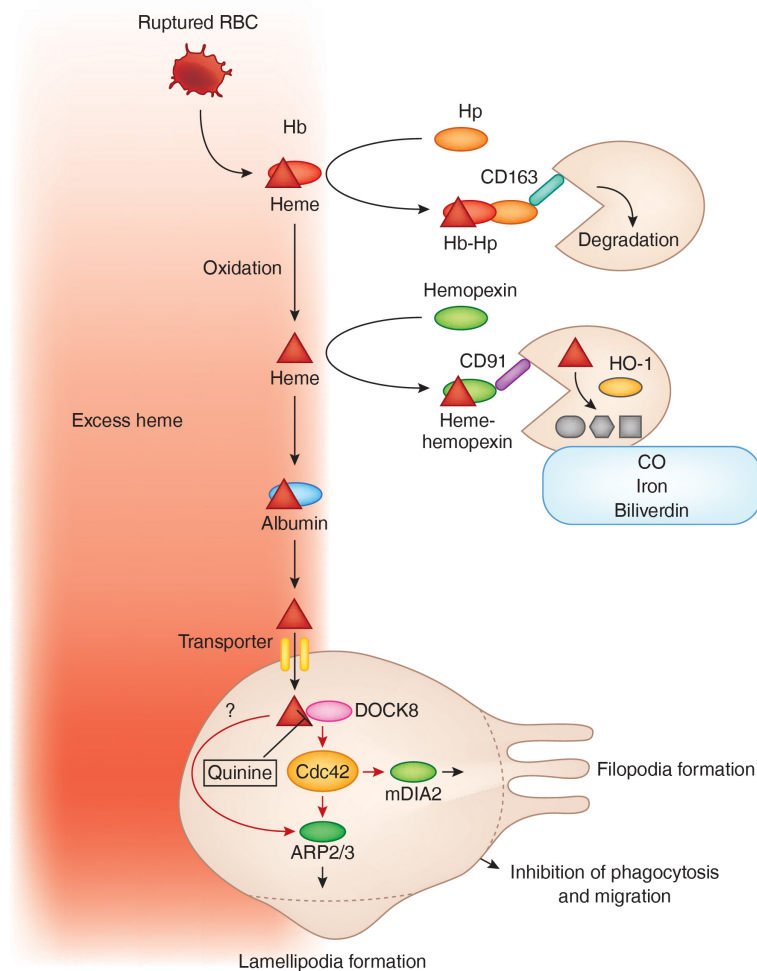


Figure 18 – Working model of how heme resulting from severe intravascular hemolysis is able to overwhelm plasma scavenging proteins and consequently disrupt phagocyte cytoskeletal dynamics, leading to inhibition of phagocytosis and chemotaxis. Hb = hemoglobin, Hp = haptoglobin. Taken from Tan & Wenginger (2016).

The discovery that excess heme affects cytoskeletal control pathways with negative consequences for innate immune responses exposes potential targets for therapeutic intervention. In line with this, a secondary aim of this thesis was to explore any possible therapeutic options geared towards reverting, or preventing the effects of heme on cytoskeletal dynamics. However, direct, target-driven manipulation of cytoskeletal pathways carries the risk of interfering with phagocytosis and cell migration by itself and is therefore not amenable for therapeutic exploration (Chimini & Chavrier, 2000, Flannagan et al., 2012, Lee et al., 2000). Instead, an unbiased approach revealed that quinine was able to prevent the inhibitory effects of heme on phagocytosis while having no influence on baseline phagocytic ability, providing a proof-of-concept approach which showed remarkable efficacy in countering the effects of excess heme in a mouse model of Gram negative sepsis. The exact mechanism by which quinine is able to prevent heme-mediated cytoskeletal disruption is an important open question as it might hold the key to engineer future therapeutic agents. Nevertheless, preliminary data seem

to indicate that quinine might specifically prevent the association of heme and DOCK8, indicating that steric hindrance could play a role. This possibility is supported by the observation that quinine is able to bind heme (Leed, DuBay et al., 2002). In agreement with this, we found that 3 out of the 6 top scoring chemicals (including quinine) were known to either bind heme, or display anti-malarial activity (data not shown), indicating that complexing heme might be a viable therapeutic strategy. Similarly, hemopexin replenishment in cases of hemopexin exhaustion due to severe intravascular hemolysis could have many-fold benefits, as evidenced already by Larsen et al. (2010). Alternatively, heme uptake by specific transporters could be targeted, to avoid increased cytosolic heme in macrophages. However, specific heme transport across plasma membranes in mammals is yet poorly described, and there's the possibility that heme is able to diffuse through membranes due to its amphipathic nature (Khan & Quigley, 2011, Khan & Quigley, 2013, Smith & McCulloh, 2015), making it an unlikely therapeutic target. Furthermore, inhibition of heme uptake would increase the concentration and half-life of circulatory heme with potential consequences for vascular homeostasis (Balla, Vercellotti et al., 2005). Finally, the immunoadjuvant therapy concept explored in this work serves as a proof-of-concept that restoring immune effector functions can help bypass the need for pathogen-targeted therapeutics (i.e. antibiotics), which in this case is accomplished by rendering phagocytic cells insensitive to heme-mediated cytoskeletal disruption. This could fuel the development of novel therapies for patients suffering from sepsis or hemolytic disorders, such as SCD, α and β thalassemia or malaria, by restoring efficient immune responses and abrogating the susceptibility to infection observed in these patients.

4. References

A-Gonzalez N, Guillen JA, Gallardo G, Diaz M, de la Rosa JV, Hernandez IH, Casanova-Acebes M, Lopez F, Tabraue C, Beceiro S, Hong C, Lara PC, Andujar M, Arai S, Miyazaki T, Li S, Corbi AL, Tontonoz P, Hidalgo A, Castrillo A (2013) The nuclear receptor LXRalpha controls the functional specialization of splenic macrophages. *Nat Immunol* 14: 831-9

Abu Kwaik Y, Bumann D (2015) Host Delivery of Favorite Meals for Intracellular Pathogens. *PLoS Pathog* 11: e1004866

Adamzik M, Hamburger T, Petrat F, Peters J, de Groot H, Hartmann M (2012) Free hemoglobin concentration in severe sepsis: methods of measurement and prediction of outcome. *Crit Care* 16: R125

Ahonkhai VI, Landesman SH, Fikrig SM, Schmalzer EA, Brown AK, Cherubin CE, Schiffman G (1979) Failure of pneumococcal vaccine in children with sickle-cell disease. *N Engl J Med* 301: 26-7

Akgul C, Edwards SW (2003) Regulation of neutrophil apoptosis via death receptors. *Cell Mol Life Sci* 60: 2402-8

Alberts B (2002) Chapter 24 The Adaptive Immune System. In *Molecular biology of the cell*, pp xxxiv, 1548 p. New York: Garland Science

Allhorn M, Berggard T, Nordberg J, Olsson ML, Akerstrom B (2002) Processing of the lipocalin alpha(1)-microglobulin by hemoglobin induces heme-binding and heme-degradation properties. *Blood* 99: 1894-901

Andrews NC, Schmidt PJ (2007) Iron Homeostasis. *Annual Review of Physiology* 69: 69-85

Ascenzi P, Bocedi A, Visca P, Altruda F, Tolosano E, Beringhelli T, Fasano M (2005) Hemoglobin and heme scavenging. *IUBMB Life* 57: 749-59

Ashley NT, Weil ZM, Nelson RJ (2012) Inflammation: Mechanisms, Costs, and Natural Variation. *Annual Review of Ecology, Evolution, and Systematics* 43: 385-406

Baccala R, Gonzalez-Quintial R, Lawson BR, Stern ME, Kono DH, Beutler B, Theofilopoulos AN (2009) Sensors of the innate immune system: their mode of action. *Nat Rev Rheumatol* 5: 448-56

Balla J, Vercellotti GM, Jeney V, Yachie A, Varga Z, Eaton JW, Balla G (2005) Heme, heme oxygenase and ferritin in vascular endothelial cell injury. *Mol Nutr Food Res* 49: 1030-43

Bamburg JR, Bernstein BW (2010) Roles of ADF/cofilin in actin polymerization and beyond. *F1000 Biol Rep* 2: 62

Berkowitz FE (1991) Hemolysis and infection: categories and mechanisms of their interrelationship. *Reviews of infectious diseases* 13: 1151-62

Bertucci E, El-Dahr JL, Kanter-Washko J (2013) Sickle Cell Disease and Poor Response to Pneumococcal Vaccination. *J Allergy Clin Immunol* 131: AB157

Beutler BA (2009) TLRs and innate immunity. *Blood* 113: 1399-407

- Beutler E (2008) Glucose-6-phosphate dehydrogenase deficiency: a historical perspective. *Blood* 111: 16-24
- Bezanilla M, Gladfelter AS, Kovar DR, Lee WL (2015) Cytoskeletal dynamics: a view from the membrane. *J Cell Biol* 209: 329-37
- Birmingham CL, Canadien V, Kaniuk NA, Steinberg BE, Higgins DE, Brumell JH (2008) Listeriolysin O allows *Listeria monocytogenes* replication in macrophage vacuoles. *Nature* 451: 350-4
- Bjornson AB, Lobel JS (1987) Direct evidence that decreased serum opsonization of *Streptococcus pneumoniae* via the alternative complement pathway in sickle cell disease is related to antibody deficiency. *J Clin Invest* 79: 388-98
- Blanchoin L, Boujemaa-Paterski R, Sykes C, Plastino J (2014) Actin dynamics, architecture, and mechanics in cell motility. *Physiol Rev* 94: 235-63
- Bloes DA, Kretschmer D, Peschel A (2015) Enemy attraction: bacterial agonists for leukocyte chemotaxis receptors. *Nature reviews Microbiology* 13: 95-104
- Booth C, Inusa B, Obaro SK (2010) Infection in sickle cell disease: a review. *International journal of infectious diseases : IJID : official publication of the International Society for Infectious Diseases* 14: e2-e12
- Brinkmann V, Reichard U, Goosmann C, Fauler B, Uhlemann Y, Weiss DS, Weinrauch Y, Zychlinsky A (2004) Neutrophil extracellular traps kill bacteria. *Science* 303: 1532-5
- Brousse V, Buffet P, Rees D (2014) The spleen and sickle cell disease: the sick(led) spleen. *Br J Haematol* 166: 165-76
- Brown SA, Palmer KL, Whiteley M (2008) Revisiting the host as a growth medium. *Nature reviews Microbiology* 6: 657-66
- Buffet PA, Safeukui I, Deplaine G, Brousse V, Prendki V, Thellier M, Turner GD, Mercereau-Puijalon O (2011) The pathogenesis of *Plasmodium falciparum* malaria in humans: insights from splenic physiology. *Blood* 117: 381-92
- Bundy DG, Strouse JJ, Casella JF, Miller MR (2010) Burden of influenza-related hospitalizations among children with sickle cell disease. *Pediatrics* 125: 234-43
- Buttery J, Moxon ER (2002) Capsulate bacteria and the lung. *Br Med Bull* 61: 63-80
- Cassat JE, Skaar EP (2013) Iron in infection and immunity. *Cell host & microbe* 13: 509-19
- Chen G, Shaw MH, Kim YG, Nunez G (2009) NOD-like receptors: role in innate immunity and inflammatory disease. *Annual review of pathology* 4: 365-98
- Chen JJ (2007) Regulation of protein synthesis by the heme-regulated eIF2 α kinase: relevance to anemias. *Blood* 109: 2693-9
- Cherfils J, Zeghouf M (2013) Regulation of small GTPases by GEFs, GAPs, and GDIs. *Physiol Rev* 93: 269-309

Chiabrando D, Vinchi F, Fiorito V, Mercurio S, Tolosano E (2014) Heme in pathophysiology: a matter of scavenging, metabolism and trafficking across cell membranes. *Front Pharmacol* 5: 61

Chimini G, Chavrier P (2000) Function of Rho family proteins in actin dynamics during phagocytosis and engulfment. *Nat Cell Biol* 2: E191-6

Chiu D, Lubin B (1989) Oxidative hemoglobin denaturation and RBC destruction: the effect of heme on red cell membranes. *Semin Hematol* 26: 128-35

Chovatiya R, Medzhitov R (2014) Stress, inflammation, and defense of homeostasis. *Mol Cell* 54: 281-8

Church J, Maitland K (2014) Invasive bacterial co-infection in African children with *Plasmodium falciparum* malaria: a systematic review. *BMC medicine* 12: 31

Cote JF, Vuori K (2002) Identification of an evolutionarily conserved superfamily of DOCK180-related proteins with guanine nucleotide exchange activity. *J Cell Sci* 115: 4901-13

Cunnington AJ, de Souza JB, Walther M, Riley EM (2012a) Malaria impairs resistance to *Salmonella* through heme- and heme oxygenase-dependent dysfunctional granulocyte mobilization. *Nat Med* 18: 120-7

Cunnington AJ, Njie M, Correa S, Takem EN, Riley EM, Walther M (2012b) Prolonged neutrophil dysfunction after *Plasmodium falciparum* malaria is related to hemolysis and heme oxygenase-1 induction. *J Immunol* 189: 5336-46

Curnock AP, Logan MK, Ward SG (2002) Chemokine signalling: pivoting around multiple phosphoinositide 3-kinases. *Immunology* 105: 125-36

Delves PJ, Roitt IM (2000a) The immune system. First of two parts. *N Engl J Med* 343: 37-49

Delves PJ, Roitt IM (2000b) The immune system. Second of two parts. *N Engl J Med* 343: 108-17

DerMardirossian C, Bokoch GM (2005) GDIs: central regulatory molecules in Rho GTPase activation. *Trends Cell Biol* 15: 356-63

Desjardins M, Huber LA, Parton RG, Griffiths G (1994) Biogenesis of phagolysosomes proceeds through a sequential series of interactions with the endocytic apparatus. *J Cell Biol* 124: 677-88

Diacovich L, Gorvel JP (2010) Bacterial manipulation of innate immunity to promote infection. *Nature reviews Microbiology* 8: 117-28

Dixon SJ, Stockwell BR (2014) The role of iron and reactive oxygen species in cell death. *Nat Chem Biol* 10: 9-17

Dobbs K, Dominguez Conde C, Zhang SY, Parolini S, Audry M, Chou J, Haapaniemi E, Keles S, Bilic I, Okada S, Massaad MJ, Rounioja S, Alwahadneh AM, Serwas NK, Capuder K, Ciftci E, Felgentreff K, Ohsumi TK, Pedergnana V, Boisson B et al. (2015) Inherited DOCK2 Deficiency in Patients with Early-Onset Invasive Infections. *N Engl J Med* 372: 2409-22

Docherty JC, Firneisz GD, Schacter BA (1984) Methene bridge carbon atom elimination in oxidative heme degradation catalyzed by heme oxygenase and NADPH-cytochrome P-450 reductase. *Arch Biochem Biophys* 235: 657-64

Dominguez R, Holmes KC (2011) Actin structure and function. *Annu Rev Biophys* 40: 169-86

Dong N, Liu L, Shao F (2010) A bacterial effector targets host DH-PH domain RhoGEFs and antagonizes macrophage phagocytosis. *EMBO J* 29: 1363-76

Dutra FF, Alves LS, Rodrigues D, Fernandez PL, de Oliveira RB, Golenbock DT, Zamboni DS, Bozza MT (2014) Hemolysis-induced lethality involves inflammasome activation by heme. *Proc Natl Acad Sci U S A* 111: E4110-8

Dutra FF, Bozza MT (2014) Heme on innate immunity and inflammation. *Front Pharmacol* 5: 115

Eber SW, Gonzalez JM, Lux ML, Scarpa AL, Tse WT, Dornwell M, Herbers J, Kugler W, Ozcan R, Pekrun A, Gallagher PG, Schroter W, Forget BG, Lux SE (1996) Ankyrin-1 mutations are a major cause of dominant and recessive hereditary spherocytosis. *Nat Genet* 13: 214-8

Esser C (2016) Environmental influences on the immune system. Springer, Vienna

Etienne-Manneville S (2004) Cdc42--the centre of polarity. *J Cell Sci* 117: 1291-300

Ferreira A, Balla J, Jeney V, Balla G, Soares MP (2008) A central role for free heme in the pathogenesis of severe malaria: the missing link? *J Mol Med* 86: 1097-111

Fibach E, Rachmilewitz E (2008) The role of oxidative stress in hemolytic anemia. *Curr Mol Med* 8: 609-19

Figueiredo RT, Fernandez PL, Mourao-Sa DS, Porto BN, Dutra FF, Alves LS, Oliveira MF, Oliveira PL, Graca-Souza AV, Bozza MT (2007) Characterization of heme as activator of Toll-like receptor 4. *J Biol Chem* 282: 20221-9

Finlay BB, McFadden G (2006) Anti-immunology: evasion of the host immune system by bacterial and viral pathogens. *Cell* 124: 767-82

Flannagan RS, Cosio G, Grinstein S (2009) Antimicrobial mechanisms of phagocytes and bacterial evasion strategies. *Nature reviews Microbiology* 7: 355-66

Flannagan RS, Jaumouille V, Grinstein S (2012) The cell biology of phagocytosis. *Annual review of pathology* 7: 61-98

Fletcher DA, Mullins RD (2010) Cell mechanics and the cytoskeleton. *Nature* 463: 485-92

Forster R, Davalos-Misslitz AC, Rot A (2008) CCR7 and its ligands: balancing immunity and tolerance. *Nat Rev Immunol* 8: 362-71

Fortes GB, Alves LS, de Oliveira R, Dutra FF, Rodrigues D, Fernandez PL, Souto-Pradon T, De Rosa MJ, Kelliher M, Golenbock D, Chan FK, Bozza MT (2012) Heme induces programmed necrosis on macrophages through autocrine TNF and ROS production. *Blood* 119: 2368-75

Freedman J (2015) Autoimmune Hemolysis: A Journey through Time. *Transfus Med Hemother* 42: 278-85

Freestone PP, Haigh RD, Williams PH, Lyte M (2003) Involvement of enterobactin in norepinephrine-mediated iron supply from transferrin to enterohaemorrhagic *Escherichia coli*. *FEMS Microbiol Lett* 222: 39-43

Gadea G, Blangy A (2014) Dock-family exchange factors in cell migration and disease. *Eur J Cell Biol* 93: 466-77

Galan JE, Lara-Tejero M, Marlovits TC, Wagner S (2014) Bacterial type III secretion systems: specialized nanomachines for protein delivery into target cells. *Annu Rev Microbiol* 68: 415-38

Ganz T (2012) Macrophages and systemic iron homeostasis. *Journal of innate immunity* 4: 446-53

Ganz T (2013) Systemic iron homeostasis. *Physiol Rev* 93: 1721-41

Ganz T, Nemeth E (2015) Iron homeostasis in host defence and inflammation. *Nat Rev Immunol* 15: 500-10

Ghirelli C, Hagemann T (2013) Targeting immunosuppression for cancer therapy. *J Clin Invest* 123: 2355-7

Ginhoux F, Jung S (2014) Monocytes and macrophages: developmental pathways and tissue homeostasis. *Nat Rev Immunol* 14: 392-404

Ginhoux F, Schultze JL, Murray PJ, Ochando J, Biswas SK (2016) New insights into the multidimensional concept of macrophage ontogeny, activation and function. *Nat Immunol* 17: 34-40

Glass CK, Natoli G (2016) Molecular control of activation and priming in macrophages. *Nat Immunol* 17: 26-33

Gozzelino R, Andrade BB, Larsen R, Luz NF, Vanoaica L, Seixas E, Coutinho A, Cardoso S, Rebelo S, Poli M, Barral-Netto M, Darshan D, Kuhn LC, Soares MP (2012) Metabolic adaptation to tissue iron overload confers tolerance to malaria. *Cell host & microbe* 12: 693-704

Gozzelino R, Jeney V, Soares MP (2010) Mechanisms of cell protection by heme oxygenase-1. *Annual review of pharmacology and toxicology* 50: 323-54

Grice EA, Segre JA (2011) The skin microbiome. *Nature reviews Microbiology* 9: 244-53

Griffith JW, Sokol CL, Luster AD (2014) Chemokines and chemokine receptors: positioning cells for host defense and immunity. *Annual review of immunology* 32: 659-702

Harada Y, Tanaka Y, Terasawa M, Pieczyk M, Habiro K, Katakai T, Hanawa-Suetsugu K, Kukimoto-Niino M, Nishizaki T, Shirouzu M, Duan X, Uruno T, Nishikimi A, Sanematsu F, Yokoyama S, Stein JV, Kinashi T, Fukui Y (2012) DOCK8 is a Cdc42 activator critical for interstitial dendritic cell migration during immune responses. *Blood* 119: 4451-61

Hardt WD, Chen LM, Schuebel KE, Bustelo XR, Galan JE (1998) *S. typhimurium* encodes an activator of Rho GTPases that induces membrane ruffling and nuclear responses in host cells. *Cell* 93: 815-26

Haslett C, Savill JS, Whyte MK, Stern M, Dransfield I, Meagher LC (1994) Granulocyte apoptosis and the control of inflammation. *Philos Trans R Soc Lond B Biol Sci* 345: 327-33

Heasman SJ, Ridley AJ (2008) Mammalian Rho GTPases: new insights into their functions from in vivo studies. *Nat Rev Mol Cell Biol* 9: 690-701

Herrmann H, Bar H, Kreplak L, Strelkov SV, Aebi U (2007) Intermediate filaments: from cell architecture to nanomechanics. *Nat Rev Mol Cell Biol* 8: 562-73

Higgs HN, Pollard TD (2001) Regulation of actin filament network formation through ARP2/3 complex: activation by a diverse array of proteins. *Annu Rev Biochem* 70: 649-76

Hill GB (1978) Enhancement of experimental anaerobic infections by blood, hemoglobin, and hemostatic agents. *Infection and immunity* 19: 443-9

Hood MI, Skaar EP (2012) Nutritional immunity: transition metals at the pathogen-host interface. *Nature reviews Microbiology* 10: 525-37

Huber F, Schnauss J, Ronicke S, Rauch P, Muller K, Futterer C, Kas J (2013) Emergent complexity of the cytoskeleton: from single filaments to tissue. *Adv Phys* 62: 1-112

Hvidberg V, Maniecki MB, Jacobsen C, Hojrup P, Moller HJ, Moestrup SK (2005) Identification of the receptor scavenging hemopexin-heme complexes. *Blood* 106: 2572-9

Inusa B, Zuckerman M, Gadong N, Afif M, Arnott S, Heath P, Marais G, Robertson P, Payne H, Wilkey O, Rees DC (2010) Pandemic influenza A (H1N1) virus infections in children with sickle cell disease. *Blood* 115: 2329-30

Jaffe AB, Hall A (2005) Rho GTPases: biochemistry and biology. *Annual review of cell and developmental biology* 21: 247-69

Janeway C (2001) The generation of diversity in immunoglobulins. In *Immunobiology 5 : the immune system in health and disease*, pp xviii, 732 p. New York: Garland Pub.

Jordan PM (1991) Biosynthesis of tetrapyrroles. Elsevier ; New York, NY, USA : Sole distributors for the USA and Canada, Elsevier Science Pub. Co., Amsterdam ; New York

Kadish KM, Smith KM, Guillard R (2000) The porphyrin handbook. Academic Press, San Diego

Kaplan W, Wirtz VJ, Mantel-Teeuwisse A, Stolk P, Duthey B, Laing R (2013) Priority Medicines for Europe and the World 2013 Update. World Health Organization, Geneva, Switzerland

Khan AA, Quigley JG (2011) Control of intracellular heme levels: heme transporters and heme oxygenases. *Biochim Biophys Acta* 1813: 668-82

Khan AA, Quigley JG (2013) Heme and FLVCR-related transporter families SLC48 and SLC49. *Molecular aspects of medicine* 34: 669-82

Kikuchi G, Yoshida T, Noguchi M (2005) Heme oxygenase and heme degradation. *Biochem Biophys Res Commun* 338: 558-67

Kolaczowska E, Kubes P (2013) Neutrophil recruitment and function in health and inflammation. *Nat Rev Immunol* 13: 159-75

Korolnek T, Hamza I (2015) Macrophages and iron trafficking at the birth and death of red cells. *Blood* 125: 2893-7

Kotas ME, Medzhitov R (2015) Homeostasis, Inflammation, and Disease Susceptibility. *Cell* 160: 816-827

Krishnaswamy JK, Singh A, Gowthaman U, Wu R, Gorrepati P, Sales Nascimento M, Gallman A, Liu D, Rhebergen AM, Calabro S, Xu L, Ranney P, Srivastava A, Ranson M, Gorham JD, McCaw Z, Kleeberger SR, Heinz LX, Muller AC, Bennett KL et al. (2015) Coincidental loss of DOCK8 function in NLRP10-deficient and C3H/HeJ mice results in defective dendritic cell migration. *Proc Natl Acad Sci U S A* 112: 3056-61

Kruger P, Saffarzadeh M, Weber AN, Rieber N, Radsak M, von Bernuth H, Benarafa C, Roos D, Skokowa J, Hartl D (2015) Neutrophils: Between host defence, immune modulation, and tissue injury. *PLoS Pathog* 11: e1004651

Kumar H, Kawai T, Akira S (2011) Pathogen recognition by the innate immune system. *Int Rev Immunol* 30: 16-34

Kvach JT, Wiles TI, Mellencamp MW, Kochan I (1977) Use of transferrin-iron enterobactin complexes as the source of iron by serum-exposed bacteria. *Infection and immunity* 18: 439-45

Kwiatkowski DP (2005) How malaria has affected the human genome and what human genetics can teach us about malaria. *Am J Hum Genet* 77: 171-92

Lai Y, Di Nardo A, Nakatsuji T, Leichtle A, Yang Y, Cogen AL, Wu ZR, Hooper LV, Schmidt RR, von Aulock S, Radek KA, Huang CM, Ryan AF, Gallo RL (2009) Commensal bacteria regulate Toll-like receptor 3-dependent inflammation after skin injury. *Nat Med* 15: 1377-82

Lambrechts A, Gevaert K, Cossart P, Vandekerckhove J, Van Troys M (2008) Listeria comet tails: the actin-based motility machinery at work. *Trends Cell Biol* 18: 220-7

Larsen R, Gozzelino R, Jeney V, Tokaji L, Bozza FA, Japiassu AM, Bonaparte D, Cavalcante MM, Chora A, Ferreira A, Marguti I, Cardoso S, Sepulveda N, Smith A, Soares MP (2010) A central role for free heme in the pathogenesis of severe sepsis. *Sci Transl Med* 2: 51ra71

Laurin M, Cote JF (2014) Insights into the biological functions of Dock family guanine nucleotide exchange factors. *Genes Dev* 28: 533-47

Lavin Y, Mortha A, Rahman A, Merad M (2015) Regulation of macrophage development and function in peripheral tissues. *Nat Rev Immunol* 15: 731-44

LeBlanc JG, Milani C, de Giori GS, Sesma F, van Sinderen D, Ventura M (2013) Bacteria as vitamin suppliers to their host: a gut microbiota perspective. *Curr Opin Biotechnol* 24: 160-8

Lee DJ, Cox D, Li J, Greenberg S (2000) Rac1 and Cdc42 are required for phagocytosis, but not NF-kappaB-dependent gene expression, in macrophages challenged with *Pseudomonas aeruginosa*. *J Biol Chem* 275: 141-6

Lee WL, Harrison RE, Grinstein S (2003) Phagocytosis by neutrophils. *Microbes Infect* 5: 1299-306

Leed A, DuBay K, Ursos LM, Sears D, De Dios AC, Roepe PD (2002) Solution structures of antimalarial drug-heme complexes. *Biochemistry* 41: 10245-55

Letoffe S, Delepelaire P, Wandersman C (2006) The housekeeping dipeptide permease is the *Escherichia coli* heme transporter and functions with two optional peptide binding proteins. *Proc Natl Acad Sci U S A* 103: 12891-6

Lucas T, Waisman A, Ranjan R, Roes J, Krieg T, Muller W, Roers A, Eming SA (2010) Differential roles of macrophages in diverse phases of skin repair. *J Immunol* 184: 3964-77

Maartens G, Celum C, Lewin SR (2014) HIV infection: epidemiology, pathogenesis, treatment, and prevention. *Lancet* 384: 258-71

Maines MD, Trakshel GM, Kutty RK (1986) Characterization of two constitutive forms of rat liver microsomal heme oxygenase. Only one molecular species of the enzyme is inducible. *J Biol Chem* 261: 411-9

Malagoli D (2016) The evolution of the immune system : conservation and diversification. Elsevier, Boston, MA

Marchesi JR, Adams DH, Fava F, Hermes GD, Hirschfield GM, Hold G, Quraishi MN, Kinross J, Smidt H, Tuohy KM, Thomas LV, Zoetendal EG, Hart A (2016) The gut microbiota and host health: a new clinical frontier. *Gut* 65: 330-9

Mattila PK, Lappalainen P (2008) Filopodia: molecular architecture and cellular functions. *Nat Rev Mol Cell Biol* 9: 446-54

McCusker C, Warrington R (2011) Primary immunodeficiency. *Allergy Asthma Clin Immunol* 7 Suppl 1: S11

Mechnikov I (1883) Untersuchungen über die intrazelluläre Verdauung bei wirbellosen Tieren. *Arb Zool Inst Univ Wien* 5: 1-28

Medzhitov R (2008) Origin and physiological roles of inflammation. *Nature* 454: 428-35

Medzhitov R, Janeway C, Jr. (2000) Innate immunity. *N Engl J Med* 343: 338-44

Medzhitov R, Schneider DS, Soares MP (2012) Disease tolerance as a defense strategy. *Science* 335: 936-41

Miller SI, Hoffman LR, Sanowar S (2007) Did bacterial sensing of host environments evolve from sensing within microbial communities? *Cell host & microbe* 1: 85-7

Milo R, Phillips R (2016) Cell biology by the numbers. Garland Science, New York, NY

Mocsai A (2013) Diverse novel functions of neutrophils in immunity, inflammation, and beyond. *J Exp Med* 210: 1283-99

Modell B, Darlison M (2008) Global epidemiology of haemoglobin disorders and derived service indicators. *Bulletin of the World Health Organization* 86: 480-7

Mostowy S, Shenoy AR (2015) The cytoskeleton in cell-autonomous immunity: structural determinants of host defence. *Nat Rev Immunol* 15: 559-73

Motterlini R, Otterbein LE (2010) The therapeutic potential of carbon monoxide. *Nat Rev Drug Discov* 9: 728-43

Moulding DA, Record J, Malinova D, Thrasher AJ (2013) Actin cytoskeletal defects in immunodeficiency. *Immunol Rev* 256: 282-99

Muller-Eberhard U, Javid J, Liem HH, Hanstein A, Hanna M (1968) Plasma concentrations of hemopexin, haptoglobin and heme in patients with various hemolytic diseases. *Blood* 32: 811-5

Muller-Eberhard U, Liem HH (1974) Hemopexin, The Heme-Binding Serum β -Glycoprotein. In *Structure and function of plasma proteins*, Allison AC (ed) London ; New York: Plenum Press

Murray PJ, Wynn TA (2011) Protective and pathogenic functions of macrophage subsets. *Nat Rev Immunol* 11: 723-37

Naik S, Bouladoux N, Linehan JL, Han SJ, Harrison OJ, Wilhelm C, Conlan S, Himmelfarb S, Byrd AL, Deming C, Quinones M, Brenchley JM, Kong HH, Tussiwand R, Murphy KM, Merad M, Segre JA, Belkaid Y (2015) Commensal-dendritic-cell interaction specifies a unique protective skin immune signature. *Nature* 520: 104-8

Nishikimi A, Kukimoto-Niino M, Yokoyama S, Fukui Y (2013) Immune regulatory functions of DOCK family proteins in health and disease. *Exp Cell Res* 319: 2343-9

Nogales E (2000) Structural insights into microtubule function. *Annu Rev Biochem* 69: 277-302

Noinaj N, Guillier M, Barnard TJ, Buchanan SK (2010) TonB-dependent transporters: regulation, structure, and function. *Annu Rev Microbiol* 64: 43-60

O'Neill LA, Golenbock D, Bowie AG (2013) The history of Toll-like receptors - redefining innate immunity. *Nat Rev Immunol* 13: 453-60

Ortega-Gomez A, Perretti M, Soehnlein O (2013) Resolution of inflammation: an integrated view. *EMBO Mol Med* 5: 661-74

Otterbein LE, Bach FH, Alam J, Soares M, Tao Lu H, Wysk M, Davis RJ, Flavell RA, Choi AM (2000) Carbon monoxide has anti-inflammatory effects involving the mitogen-activated protein kinase pathway. *Nat Med* 6: 422-8

Otto BR, van Dooren SJ, Dozois CM, Luirink J, Oudega B (2002) *Escherichia coli* hemoglobin protease autotransporter contributes to synergistic abscess formation and heme-dependent growth of *Bacteroides fragilis*. *Infection and immunity* 70: 5-10

Overturf GD, Field R, Edmonds R (1979) Death from type 6 pneumococcal septicemia in a vaccinated child with sickle-cell disease. *N Engl J Med* 300: 143

Overturf GD, Selzer JW, Chan L, Weiss J, Field R, Rigau-Perez JG, Powars D, Uy C, Pang EJ, Honig G, Steele R, Edmonds R, Portnoy B (1982) Pneumococcal polysaccharide immunization of children with sickle cell disease. II. Serologic response and pneumococcal disease following immunization. *Am J Pediatr Hematol Oncol* 4: 25-35

Paoli M, Anderson BF, Baker HM, Morgan WT, Smith A, Baker EN (1999) Crystal structure of hemopexin reveals a novel high-affinity heme site formed between two beta-propeller domains. *Nat Struct Biol* 6: 926-31

Perdiguero EG, Geissmann F (2016) The development and maintenance of resident macrophages. *Nat Immunol* 17: 2-8

Pollard TD, Blanchoin L, Mullins RD (2000) Molecular mechanisms controlling actin filament dynamics in nonmuscle cells. *Annu Rev Biophys Biomol Struct* 29: 545-76

Premkumar L, Bobkov AA, Patel M, Jaroszewski L, Bankston LA, Stec B, Vuori K, Cote JF, Liddington RC (2010) Structural basis of membrane targeting by the Dock180 family of Rho family guanine exchange factors (Rho-GEFs). *J Biol Chem* 285: 13211-22

Prestia K, Bandyopadhyay S, Slate A, Francis RO, Francis KP, Spitalnik SL, Fidock DA, Brittenham GM, Hod EA (2014) Transfusion of stored blood impairs host defenses against Gram-negative pathogens in mice. *Transfusion* 54: 2842-51

Puntarulo S (2005) Iron, oxidative stress and human health. *Molecular aspects of medicine* 26: 299-312

Raftopoulou M, Hall A (2004) Cell migration: Rho GTPases lead the way. *Dev Biol* 265: 23-32

Ramakrishnan M, Moisi JC, Klugman KP, Iglesias JM, Grant LR, Mpoudi-Etame M, Levine OS (2010) Increased risk of invasive bacterial infections in African people with sickle-cell disease: a systematic review and meta-analysis. *The Lancet Infectious diseases* 10: 329-37

Rees DC, Williams TN, Gladwin MT (2010) Sickle-cell disease. *Lancet* 376: 2018-31

Reikine S, Nguyen JB, Modis Y (2014) Pattern Recognition and Signaling Mechanisms of RIG-I and MDA5. *Front Immunol* 5: 342

Ridley AJ (2011) Life at the leading edge. *Cell* 145: 1012-22

RossBoswell (2012) Heme B biosynthesis pathway and its modulators. In *Wikimedia commons*

Rossmann KL, Der CJ, Sondek J (2005) GEF means go: turning on RHO GTPases with guanine nucleotide-exchange factors. *Nat Rev Mol Cell Biol* 6: 167-80

Runyen-Janecky LJ (2013) Role and regulation of heme iron acquisition in gram-negative pathogens. *Front Cell Infect Microbiol* 3: 55

Ryter SW, Alam J, Choi AM (2006) Heme oxygenase-1/carbon monoxide: from basic science to therapeutic applications. *Physiol Rev* 86: 583-650

Saclier M, Yacoub-Youssef H, Mackey AL, Arnold L, Ardjoune H, Magnan M, Sailhan F, Chelly J, Pavlath GK, Mounier R, Kjaer M, Chazaud B (2013) Differentially activated macrophages orchestrate myogenic precursor cell fate during human skeletal muscle regeneration. *Stem Cells* 31: 384-96

Sarantis H, Grinstein S (2012) Subversion of phagocytosis for pathogen survival. *Cell host & microbe* 12: 419-31

Savill JS, Wyllie AH, Henson JE, Walport MJ, Henson PM, Haslett C (1989) Macrophage phagocytosis of aging neutrophils in inflammation. Programmed cell death in the neutrophil leads to its recognition by macrophages. *J Clin Invest* 83: 865-75

Schaer DJ, Buehler PW, Alayash AI, Belcher JD, Vercellotti GM (2013) Hemolysis and free hemoglobin revisited: exploring hemoglobin and heme scavengers as a novel class of therapeutic proteins. *Blood* 121: 1276-84

Schmidt A, Hall A (2002) Guanine nucleotide exchange factors for Rho GTPases: turning on the switch. *Genes Dev* 16: 1587-609

Schmitt TH, Frezzatti WA, Jr., Schreier S (1993) Hemin-induced lipid membrane disorder and increased permeability: a molecular model for the mechanism of cell lysis. *Arch Biochem Biophys* 307: 96-103

Scrimshaw NS, Taylor CE, Gordon JE, World Health Organization. (1968) Interactions of nutrition and infection. World Health Organization, Geneva

Sekirov I, Russell SL, Antunes LC, Finlay BB (2010) Gut microbiota in health and disease. *Physiol Rev* 90: 859-904

Severance S, Hamza I (2009) Trafficking of heme and porphyrins in metazoa. *Chem Rev* 109: 4596-616

Shi C, Pamer EG (2011) Monocyte recruitment during infection and inflammation. *Nat Rev Immunol* 11: 762-74

Sit ST, Manser E (2011) Rho GTPases and their role in organizing the actin cytoskeleton. *J Cell Sci* 124: 679-83

Skaar EP (2010) The battle for iron between bacterial pathogens and their vertebrate hosts. *PLoS Pathog* 6: e1000949

Smith A, McCulloh RJ (2015) Hemopexin and haptoglobin: allies against heme toxicity from hemoglobin not contenders. *Front Physiol* 6: 187

Soares MP, Bozza MT (2016) Red alert: labile heme is an alarmin. *Curr Opin Immunol* 38: 94-100

Soares MP, Gozzelino R, Weis S (2014) Tissue damage control in disease tolerance. *Trends Immunol* 35: 483-94

Soares MP, Hamza I (2016) Macrophages and Iron Metabolism. *Immunity* 44: 492-504

Soehnlein O, Lindbom L (2010) Phagocyte partnership during the onset and resolution of inflammation. *Nat Rev Immunol* 10: 427-39

Sokolic R (2013) Neutropenia in primary immunodeficiency. *Curr Opin Hematol* 20: 55-65

Stender S, Friebel A, Linder S, Rohde M, Miold S, Hardt WD (2000) Identification of SopE2 from *Salmonella typhimurium*, a conserved guanine nucleotide exchange factor for Cdc42 of the host cell. *Mol Microbiol* 36: 1206-21

Strouse JJ, Reller ME, Bundy DG, Amoako M, Cancio M, Han RN, Valsamakis A, Casella JF (2010) Severe pandemic H1N1 and seasonal influenza in children and young adults with sickle cell disease. *Blood* 116: 3431-4

Stull TL (1987) Protein sources of heme for *Haemophilus influenzae*. *Infection and immunity* 55: 148-53

Szczepanek SM, McNamara JT, Secor ER, Jr., Natarajan P, Guernsey LA, Miller LA, Ballesteros E, Jellison E, Thrall RS, Andemariam B (2012) Splenic morphological changes are accompanied by altered baseline immunity in a mouse model of sickle-cell disease. *Am J Pathol* 181: 1725-34

Szczepanek SM, Secor ER, Jr., Bracken SJ, Guernsey L, Rafti E, Matson A, Thrall RS, Andemariam B (2013) Transgenic sickle cell disease mice have high mortality and dysregulated immune responses after vaccination. *Pediatr Res* 74: 141-7

Takeuchi O, Akira S (2010) Pattern recognition receptors and inflammation. *Cell* 140: 805-20

Tan SY, Weninger W (2016) Phagocyte mayHEME caused by severe hemolysis. *Nat Immunol* 17: 1335-1337

Thomsen JH, Etzerodt A, Svendsen P, Moestrup SK (2013) The haptoglobin-CD163-heme oxygenase-1 pathway for hemoglobin scavenging. *Oxid Med Cell Longev* 2013: 523652

Tolosano E, Fagoonee S, Morello N, Vinchi F, Fiorito V (2010) Heme scavenging and the other facets of hemopexin. *Antioxid Redox Signal* 12: 305-20

Underhill DM, Ozinsky A (2002) Phagocytosis of microbes: complexity in action. *Annual review of immunology* 20: 825-52

Vallelian F, Deuel JW, Opitz L, Schaer CA, Puglia M, Lonn M, Engelsberger W, Schauer S, Karnaukhova E, Spahn DR, Stocker R, Buehler PW, Schaer DJ (2015) Proteasome inhibition and oxidative reactions disrupt cellular homeostasis during heme stress. *Cell Death Differ* 22: 597-611

Vicente-Manzanares M, Sanchez-Madrid F (2004) Role of the cytoskeleton during leukocyte responses. *Nat Rev Immunol* 4: 110-22

Vilcek J, Feldmann M (2004) Historical review: Cytokines as therapeutics and targets of therapeutics. *Trends Pharmacol Sci* 25: 201-9

Vincent SH (1989) Oxidative effects of heme and porphyrins on proteins and lipids. *Semin Hematol* 26: 105-13

- Vincent SH, Grady RW, Shaklai N, Snider JM, Muller-Eberhard U (1988) The influence of heme-binding proteins in heme-catalyzed oxidations. *Arch Biochem Biophys* 265: 539-50
- Voll RE, Herrmann M, Roth EA, Stach C, Kalden JR, Girkontaite I (1997) Immunosuppressive effects of apoptotic cells. *Nature* 390: 350-1
- Wandersman C, Stojiljkovic I (2000) Bacterial heme sources: the role of heme, hemoprotein receptors and hemophores. *Curr Opin Microbiol* 3: 215-20
- Wang J, Pantopoulos K (2011) Regulation of cellular iron metabolism. *Biochem J* 434: 365-81
- Warren MJ, Smith AG (2009) *Tetrapyrroles : birth, life, and death*. Landes Bioscience ; New York, New York, Austin, Tex. Springer Science+Business Media ;
- Wegiel B, Otterbein LE (2012) Go green: the anti-inflammatory effects of biliverdin reductase. *Front Pharmacol* 3: 47
- Wickstead B, Gull K (2011) The evolution of the cytoskeleton. *J Cell Biol* 194: 513-25
- Wiener E (2003) Impaired phagocyte antibacterial effector functions in beta-thalassemia: a likely factor in the increased susceptibility to bacterial infections. *Hematology* 8: 35-40
- Williams SE, Wootton P, Mason HS, Bould J, Iles DE, Riccardi D, Peers C, Kemp PJ (2004) Hemoxygenase-2 is an oxygen sensor for a calcium-sensitive potassium channel. *Science* 306: 2093-7
- World Health Organization (2015) WHO estimates of the global burden of foodborne diseases. Foodborne diseases burden epidemiology reference group 2007-2015. World Health Organization, Geneva
- World Health Organization. (2013) World malaria report 2013. World Health Organization, Geneva
- Yikrazuul (2010) Molecular structure of heme b. In
- Yin L, Wu N, Lazar MA (2010) Nuclear receptor Rev-erbalpha: a heme receptor that coordinates circadian rhythm and metabolism. *Nucl Recept Signal* 8: e001
- Zhang Q, Davis JC, Lamborn IT, Freeman AF, Jing H, Favreau AJ, Matthews HF, Davis J, Turner ML, Uzel G, Holland SM, Su HC (2009) Combined immunodeficiency associated with DOCK8 mutations. *N Engl J Med* 361: 2046-55
- Zhang Q, Dove CG, Hor JL, Murdock HM, Strauss-Albee DM, Garcia JA, Mandl JN, Grodick RA, Jing H, Chandler-Brown DB, Lenardo TE, Crawford G, Matthews HF, Freeman AF, Cornall RJ, Germain RN, Mueller SN, Su HC (2014) DOCK8 regulates lymphocyte shape integrity for skin antiviral immunity. *J Exp Med* 211: 2549-66

Curriculum vitae

PERSONAL INFORMATION

Name: Martins, Rui

Date of birth: 24-9-1982

Nationality: Portuguese

Address: Währinger Gürtel 112, Top 10/11, A-1090 Austria

E-mail: Rui.Martins@meduniwien.ac.at

ORCID ID: orcid.org/0000-0001-8106-6324

RESEARCH INTERESTS

Basic and translational immunology, with a focus on innate immunity and inflammation. The interface between immunity, inflammation and microbiota, and how these factors shape the immune response. Therapeutic development, high-throughput imaging and computational approaches.

EDUCATION

- Oct. 2010-Present **PhD in Infection Biology** – CeMM Research Center for Molecular Medicine of the Austrian Academy of Sciences and Department of Internal Medicine I, Medical University of Vienna, under the supervision of Prof. Sylvia Knapp
- Jan. 2010 **MSc Molecular Genetics and Biomedicine** - Universidade Nova de Lisboa, Faculdade de Ciências e Tecnologia
- Jul. 2007 **BSc Natural Sciences (Biology and Geology)** – Universidade Nova de Lisboa, Faculdade de Ciências e Tecnologia

RESEARCH TRAINING

- Oct. 2010-Present **PhD Thesis:** "The impact of hemolysis and heme on the susceptibility to bacterial infections" Laboratory of Infection Biology, CeMM - Research Center for Molecular Medicine of the Austrian Academy of Sciences, Vienna, Austria
Supervisor: Prof. Sylvia Knapp
- 2009-2010 **Research Stipend:** "Transcriptional Profile of Microglia upon Interferon gamma Stimulation."
Center for Brain Research – Medical University of Vienna
Supervisor: Prof. Monika Bradl
- 2008-2009 **Master Thesis:** "The microglial response to transforming growth factor beta"
Center for Brain Research – Medical University of Vienna
Supervisor: Prof. Monika Bradl

TEACHING

-
- | | |
|--------------|---|
| 2015-Present | Federica Quattrone – PhD student
Experimental supervisor |
| 2013-2014 | Julia Maier - Master Student
Master Thesis: “The Effect of Heme on the Innate Immune System”
(Co-supervised with Prof. Sylvia Knapp) |

AWARDS

-
- | | |
|------|---|
| 2016 | Poster prize at the European Macrophage and Dendritic Cell Society (EMDS) meeting in Amsterdam, Netherlands |
| 2013 | Best oral presentation prize at the 1 st Vascular Biology Meeting of the Medical University of Vienna |
| 2012 | Poster prize at the symposium of The Austrian Society of Allergology and Immunology (ÖGAI) |

PUBLICATIONS

Research articles

1. **Martins, R.**, Maier, J., Gorki A.D., Huber, K.V.M., Sharif, O., Starkl, P., Saluzzo, S., Quattrone, F., Gawish, R., Lakovits, K., Aichinger, M.C., Radic-Sarikas, B., Lardeau, C.H., Hladik, A., Korosec, A., Brown, M., Vaahtomeri, K., Duggan, M., Kerjaschki, D., Esterbauer, H., Colinge, J., Eisenbarth, S.C., Decker, T., Bennett, K.L., Kubicek, S., Sixt, M., Superti-Furga, G., and Knapp, S. *Heme drives hemolysis-induced susceptibility to infection and sepsis via disruption of phagocyte cytoskeletal dynamics* *Nature Immunology*, (2016), Vol(17), p1361–1372.
2. Willmann, K. L., Sacco, R.*, **Martins, R.***, Garncarz, W.*, Krolo, A., Knapp, S., Bennett, K. L. & Boztug, K., *Expanding the interactome of the non-canonical NF-kB signaling pathway.* *Journal of Proteome Research*, (2016), Vol(15), Issue:9, p2900–2909.
(* equal contribution)
3. Maier, B. B., Hladik, A., Lakovits, K., Korosec, A., **Martins, R.**, Kral, J. B., Mesteri, I., Strobl, B., Muller, M., Kalinke, U., Merad, M. & Knapp, S., *Type I interferon promotes alveolar epithelial type II cell survival during pulmonary Streptococcus pneumoniae infection and sterile lung injury in mice.* *European Journal of Immunology*, (2016), Vol(46), Issue:9, p2175-86.
4. Gawish, R., **Martins, R.**, Bohm, B., Wimberger, T., Sharif, O., Lakovits, K., Schmidt, M. & Knapp, S., 2015, *Triggering receptor expressed on myeloid cells-2 fine-tunes inflammatory responses in murine Gram-negative sepsis.* *FASEB Journal*, (2015), Vol. (29), Issue:4, p1247-57
5. Sharif, O., Gawish, R., Warszawska, J. M., **Martins, R.**, Lakovits, K., Hladik, A., Doninger, B., Brunner, J., Korosec, A., Schwarzenbacher, R. E., Berg, T., Kralovics, R.,

- Colinge, J., Mesteri, I., Gilfillan, S., Salmaggi, A., Verschoor, A., Colonna, M. & Knapp, S., *The triggering receptor expressed on myeloid cells 2 inhibits complement component 1q effector mechanisms and exerts detrimental effects during pneumococcal pneumonia. PLoS Pathogens*, (2014), 10(6), e1004167
6. Jais, A.*, Einwallner, E.*, Sharif, O., Gossens, K., Lu, T. T., Soyol, S. M., Medgyesi, D., Neureiter, D., Paier-Pourani, J., Dalgaard, K., Duvigneau, J. C., Lindroos-Christensen, J., Zapf, T. C., Amann, S., Saluzzo, S., Jantscher, F., Stiedl, P., Todoric, J., **Martins, R.**, Oberkofler, H., Muller, S., Hauser-Kronberger, C., Kenner, L., Casanova, E., Sutterluty-Fall, H., Bilban, M., Miller, K., Kozlov, A. V., Krempler, F., Knapp, S., Lumeng, C. N., Patsch, W., Wagner, O., Pospisilik, J. A. & Esterbauer, H., *Heme oxygenase-1 drives metaflammation and insulin resistance in mouse and man, Cell*, (2014), Vol(158), Issue:1, p25-40
(* equal contribution)
7. Pohl, M., Kawakami, N., Kitic, M., Bauer, J., **Martins, R.**, Fischer, M. T., Machado-Santos, J., Mader, S., Ellwart, J. W., Misu, T., Fujihara, K., Wekerle, H., Reindl, M., Lassmann, H. & Bradl, *T cell-activation in neuromyelitis optica lesions plays a role in their formation. Acta Neuropathologica Communications*, (2013), Vol(1), p85
8. Matt, U.*, Sharif, O.*, **Martins, R.**, Furtner, T., Langeberg, L., Gawish, R., Elbau, I., Zivkovic, A., Lakovits, K., Oskolkova, O., Doninger, B., Vychytil, A., Perkmann, T., Schabbauer, G., Binder, C. J., Bochkov, V. N., Scott, J. D. & Knapp, S., *WAVE1 mediates suppression of phagocytosis by phospholipid-derived DAMPs. Journal of Clinical Investigation*, (2013), Vol(123), Issue:7, p3014-24.
(* equal contribution)

Review articles

1. Matt, U., Sharif, O., **Martins, R.** & Knapp, S. *Accumulating evidence for a role of oxidized phospholipids in infectious diseases. Cellular and molecular life sciences*, (2015), Vol(72), p1059-1071

NON-ACADEMIC/SCIENTIFIC PROFESSIONAL EXPERIENCE

- 2005-2007 Computer hardware technician, web-designer – Páginas Comerciais, Lda.
2001-2007 Graphic designer, 3D modeler – Ciscofran Comunicação Visual, Lda.

LANGUAGES

- English Full professional proficiency
Portuguese Mother tongue
German Professional proficiency
Spanish Professional proficiency
French Elementary proficiency